INFORMATION TO USERS

This manuscript has been reproduced from the microfilm master. UMI films the text directly from the original or copy submitted. Thus, some thesis and dissertation copies are in typewriter face, while others may be from any type of computer printer.

The quality of this reproduction is dependent upon the quality of the copy submitted. Broken or indistinct print, colored or poor quality illustrations and photographs, print bleedthrough, substandard margins, and improper alignment can adversely affect reproduction.

In the unlikely event that the author did not send UMI a complete manuscript and there are missing pages, these will be noted. Also, if unauthorized copyright material had to be removed, a note will indicate the deletion.

Oversize materials (e.g., maps, drawings, charts) are reproduced by sectioning the original, beginning at the upper left-hand corner and continuing from left to right in equal sections with small overlaps.

Photographs included in the original manuscript have been reproduced xerographically in this copy. Higher quality 6" x 9" black and white photographic prints are available for any photographs or illustrations appearing in this copy for an additional charge. Contact UMI directly to order.

Bell & Howell Information and Learning
300 North Zeeb Road, Ann Arbor, MI 48106-1346 USA
800-521-0600

UMI®

Université d'Ottawa • University of Ottawa

Dedicated to the loving memory

of my mother, who passed

away from cancer during the

writing of this thesis.

She will always be

an inspiration.

Acknowledgments

I would like to thank the people who have helped support me in my graduate studies. To my Ph.D. supervisor Dr. J.C. Scaiano, for always being available to listen both on a professional and personal level. His relations and concern for his students render him a truly unique supervisor. To Dr. H. García, with whom I colloborated on many projects; your friendship will never be forgotten. My fellow group members also deserve special mention.

During my time at Ottawa U, the post-docs and students in the group have made it truly memorable. To Will, who constantly looked out for me, better than any brother could. To Gonzalo, with whom I share a close friendship that will always remain with me. To the post-docs, Terry and Gerd, who supervised some projects of mine. Their patience and willingness to address my questions were greatly appreciated. To Nadereh, who is one of the most kind and generous people I have had the pleasure of calling my friend. To Lydia, who has become the big sister I've never had. She is a role model to me, demonstrating independence and compassion. You all are so special to me.

During my graduate studies, I have met people outside the lab who have helped immensely. One of these people deserves the highest praise for his positive influence on my life. To Tim, who has added a whole new dimension to my life, and continues to teach me many important lessons.

And finally to my family, who have been cheering me on my whole life and have always been there to motivate me. I especially want to bestow a special

thanks to my parents, who have been a continuing source of inspiration in my life and have always encouraged me to do my very best. I love you both dearly.

Table of Contents

List of Tables

List of Schemes

List of Figures

List of Abbreviations

LFP	=	laser flash photolysis
DR LFP	=	diffuse reflectance laser flash photolysis
IR	=	infrared
PMT	=	photomultiplier tube
J	=	light intensity of the monitoring beam (diffuse reflectance)
ΔJ	=	change in reflectance after excitation
NMR	=	nuclear magnetic resonance
THF	=	tetrahydrofuran
DMSO	=	dimethylsulfoxide
DMF	=	dimethylformamide
EtOH	=	ethanol
MeOH	=	methanol
EMM	=	effective mass model
PDMS	=	polydimethylsiloxane
ESM	=	exponential series method
PTI	=	Photon Technology International
K	=	absorption coefficient
S	=	scattering coefficient
F(R)	=	remission function
EFAL	=	extra-framework aluminum
IP	=	ionization potential

CT = charge-transfer

et = electron transfer

RP = radical pair

TTL = transistor-transistor linked

XANES = X-ray Absorption Near Edge Spectroscopy

k = rate constant

Abstract

This thesis gives a detailed account of photochemical processes that occur upon excitation of guest species included inside zeolite host cavities. The use of zeolites, which contain an internal pore structure, as 'microreactors' that can house a variety of molecules differing in size and shape has a remarkable influence on the outcome of photochemical processes, as well as on the behaviour of the transient species formed.

The work presented in the various chapters all have an underlying theme: to acquire an understanding of the photochemical and photophysical processes of guest species encapsulated in a constricted medium, and to use this knowledge in the development of new applications of zeolite materials. Thus, the work presented in this thesis explores many different probe molecules in order to acquire a broad view of how the intrazeolite environment influences the photochemical behaviour of encapsulated species. The topics investigated range from the acid-base properties of coumarin 6 in a series of zeolites, to the effect of spectators on the transient and product formation of encapsulated carbonyl compounds, to the characterization of transparent zeolite films. The relevance of these results in context with other work in the field will also be discussed.

1. Introduction

1.1 Characteristics of Zeolites

1.1.1 *Background on Zeolite Materials*

Zeolites form a family of aluminosilicates containing an internal pore structure and have been studied by mineralogists for more than 200 years. The term zeolite was coined in 1756 by a Swedish mineralogist, taken from the Greek 'zeo' to boil and 'lithos' for stone, due to the appearance of the material boiling when heated.[1] Since then, approximately forty naturally occurring zeolite minerals have been discovered. Initial attempts at synthesizing new zeolite materials began in the 1860's. The characterization of these materials did not occur until the 1940's, when x-ray diffraction techniques became available.

Zeolite research covers a fairly broad spectrum, ranging from catalytic studies to their use as supramolecular hosts in photochemical reactions. While the catalytic behaviour of zeolites in many different types of reactions has been investigated for over three decades,[2-6] the interest in the photochemical properties of a guest molecule included within the zeolite pores has only received appreciable interest during the past fifteen years.[7,8] The current interest in supramolecular photochemistry[9] arises from the influence that organized and constrained media have on the abilities of guest molecules to change their shape during the course of a photoreaction. In addition, zeolites are extremely versatile hosts, with a wide range of both geometry and pore dimensions to accomodate

many sizes and shapes of guest molecules.[10-14] This chapter will examine in detail the specific characteristics of zeolites that make them such an attractive medium for photochemical reactions, as well as a brief review on some unique findings by other groups using zeolites as supramolecular microreactors.

1.1.2 *Zeolite Structure*

Zeolites are crystalline aluminosilicates containing an internal pore structure consisting of either nanosized cages or channels that are repeated along the tri-directional structure of the lattice. The internal zeolite surface occurs in a periodic fashion because of the crystalline nature of the framework. The framework of the zeolite is made up of $[SiO_4]^{4-}$ and $[AlO_4]^{5-}$ tetrahedra sharing their edges.[10,11] The lower valence of Al relative to Si results in a net negative charge, one per Al, which is compensated for by the presence of charge-balancing cations, such as H^+, Na^+, Ca^{2+}, etc. This keeps the framework neutral.

The $[SiO_4]^{4-}$ and $[AlO_4]^{5-}$ tetrahedra are arranged in substructures that form the building blocks of the zeolite.[15] These include the sodalite cage, which makes up the faujasite zeolite A, X and Y, and sodalite zeolite; the pentasil cage, which makes up the zeolites mordenite, ZSM-5 and ZSM-11. Zeolites X and Y have the same three dimensional structure, but different Si/Al ratios, resulting in differences between the number of cations per unit cell (86 for NaX and 56 for NaY). The structures of the building blocks and corresponding zeolites are given in Figure 1.1. This simplified representation does not show each individual Al, Si and O atom; rather, the vertex represents Si or Al and the line represents the oxygen link

between them. The charge-balancing cations are also not included for clarity sake. In Figure 1.2, a different view of the pentasil zeolites ZSM-5 and ZSM-11, illustrating their channel structure, is given. In this figure, only the void spaces are indicated; the framework is omitted for clarity.

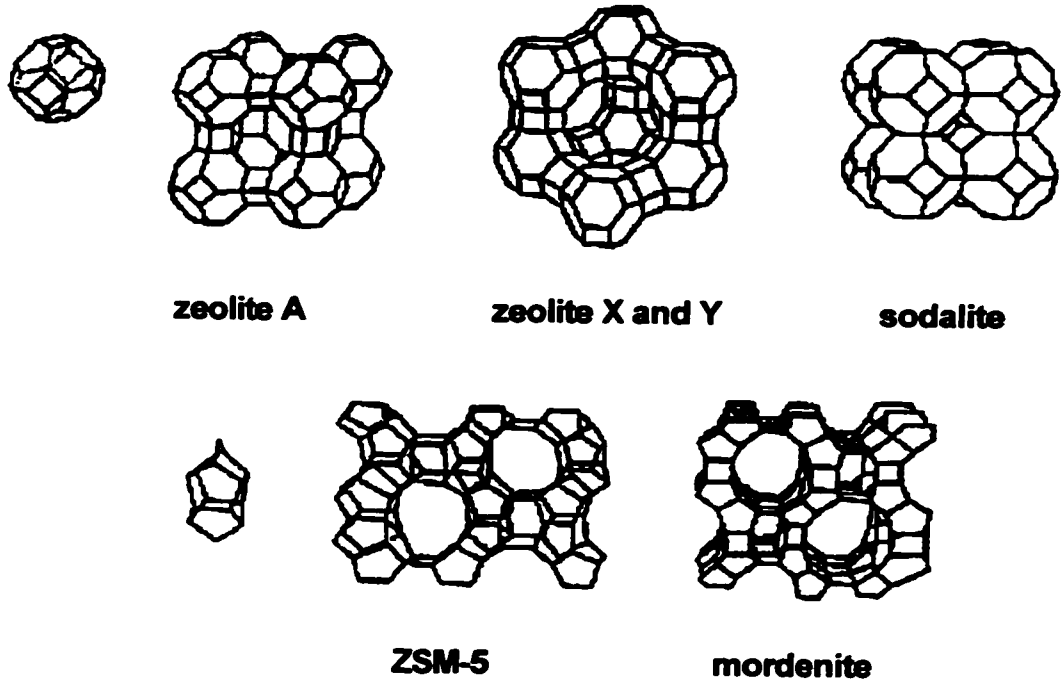

Figure 1-1: Structures of faujasite and pentasil zeolites. (*Top*) sodalite cage, which makes up structures of zeolite A, X and Y, and sodalite. (*Bottom*) pentasil cage, which makes up structures of ZSM-5 and mordenite. Reprinted from reference 9

ZSM-5 ZSM-11

Figure 1-2: Channel structure of zeolites ZSM-5 and ZSM-11. Note that ZSM-5 has two channel types: the zig-zag and linear types, whereas ZSM-11 has straight channels only. Reprinted from ref 15

The faujasite family of zeolites contain large spherical cavities called supercages, which are tetrahedrally coordinated to four other supercages. The window opening to the supercage in zeolite Y is approximately 7.4 Å in diameter, while the interior of the supercage has a diameter of ~ 13 Å.[12] These dimensions control the possible guest uptake and intercavity diffusion, since only guest molecules of kinetic size less than the window opening can be readily included. Supercages are large, as they can hold 28 molecules of water and over 5 molecules of benzene. The sodalite cages themselves have pore openings that are too small to allow any organic molecule through.

The charge-compensating cations in faujasite zeolites X and Y occupy three different sites. The first location, referred to as site I, with 16 per unit cell for both X and Y, is located on the hexagonal prism faces between the sodalite units. Site II, with 32 cations per unit cell for both X and Y, is located in the open hexagonal faces. The third location, site III, with 8 per unit cell for Y and 38 per unit cell for X,

is located on the walls of the larger supercage cavity. Each unit cell consists of eight supercages. Only cations occupying sites II and III are expected to be readily accessible to the included organic molecules. Figure 1.3 illustrates the cation locations in faujasite zeolites.

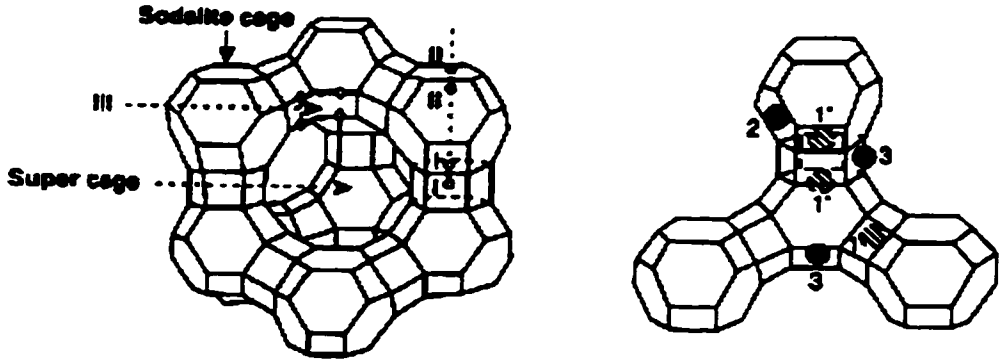

Figure 1-3: Structure of the faujasite zeolite, illustrating the cages present as well as cation location. Reprinted from reference 16

The pentasil-based zeolites have a different three-dimensional structure; these zeolites contain two intersecting channels. ZSM-5 contains straight and sinusoidal channels. The straight channels have dimensions of 5.4 x 5.6 Å and the sinusoidal channels have a diameter of 5.1 x 5.5 Å. In contrast, ZSM-11 contains both straight channels with diameters of about 5.3 x 5.4 Å (see Figure 1.2). In mordenite zeolite, the channel dimensions are 7.0 x 6.7 and 2.6 x 5.7 Å.[15] Figure 1.4 shows a simple representation of a two dimensional slice of zeolite Y and ZSM classes of zeolites.

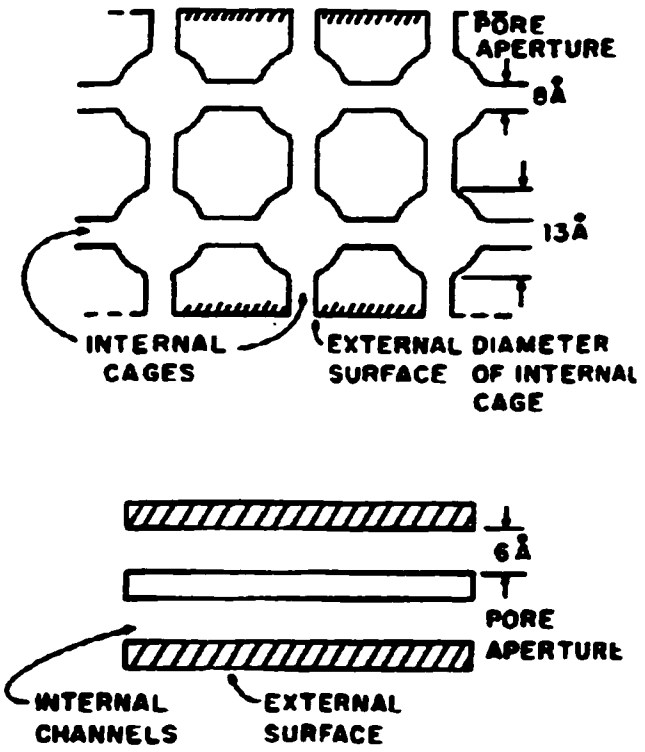

Figure 1-4: Topological representation of the X and Y zeolite (*top*) and the ZSM zeolite (*bottom*). The representation shows a two dimensional slice of the solid. Reprinted from reference 1

The term zeolite is reserved strictly for molecular sieves containing $[SiO_4]^{4-}$ and $[AlO_4]^{5-}$ tetrahedra. Other types of molecular sieves that are similar to zeolites exist, differing in terms of their chemical framework; that is, the tetrahedral sites are occupied by cations other than Al^{3+} and Si^{4+}.[13] One example of such a zeolite type material is derived from Al and P. This material has no framework charge and therefore no ion-exchange capacity. The pore system consists of one-dimensional channels. Zeolite-type materials which fall into this category include VIP-5[16] and $AlPO_4$-5.[17] Another example of a zeolite type material includes one derived from Ga and P. One particular gallophosphate molecular sieve is

cloverite,[18] which has a four-leaf-clover-shaped pore opening. The large interior supercage has a diameter of 30 Å with a pore aperture of ~ 13 Å. The interior of the supercage contains some hydroxyl groups in the framework. The structures of these two categories of zeolite type materials are illustrated in Figures 1.5 and 1.6. The simplified representation of the structures is similar as that given for the zeolite framework: the vertex represents a tetrahedral atom, and the line joining them represents an oxygen bridge. For the structure of cloverite given in Figure 1.6, the solid circles represent some of the terminal hydroxyl groups.

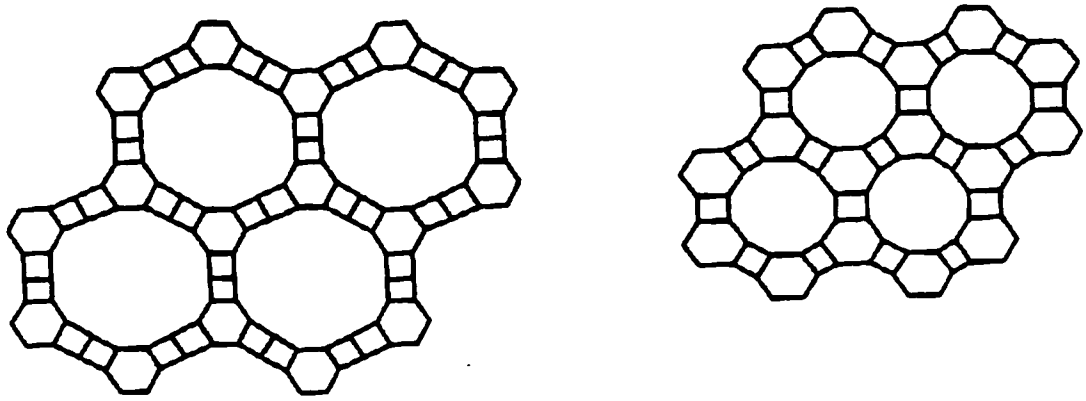

VPI-5 **$AlPO_4$-5**

Figure 1-5: Channel openings of VPI-5 and $AlPO_4$-5. Reprinted from reference 15

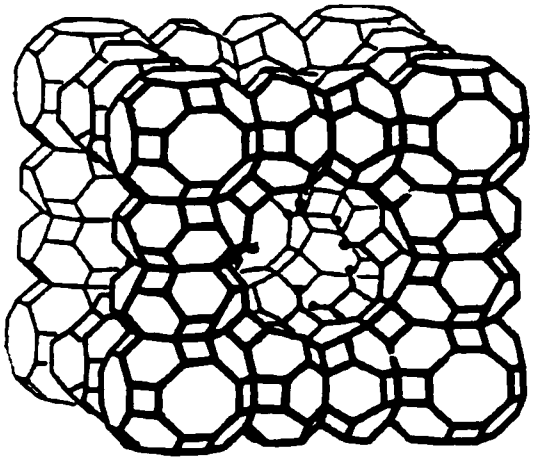

Figure 1-6: Framework structure of cloverite. Reprinted from reference 13

Zeolites can be classified as small, medium or large pore, depending on the number of oxygen atoms defining the pore opening. Small pore zeolites contain 8 oxygen atoms, medium pore zeolites have 10 and large pore zeolites have 12 oxygen atoms in the pore opening. Using this definition, zeolite X and Y are classified as large pore zeolites and ZSM-5 and ZSM-11 are medium pore zeolites. Extending the same classifications to zeolite type materials, $AlPO_4$-5 is a large pore molecular sieve, and VIP-5 is a very large pore molecular sieve (18 oxygen atoms). Cloverite, on the other hand, has 20 oxygen atoms in the pore opening. Due to the pore sizes of these zeolite-type molecular sieves, they are often referred to as microporous materials, rather than nanoporous materials which classify zeolites. Molecular sieves with larger pore openings (> 13 Å) are referred to as mesoporous molecular sieves. An example is MCM-41[19,20] (MCM stands for **M**obil's **C**omposition of **M**atter), which has a hexagonal arrangement of parallel channels. The channel diameter is tunable between 15 Å and 100 Å,

depending on the size of the template used during synthesis of this material. The pore size distribution is nearly as sharp as conventional zeolites.

1.1.3 Synthesis and Manipulations of Zeolite Materials

The usual technique for synthesizing zeolites is through hydrothermal treatments of aluminosilicate gels or solutions[10] containing metal (such as alkali or alkaline earths), or organic ions (such as tetraalkylammonium) or molecules (such as amines). The ions or molecules present in the treated gel act as templates during the crystallization process. Templates direct the formation of the specific zeolite framework, including the pore size. During crystallization, the aluminosilicate solution present between the template assemblies becomes the walls of the porous solid.

The conditions applied during the hydrothermal treatment affect the Si/Al ratio of the zeolite as well as its water content. This may result in a series of zeolites that are structurally similar, but exhibit different properties.

Manipulations of the zeolite material, either before or after synthesis, can easily be achieved. One such manipulation is the altering of the Si/Al ratio of the zeolite. Generally,the Si/Al ratio varies from zeolite to zeolite, ranging from 1 to ∞. A Si/Al ratio less than one is unattainable; this is a direct consequence of the proximity of the charge-balancing cations near the Al in the zeolite framework. This ensures that no Al-O-Al bonds are formed because of the unfavourable interaction of two positively charged ions close together. The Si/Al ratio of a zeolite determines whether the zeolite is hydrophobic or hydrophilic. Zeolites with a Si/Al

ratio close to one have a high framework charge and therefore many cations are present. This leads to a very hydrophilic zeolite. On the other hand, zeolites with a high Si/Al ratio have very few cations in the interior, and hence are very hydrophobic.

Another manipulation of the zeolite material involves altering the charge-balancing cations. The cations present in the zeolite pores can be readily replaced using conventional ion exchange techniques.[10,11,14] This is discussed further in Section 1.1.5. Zeolites with the same three-dimensional structure but with different charge-balancing cations exhibit different properties. For example, exchanging Na^+ for K^+ or Cs^+ results in a less acidic zeolite, whereas exchanging Na^+ for any of the Group II cations results in an acidic zeolite. Changing the counterion also determines the available space in the zeolite pores. For example, replacing Na^+ for the larger Cs^+ in zeolite Y reduces the vacant space in the supercage,[21] from 827 $Å^3$ to 781 $Å^3$. This dramatically influences the guest uptake as well as guest mobilities. In addition, the electrostatic field within the supercage is strongly dependent upon the countercation; this is due mainly to size effects. The smaller Li^+ induces a stronger field in its proximity than does Cs^+. The measured electrostatic field within the supercages of LiY is 2.1 V/Å, compared to 0.6 V/Å for CsY.[21] All of the above parameters have a significant influence on the photochemistry and photophysics of included organic guest molecules.[6,15,21-25]

1.1.4 *Location and Distribution of Guest Molecules*

To be able to understand or predict the photochemical behaviour of guest molecules included in zeolites, their location and distribution within the zeolite pore structure must be known. Characterization of guest location within a zeolite has been accomplished using techniques such as x-ray and neutron diffraction, NMR, IR and time-resolved methods.[7,8,26-31]

The amount, or loading, of guest molecules included in zeolite pores is often given in terms of the occupancy number, <S>. This value is a ratio of the number of guest molecules to the number of supercages. This number is only an average number, since the distribution of guest molecules in the zeolite is not expected to be uniform. That is, some cages may be singly occupied, some may be doubly occupied, whereas others may not be occupied at all. This occupancy number, <S>, is used to indicate the loading levels, but may not reflect the true inhomogeneity of guest distribution in zeolites.

The loading level of an organic molecule in zeolite pores has an effect in determining the location of the guest molecule. Small loadings in pentasil zeolites such as ZSM-5 results in the organic guest molecules preferably residing at the intersection of channels. At high loadings in a pentasil zeolite such as ZSM-5, occupation of both the straight and sinusoidal channels occurs.[15,21] In the case of faujasite zeolite Y, small loadings of guest molecules results in their location inside the supercage. Occupation of > 1 molecule per supercage occurs when higher loadings are introduced. To illustrate the locations of guest molecules in faujasite zeolites, the inclusion of benzene in NaY will be used as an example.

There are three distinct locations of benzene in the supercages of zeolite Y. One is at the cation site (site II or III), one at the 12 ring window site, and the other corresponding to benzene clusters within the cage. At low loading levels, this clustering is avoided; instead, there is a distribution between the cation site and the window site.[15] Benzene, as well as other aromatic molecules, are stabilized at the cation site through a cation-π interaction with the π cloud of the benzene ring. At the window site, stabilization occurs through van der Waals forces. The two sites are shown in Figure 1.7.

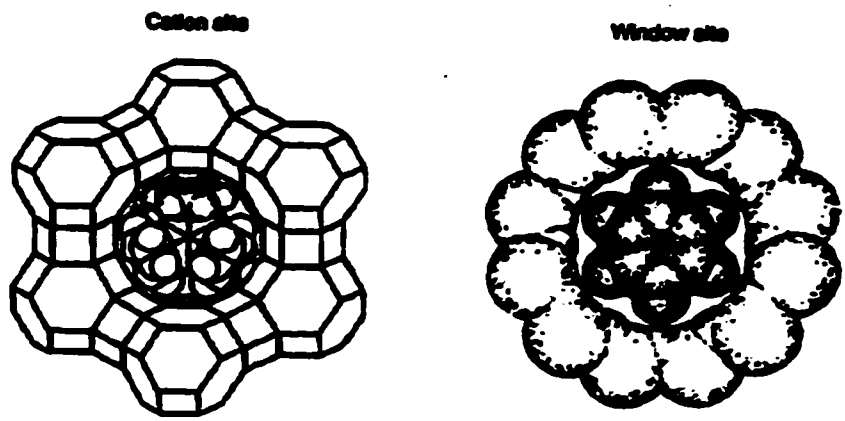

Figure 1-7: Two sites in which benzene is located upon small loadings in the faujasite zeolite. The diagram on the left illustrates benzene located at the cation site, while the diagram on the right shows the location of benzene at the window site. Reprinted from reference 15

Another example which illustrates the effect of guest location is the fluorescence of pyrene in NaY. On freshly prepared samples of pyrene in NaY, excimer (**excited dimer**) formation is detected, which can only occur when the supercages are doubly occupied. Aging of the samples causes the pyrene molecules to redistribute, resulting in an equilibrium distribution where the supercages are

singly occupied. This is verified by monomer emission and lack of excimer emission.[32] These results also reinforce the necessity to examine intrazeolite photophysical properties as a function of sample age, since guest molecules in zeolites are very mobile, depending on their size, and an equilibrium guest distribution may take months to occur.

In a supramolecular host such as a zeolite, the distribution of guest molecules is such that there often is more than one site for the reacting guest. This possibility is rarely discussed in homogeneous solution, since fluid solutions allow reacting molecules to experience an average microenvironment. This is attributed to the fast relaxation time of the solvent and the mobility of reactant molecules. In solution, all reactant molecules experience a single environment. Unlike solvents, the zeolite structure is time-independent. Thus, photoexcited guest molecules may experience different environments or a single environment, depending on the guest migration rate and the excited state lifetime. This is a contributing factor to the differences seen between solution and intrazeolite photoreactions, as will be examined in more detail in the last section of this chapter.

1.1.5 *Preparation of Zeolite Complexes*

1.1.5.1 Method of Exchanging Charge-Balancing Cations

Methods of exchanging the charge-balancing cations are well established.[10,11,14] This is accomplished through contact of the Na^+ of the zeolite with an aqueous solution of the desired cation (in the form of the corresponding

chloride or nitrate). The complex is then dried at high temperatures, and the entire process repeated twice more. It should be noted that only partial exchange of cations such as Rb^+ or Cs^+ occurs; the size of the cations excludes complete exchange.

The cation to be introduced into the cavities may also be a proton, rendering the zeolite with Brønsted acid sites. Proton-exchanged zeolites are prepared[33,34] by a partial exchange of Na^+ by NH_4^+, followed by calcination at high temperature (< 600°C). Further ion-exchange is required in order to reduce the sodium content. In this process, the unit cell size of the original NaY is reduced (by < 0.02 nm)[34] because of the dealumination that occurs. Generally, an increase in the Si/Al ratio results in a decrease in the unit cell dimensions, due to the shorter Si-O bond compared to the Al-O bond. This process of forming proton-exchanged zeolites does retain the zeolite crystallinity.

Removing the Al from the framework results in Al remaining on the crystal and migrating to the surface.[35] This Al species is referred to as extra-framework aluminum (EFAL). This species contributes to the Lewis acid sites that are also present in the proton-exchanged zeolites. Further treatment of the zeolites using $(NH_4)_2SiF_6$ removes partially or completely the EFAL produced,[34] depending upon the $(NH_4)_2SiF_6$-to-zeolite ratio. The presence of EFAL is important, since EFAL may play a crucial role in catalytic processes.[36,37]

This simple process of exchanging the charge-balancing cation allows small changes to be made to the zeolite, while greatly altering its properties such as polarity, acidity and electrostatics.

1.1.5.2 Inclusion of Neutral Guest Molecules

The size of the window opening of a zeolite pore defines which guest molecules may be readily included. If a guest molecule has dimensions that are smaller than the pore window, then guest uptake may occur upon contact with the zeolite in a suitable solvent. For a hydrophilic zeolite such as NaY, pretreatment of the zeolite prior to guest inclusion must occur. This involves calcining the zeolite sample at 400-550°C in order to remove the water that fills the cages. Once the water is removed, the dry zeolite is added to a solution of the desired guest. Since the interior of NaY is very polar, the solvent of choice is a non-polar, volatile one such that preferential migration of the guest into the zeolite interior dominates. The zeolite complex is then removed from the solvent, and washed with fresh solvent in order to remove any molecules that are bonded to the zeolite exterior surface. The method in which the zeolite complexes are dried has a significant influence on the ensuing photochemistry. The differences in drying methods lies in how much residual solvent, water and oxygen are removed. Complexes that do have residual solvent and water will effect the overall crowding of the cages, which may restrict the mobility of the guest molecules in the cages. The presence of oxygen may lead to quenching of the transient formed, such as triplet states. Thus, photoproduct formation may be altered, as well as transient lifetimes.

Other approaches must be employed if the desired guest molecule to be located in the zeolite pore is larger than the pore opening. A method termed 'ship in a bottle synthesis'[38,39] has been developed to overcome such difficulties. This

procedure synthesizes the desired molecules within the zeolite framework. This is accomplished by using building blocks or precursors that are small enough to diffuse into the zeolite pores which combine to produce the desired molecule, using the zeolite as a catalyst. The synthesized molecules, once formed, cannot leave or relocate within the zeolite, due to their molecular dimensions. Ship in a bottle strategies for synthesizing organic molecules locked in the supercages involve the formation of new C-C bonds.[39] An example of this type of approach is the in-situ synthesis of trialkylmethylium cations using zeolites HY, Hβ and HZSM-5. These molecules are prepared by the acid-catalyzed condensation of benzaldehydes and activated arenes. Refluxing these precursors in proton-exchanged zeolites leads to the formation of the substituted trityl cationic dyes within the zeolite (for HY and Hβ), catalyzed by the acidic zeolite. Conventional Lewis acid catalysts such as $AlCl_3$ are generally very inefficient for this reaction process. It should be noted that the formation of the trityl dye in the case of HZSM-5 occurred exclusively at the zeolite surface. This is due to the inability of the zeolite to accomodate the bulky trityl cation in its pores. This indicates that the synthesis of large species from smaller precursors does not necessarily guarantee the internal location of the guest. Figure 1.8 depicts how the trityl cations are formed via ship in a bottle synthesis. The incorporation of these cations in the zeolite supercages make up part of the charge-compensating cations. The method of ship in a bottle synthesis was used to prepare the zeolite samples examined in Chapter 6.

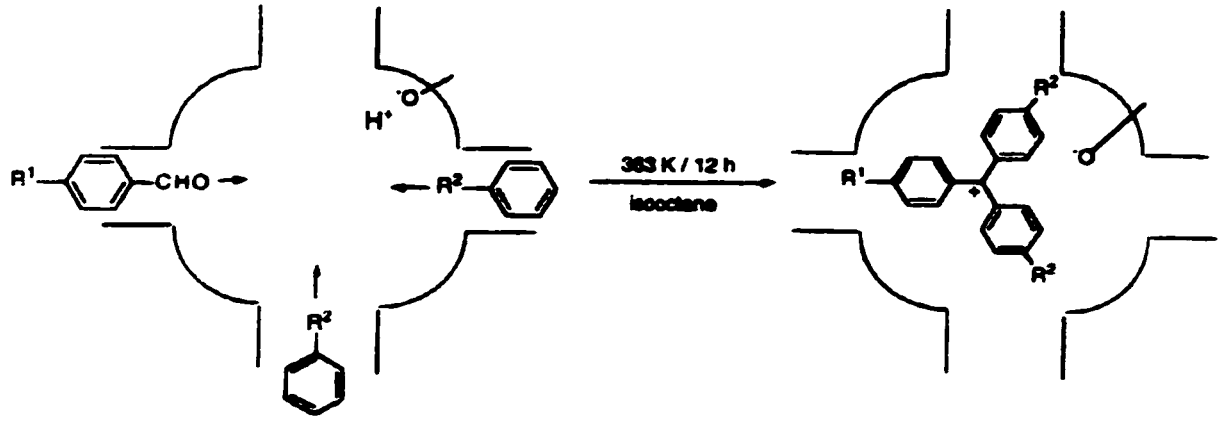

Figure 1-8: Ship in a bottle synthesis of triarylmethylium cations by acid-catalyzed condensation of benzaldehydes and activated arenes. Reprinted from reference 40

1.1.6 Role of Water in Intrazeolite Photochemistry

The role of water in intrazeolite photochemistry is extremely important. It has a substantial influence on the photochemical and photophysical behaviour of included guest molecules. Zeolites are hygroscopic; thus, the preparation of samples of organic molecules encapsulated in zeolites by different groups often results in the samples containing different amounts of water. The impact of this is outlined below.

Recent work on the photophysics and photochemistry of ketones included in 'dry' and 'wet' zeolite NaX has produced some very interesting results.[40] 'Wet' zeolites are simply the 'dry' zeolites containing the included ketone, which has been exposed to water vapour, the amount of water quantified by the resulting change in mass. The conclusion drawn from these studies is that the location of the guest molecules changes between the 'dry' and 'wet' zeolite in a predictable

fashion. In the 'dry' zeolite, the guest is included inside the supercage whereas in the 'wet' zeolite, the guest has been displaced to the exterior surface due to water filling up the void volume. This causes the guest molecules to experience much less restriction in its diffusional and rotational motions, as well as to experience a much less polar environment. This affects not only the triplet lifetime of the ketone, but also the product distributions. It has been established that the first five water molecules that enter the supercage bind to the Type III cations, and the subsequent water molecules bind the Type I and Type II cations, and then fill the void spaces within the supercage.[41] Thus, the first five water molecules will have less influence on the product distribution, although the triplet lifetimes will still be affected. These conclusions about the location of guest molecules were drawn upon studying the emission of xanthone in 'dry' and 'wet' zeolites, through product studies of Type I cleavage of dibenzylketones (homolytic α-cleavage) and the Type II reaction of aryl alkyl ketones (intramolecular H-abstraction to form 1,4-diradicals).[42]

Another influence that the presence of water in the supercages has is illustrated by using the cationic dye thionin as an example. Thionin-exchanged Y zeolite was prepared, and it was found that for the hydrated zeolite, both the monomeric and H-aggregated forms of thionin were detected. When the water was removed (by drying at 100°C), only the monomeric form of thionin was detected.[43] Similar results were obtained by an independent group, however, their interpretation of the results is different.[44] While they believe that in fact aggregation of the dye does occurs with increasing degree of hydration, they state that the

formation of the dimer must occur on the external surface of the zeolite. This is based on molecular modeling calculations that show that it is highly unlikely for aggregation to occur inside the cages. Whether or not aggregation occurs in the interior or on the external surface of the zeolite, it is apparent in any case that water does affect the form of thionin detected. Thus, intracavity water does have a significant influence on the properties of guest molecules included within zeolites.

1.2 Comparison to Other Constrained Media

Other supramolecular systems have been employed as hosts for photochemical studies. This includes, but is not limited to, silica gel[45-50] and clays.[51-56] This section will illustrate some of the features of these other constrained media in relation to zeolites.

Silica gel is one of the amorphous silicas with a rigid network of spherical particles of colloidal silica. It has been used as a surface onto which molecules can be adsorbed. The binding of molecules to silica occurs through the surface silanol groups. The types of silanol groups found on silica may be divided into three categories: vicinal, geminal and isolated. The number of silanol groups is dependent upon the pretreatment conditions of the silica gel. Heating silica gel at high temperatures (~500°C) reduces the surface silanol content, which has an effect on the rate of adsorbate diffusion on the silica gel, since the adsorbate adheres to the surface through the silanol. Molecular diffusion is slow on most surfaces, due to the strong adhesion to the surface.[25] Silica gel thus restricts the lateral movement of the adsorbent in one dimension only. The actual volume of

the reaction cavity that the adsorbent on a silica gel surface experiences is, however, undefinable because of the lack of a boundary in at least one dimension.

Clays are chemically similar to zeolites, but are comprised of two dimensional layers or sheets of aluminosilicates with the charge compensating cations located between the anionic layers.[25,57,58] Intercalation of various guest molecules within the clay minerals using water or polar solvents causes the layered structure to swell significantly.

Photochemistry of clays, for the most part, has been restricted to aqueous colloidal clay systems. Colloidal clays can only adsorb cationic species through an ion-exchange process. Organic species, such as arenes, can be adsorbed onto the clay once the clay has been pretreated such that the adsorbed water is expelled. The volume of the reaction cavity, unlike silica gel, in the interplanar regions of the clay, is time-independent, i.e. the free volume is essentially constant.

When comparing constrained media such as silica gel, clays and zeolites, one thing becomes readily apparent: silica gel restricts movement of adsorbates in one dimension, clays in two dimensions, whereas zeolites restrict movement in three dimensions. This is dictated by the shape and size of the zeolite pores. In this context, the zeolite medium can be considered a 'passive' host,[59] that is, predictions on the behaviour of a guest molecule can be made solely on the basis of zeolite cavity size, shape and flexibiliy. How does this feature of zeolites alter photochemical reactions? One important way is through confinement of molecules[60] located in the intracrystalline volume. Only certain reactants will be

able to access the internal pore openings of the shape selective zeolite medium. Once confined, the reactant may face further constraints on the reactive intermediate or transient that may be accessed, preventing the occurrence of certain reactions while greatly enhancing others. Thus, not only can zeolites act as molecular sieves for reactant molecules, but they can also alter the products of a photoreaction simply by the size and shape of the internal pores. The variety of zeolite geometries leads to photoproduct or photoproduct ratios that change from zeolite to zeolite, and not just from zeolite to solution irradiations.

Another manner in which zeolites can alter photochemical reactions is through molecular traffic control.[60,61] This derives from the ability of the pore system of zeolites to control chemical reactivity through the dynamics of molecular diffusion. A zeolite with a pore network of differentiated channels results in reactants or products having distinct steric requirements to diffuse along different paths in the intracrystalline space. The ease with which the molecules can diffuse will depend upon the congestion within the pores. This will dictate the distance that a transient or reactive intermediate can travel during the excited state lifetime or before reaction occurs. This will impact the types of products and the reaction pathway that is followed. The concept of molecular traffic control is used to explain the photochemistry of aryl alkyl ketones in zeolites, which will be examined in detail in the next section.

Through confinement and molecular traffic control alone, the altering of photochemical properties of included guest molecules in zeolites is apparent, by only examining the zeoltie as a 'passive' host. An examination of the zeolite as an

'active' host[59] will illustrate other ways in which photochemistry can be modified in zeolite pores compared to solution.

Zeolites as 'active' hosts refers to the interaction of the zeolite and the included molecule. These interactions may vary from weak van der Waals forces, to strong H-bonds, to electrostatic interactions with the charge-balancing cations. These factors can influence significantly the course of photophysical and photochemical events. The influence of the charge-balancing cations can be grouped into two different categories: light-atom and heavy-atom effects.[15,62-64] The light-atom effect, as the name implies, refers to phenomena observed with smaller and lighter cations. These cations have a higher charge density and electrostatic potential, resulting in a stronger binding interaction between the cation and the guest molecule. A classical example of the light-atom effect is the interaction of pyrene with the cation present in the supercages of X and Y zeolites. It was determined that the intensity of the 0-0 transition of the S_o to S_1 band is dependent upon the charge density of the charge-balancing cation. It was suggested that the symmetry reduction of the aromatic molecule occurs because of the strong interaction between the cation and the π ring, causing a slight bending of the aromatic plane.[15,21] The heavy-atom effect, on the other hand, deals with the weaker interaction between heavier cations such as Rb^+, Cs^+ and Tl^+ with guest molecules. This interaction leads to unique effects in the photobehaviour of guest molecules. An example of this effect is the enhanced phosphorescence of guest molecules included within heavy cation exchanged zeolites. Even molecules that do not phosphoresce under normal conditions,

such as alkenes, emit from their triplet states when included in Tl^+-exchanged zeolites.[15,21,64]

An additional guest-cation interaction includes acid-base interactions. This property is very influential in the photobehaviour of encapsulated guest molecules, as is demonstrated in Chapter 3 of this thesis.

Zeolites can be used as nanoscopic reaction vessels to alter and influence the photochemistry and photophysics of guest molecules in many ways: confinement, molecular traffic control, size and shape of pores, electrostatic interactions and acid-base interactions, to highlight a few. These characteristics are not all found in solution or in other confined media such as silica gel and clays to the same extent as occurs in zeolites. This makes the use of zeolites as supramolecular hosts an attractive medium for tuning the photobehaviour of encapsulated molecules. The next section will illustrate these effects with representative examples from the literature. As well, the following chapters will expand upon or offer new insight into the role of zeolites in supramolecular photochemistry.

1.3 Differences in Photochemical Properties of Organic Species in Solution and in Zeolites

1.3.1 Photolysis of Dibenzylketones in Zeolites

The first example will deal with aryl alkyl ketones. The photochemistry of aryl alkyl ketones has been extensively studied in solution[65,66] and a variety of supramolecular systems[67-69] including zeolites.[70-74] A few representative

examples will be presented here. Solution irradiation of an unsymmetrical dibenzyl ketone, designated as A(CO)B for simplicity, is characterized by the formation of benzyl radicals following α-cleavage and decarbonylation, resulting in formation of 3 radical coupling products AA, AB and BB, in the ratio of 1:2:1 as dictated by statistics for random radical encounters. Once the A(CO)B molecule is included in a constrained medium, the outcome of the reaction is expected to differ compared to solution, due to the zeolite microenvironment.[70,71,74] The zeolite structure may inhibit the diffusion of the primary radical pair generated, following α-cleavage, leading to distinct product formation. Another possibility is that the primary radical pair may decarbonylate to produce a secondary radical pair, with a high probability of geminate pair coupling, rather than random pair coupling, due to hindering of the escape of the radical pairs. This leads to a non-statistical distribution of radical coupling products, as compared to solution. This phenomenon is known as the cage effect, which is the percent of geminate radical pairs that undergo reaction to form coupling products. The cage effect can be expressed in the following manner:

$$\% \text{ cage effect} = \frac{AB - (AA + BB)}{AA + AB + BB} \qquad \textbf{Equation 1-1}$$

If only product AB could form, then the cage effect would be 100 %. If random radical coupling occurs (due to escape of the radical pair), as in solution, then there in no cage effect. Scheme 1.1 illustrates the photochemical reaction

pathway of an unsymmetrical aryl alkyl ketone, in this case partially deuterated dibenzyl ketone, d_5 - DBK, in a confining environment.

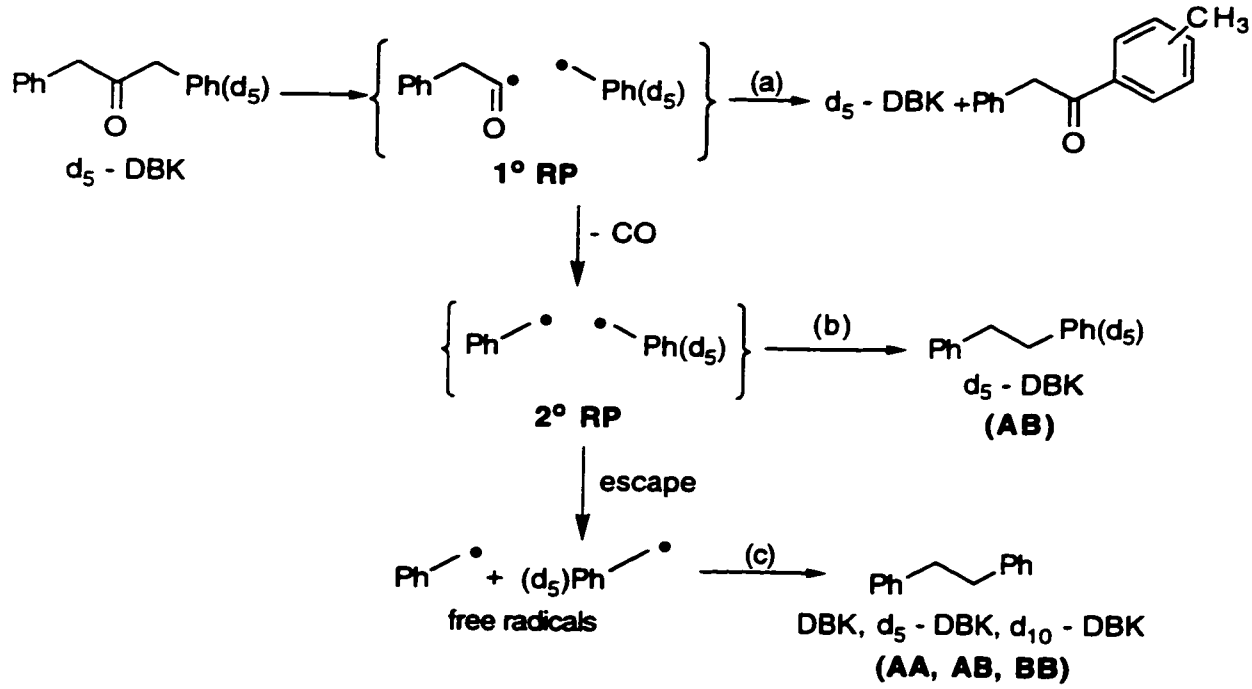

Scheme 1-1: Photolysis of d_5 - DBK in a constrained medium

For inclusion of d_5 - DBK in NaX, it was determined that the cage effect was dependent upon the guest loading in the zeolite.[74] Both low and high loadings of d_5 - DBK were used (<S> ranged from 0.1 to 1), with very different product distributions occurring for each case. As shown in Scheme 1.1, α-cleavage from the triplet state produces the primary radical pair (1° RP). This primary radical pair may undergo recombination, forming isomeric products of d_5 - DBK or recovered d_5 - DBK [path (a)]. Alternately, the primary radical pair may decarbonylate prior to recombination, forming the secondary radical pair (2° RP) which may recombine

to give the cage effect product, DPE (diphenylethane) geminate [path (b)], or escape and randomize in the global space to give random DPE products [path (c)].

For low loadings of d_5 - DBK in NaX, it was found that there were low yields of rearranged products [path (a)], high yields of diphenylethanes but a low cage effect. This is rationalized in terms that the formation of the 1° RP (consisting of benzyl radical and phenylacetyl radical) would result in the benzyl radical exploring more of the zeolite environment, while the phenylacetyl radical would remain closer to the reaction site. This is based on the expectation that the benzyl radical is more likely to diffuse at a faster rate than the phenylacetyl radical, due to their differences in polarity and size. It was estimated that the benzyl radical, during the time that decarbonylation occurs (~ 100 ns)[75] can explore up to 25 supercages. Therefore, the probability of the radical returning to the geminate site within 100 ns should be very small when there is free molecular traffic (less congestion). This leads to a large amount of DPE formed randomly, resulting in the low cage effect.

A high loading of d_5 - DBK in NaX, on the other hand, produced very different results upon irradiation. In this case, high yields of rearranged products were detected, with low yields of DPE but a large cage effect. This is explained in terms of the decrease in the number of escape routes and space available to the primary radical pair, due to the congestion in the cages. This results in a greater chance for the primary radical pair to intersystem cross and recombine before decarbonylation, resulting in high yields of rearranged products, and a low yield of DPE. The DPE that does form, however, occurs because of geminate coupling of the secondary radical pair, which is indicated by the large cage effect. These

processes are summarized in Scheme 1.2. This particular example of DBK in NaX illustrates nicely the concept of molecular traffic control introduced in an earlier section, and the consequences on the outcome of the product distribution.

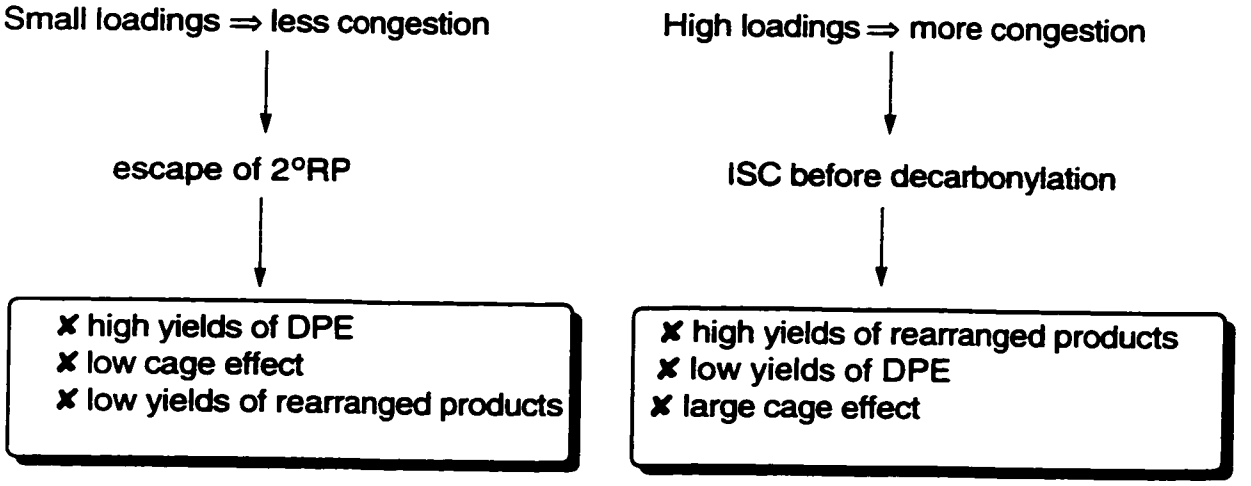

Scheme 1-2: Summary of processes that occur upon photolysis of low and high loadings of d_5 - DBK in NaX.

Ortho- and para-substituted DBK (designated as o-ACOB and p-ACOB, respectively) were used in the study of DBK photolysis using zeolite ZSM-5.[1] Because of size restraints, only p-ACOB is expected to be located on the internal surface, whereas o-ACOB is larger than the channel opening and therefore remains on the external surface. Photolysis of the substituted DBK molecules results in the formation of oA• and •B on the external surface of ZSM-5, and pA• and •B in the interior of ZSM-5.

Irradiation of p-ACOB leads to pAB being the major product (the geminate coupling product), which is consistent with the 2° RP being in a tight fitting channel; therefore, diffusion is slow and coupling to form pAB is efficient. The cage effect in

this case approaches 100%. The photolysis of oACOB results in oAoA and BB being the major products. This is consistent with the idea that the •B radicals formed on the surface diffuse into the pores (into which oA cannot fit), faster than they combine with oA. Thus, BB formation occurs inside the zeolite channels and formation of oAoA occurs on the surface. In this case, the cage effect is -100% (no geminate coupling occurs). This is shown in Scheme 1.3.

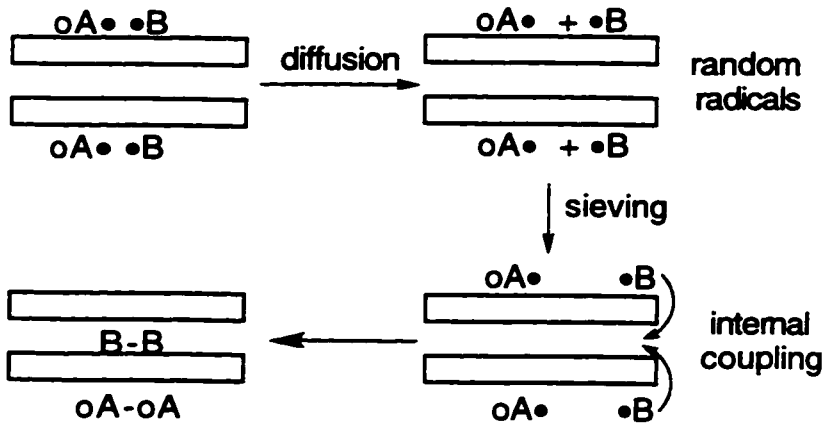

Scheme 1-3: Irradiation of o-ACOB on the external surface of ZSM-5

This example of pACOB and oACOB using ZSM-5 zeolites illustrates the remarkable shape selective ability of the zeolite in controlling photochemical reactions. This is also an example of molecular traffic control[61] since the chemical reactivity is controlled through the dynamics of molecular diffusion through the channel systems of zeolites.

1.3.2 Selective Photooxidations

Photooxidation reactions have been performed using O_2 as the oxidant in media such as O_2 gas, O_2 saturated solutions and solid O_2 matrices.[76] The limitation to this approach is that, due to the need to use UV light to induce the reaction, no product selectivity occurs. An alternative approach is to use zeolites as hosts for photooxidation reactions. The group of Frei has investigated such approaches, using small alkenes such as 2, 3-dimethyl-2-butene (DMB), and cis- and trans-2-butene, as well as cyclohexane in zeolite NaY.[77-80]

The results from these studies are striking. It was determined that the cyclohexane or alkene•O_2 charge-transfer (CT) states are highly stabilized in NaY, by > 10,000 cm^{-1} compared to the other media mentioned above. This is characterized by an absorption tail that extends out into the visible spectral region. For DMB, the absorption extends out to 750 nm and for 2-butene, the absorption extends out to 450 nm. This allows for the use of low energy visible photons instead of UV photons to access the excited state, resulting in a tightly controlled chemistry.

The significant degree of stabilization of the excited CT state is attributed to the electrostatic interactions inside the charged cages of NaY. After excitation, a large dipole moment develops across the cyclohexane•O_2 or alkene•O_2 system, due to the charge separation that occurs in the excited state. Depending upon the orientation of the charge-transfer complex, the electrostatic field of the cage (with a +1 charge on the Na^+ and a -1/8 partial charge on the framework oxygens)[81] can strongly stabilize the dipole moment that is generated. This stabilization (~2eV),

as previously mentioned, results in selective photooxidation. For cyclohexane, the sole products that are formed upon photooxidation in NaY are cyclohexyl hydroperoxide and cyclohexanone.[80] The hydroperoxide thermally rearranges to give cyclohexanone, with no side reactions. No byproducts, such as cyclohexanol, which forms in the liquid phase reaction, are observed. The processes that account for the loss of product selectivity in liquid phase oxidation reactions include the coupling of cyclohexyl peroxy radicals and secondary bimolecular chemistry of cyclohexyl hydroperoxide,[82] which do not occur in NaY due to the constraints imposed by the zeolite matrix. The selective oxidation of cyclohexane to the final product, cyclohexanone, in NaY was the first reported selective oxidation of this compound.[80] The mechanism for this reaction is given in Scheme 1.4.

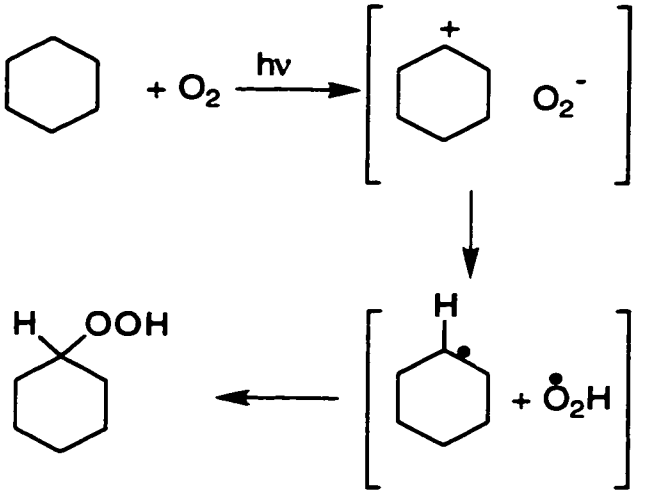

Scheme 1-4: Mechanism for the photooxidation of cyclohexane in NaY

The step following excitation is proton transfer from the cyclohexane radical cation to O_2^-. The cyclohexyl and hydroperoxy radical produced undergo cage recombination to yield cyclohexyl hydroperoxide.

For the alkene systems, photooxidation in NaY[77-79] results in the selective formation of the corresponding alkene hydroperoxide in each case, except for DMB which forms acetone as a small coproduct, which is attributed to the transient formation of dioxetane. The mechanism for the formation of the hydroperoxide is given in Scheme 1.5 for trans-2-butene.

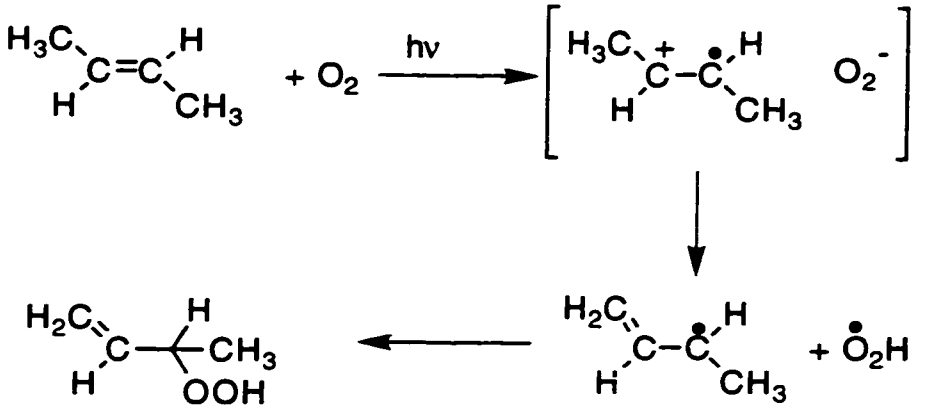

Scheme 1-5: Formation of peroxide upon irradiation of trans-2-butene in NaY

The proposed mechanism for the excited alkene•O_2 CT complex is deprotonation of the alkene to form an allyl radical and hydroperoxy radical. These radicals are expected to undergo cage recombination to generate the allylic hydroperoxide product.

Red-shifts of CT bands of other complexes included in zeolites have been reported, but the magnitude of the shift was much smaller. For example, studies

on aromatic-pyridinium (donor-acceptor complexes) in faujasite zeolites resulted in a red shift of the CT complex in the range of 10-30 nm.[83,84] For cyclohexane•O_2, the absorption onset in the O_2 -saturated liquid is 275 nm,[85] compared to 500 nm in NaY.

1.3.3 Photochemical Asymmetric Induction Reactions Using Zeolites as Hosts

In recent years, chirally modified zeolites have been used as hosts for photochemical reactions.[86-89] The purpose behind this type of host is to induce chirality in photochemical reactions conducted in its intracrystalline volume. The chirally-modified zeolites are made chiral by inclusion of an optically active inductor molecule in the cages; this inductor molecule may interact with the guest molecule throughout the course of the reaction by formation of hydrogen bonds. The first example of this was reported by Ramamurthy et al. in the Norrish Type II reaction of cyclohexyl ketones into the corresponding cyclobutanols, using NaY as the zeolite.[89] The reaction is shown in Sheme 1.6

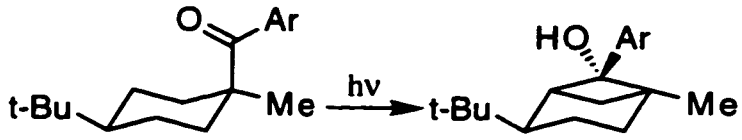

(a) Ar = Ph
(b) Ar = p-Ph-CN
(c) Ar = p-Ph-COOMe
(d) Ar = p-Ph-COOH

Scheme 1-6: Photolysis of cyclohexyl ketones in NaY, yielding chiral cyclobutanol products

Low to moderate %ee were obtained using this series of substrate molecules and chiral auxilliary inductors. The inductor that gave the highest %ee was (-)- ephedrine, at 25 - 30%. The use of (+)-ephedrine gave the optical antipode of the product produced by using (-)-ephedrine. It was found that the supercage free volume plays[90] a role in determining the extent of the enantioselectivity that occurs in chiral zeolite medium. A tight fit between the guest molecule and the chiral inductor molecule is crucial in optimizing the degree of enantioselectivity. Moreover, the loading of the inductor molecule must be at least one per supercage to also optimize the %ee.[89]

Other reactions besides the Norrish Type II have been investigated for the purpose of inducing chirality in the photoproduct.[87,88] This includes photoelectrocyclization within zeolite Y of tropolone methyl ether.[87] As seen in Scheme 1.7, irradiation of tropolone methyl ether results in 4π-disrotatory electrocyclic ring closure to yield the bicyclic product.

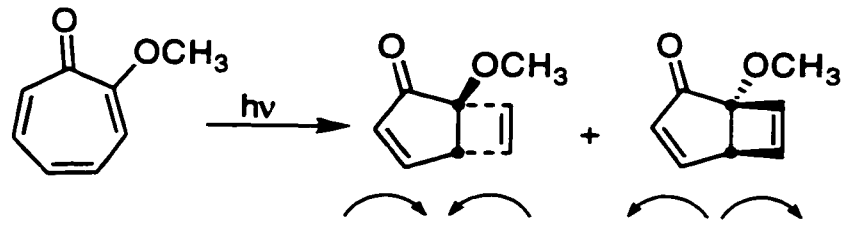

Scheme 1-7: Irradiation of tropolone methyl ether in zeolite Y

Adsorption of the ether in a chirally modified zeolite may result in preferential adsorption from one of the two enantiotopic faces, ultimately forming the

enantioselective product, rather than the racemic mixture that occurs in solution. Formation of the enantioselective product would occur due to hindering of one of the two modes of rotation of tropolone methyl ether by the zeolite. Generally, it was found that chiral inductor molecules that contain two functional groups yielded better %ee compared to inductors that contained only one functional group. The %ee ranged from <1 to 40%. The complete favouring of adsorption of one enantiotopic face over another did not occur, since 100% enantioselectivity was not achieved. However, the results presented do indicate the possible use of chirally modified zeolites as effective hosts for influencing chirality in photochemical reactions, especially when these reactions fail to produce any chirality in solution. Again, the constricted environment of the zeolite host has a significant influence on the outcome of photochemical reactions. Examples of chirally modified zeolites as hosts are given in Chapter 8.

1.3.4 Charge-Transfer and Electron Transfer (et) Reactions in Zeolites

Charge-transfer reactions within zeolite pores have been extensively studied by Kochi et al.[83,91-93] The rigid orientation and constraint imposed by the zeolite framework, as well as its highly electrostatic interior make it an interesting solid state host for these types of reactions.

Photolysis of CT complexes leads to an ion pair which can either collapse to yield the starting material or react further to form products.[94,95] The CT complexes studied included pyridinium acceptors and arene donors.[91,92] The use of cationic acceptor molecules was advantageous, since it allowed for easy

incorporation into zeolite Y by ion exchange, and the acceptors did not leach out during the subsequent inclusion of the arene donors in organic solvents. Excitation of the CT complexes led to transient radical ion pairs that could be monitored using time-resolved diffuse reflectance techniques. In general, it was found that the lifetimes of the ion pairs in zeolite cavities were much longer (μs) than those measured in organic solvents (ps). This suggests the increased stabilization of the ion pairs in the zeolite (as seen in a previous section), and suggests the potential that the zeolite has in controlling the energy-wasting back electron transfer step. This may originate from steric effects of the zeolite cages, as well as to the Coulombic interactions between the positively charged transients and the negatively charged zeolite framework (since positively charged acceptor molecules were used, no negatively charged transients were formed upon the electron transfer process). The decay kinetics measured for the transient were complex. It was suggested that the complex kinetics occurred due to the interaction of the transient with the framework, which acts as the solvent in controlling the radical ion distance. Thus, short lived species result from the ion pairs being close together (similar to contact radical ion pairs in solution) and the longer lived species are due to the electron transfer partners moving further and further apart, undergoing favourable interactions with the zeolite framework. Thus, different distances between the ion pairs can be obtained, resulting in complex decay kinetics.

Based on the results of stabilization of CT complexes in zeolites, it is likely that the confined space of the zeolite pores should provide an ideal environment

for performing photosensitized et reactions.[96-98] This is especially true if zeolite confinement can overcome the limitation of back et. The example chosen to illustrate photosensitized et in zeolite cavities involves singlet sensitized processes, using a series of both neutral and positively charged cyanoaromatic sensitizers, and arylalkene donors in zeolite NaX.

It was found that the selectively excited sensitizers decayed by two pathways: et from the aryl alkene donor to give a radical ion pair, and through photoionization to give a trapped electron. These two processes are summarized below, where D is the donor molecule and A is the acceptor molecule:

$$D + A \xrightarrow{h\nu} D^{\bullet+} + A^{\bullet-}$$

$$A \xrightarrow{h\nu} A^{\bullet+} + e^{-} \xrightarrow{4\,Na^{+}} Na_4^{3+}$$

The electron that is released by the acceptor molecule is trapped by the charge-balancing cations of the zeolite, yielding cationic clusters, in this case sodium cationic clusters. These clusters have been characterized spectroscopically through γ-irradiation of zeolites.[99-103]

The long lifetimes and the strong aryl alkene radical cation signals generated indicate that the energy wasting back electron transfer step is several orders of magnitude slower in the zeolite medium than for the same radical ion pairs in solution.[104] This illustrates the ability of zeolites to stabilize radical ion pairs and overcome the limitation of back et.

Product studies of the radical cation initiated dimerization were also performed with the series of aryl alkene donors. This was done to establish the

effect of the zeolite cavity on the geometry of the product dimers. In general, it was found that the zeolite supercage favours a product that has a spherical shape, rather than an elongated shape, resulting in more of the cis/syn dimers being preferred over the trans/anti dimers.

1.4 Concluding Remarks

It is clear from this brief overview that zeolite materials offer the chemist a variety of versatile hosts to employ in supramolecular photochemical reactions. Selected examples from the literature depicted how photochemistry of guest molecules is modified within zeolite pores, which is often different compared to solution irradiations. This occurs through the unique characteristics inherent to zeolites that are not present in homogeneous media. These examples were chosen to highlight the results presented within the following chapters where other examples of zeolite modified photochemistry are given.

The objectives of this thesis were to investigate even further how photochemistry inside zeolite pores can be modified simply by inclusion of guest molecules. This modification can lead to unique pathways that are not available in solution. This thesis explores the factors that result in the different photochemical processes to be observed. This aquired knowledge is used in the development of new applications of zeolite materials.

The use of zeolites in photochemical reactions is still a fairly new field. Thus, a better understanding of the influence of the intrazeolite environment on

certain probe molecules is essential, since it allows the chemist to use these factors to design reaction in intrazeolite cavities that are unique to this medium.

1.5 References

(1) Turro, N. J. *Pure Appl. Chem.* **1986**, *58*, 1219.

(2) Weisz, P. B.; Frilette, V. J.; Mastman, R. W.; Mower, E. B. *J. Catal.* **1962**, *1*, 307.

(3) Weitkamp, J. In *Catalysis and Absorption by Zeolites*; G. Ohlmann, Ed.; Elsevier Science Publishers: Amsterdam, 1991; pp 21.

(4) Wada, Y.; Yoshizawa, Y.; Morikawa, A. *Chem. Commun.* **1990**, 319.

(5) Chen, N. Y.; Garwood, W. E.; Dwyer, F. G. *Shape Selective Catalysis in Industrial Applications*; Marcel Dekker: New York, 1989.

(6) Davis, M. E. *Acc. Chem. Res.* **1993**, *26*, 111.

(7) Casal, H. L.; Scaiano, J. C. *Can. J. Chem.* **1984**, *62*, 628.

(8) Casal, H. L.; Scaiano, J. C. *Can. J. Chem.* **1985**, *63*, 1308.

(9) *Photochemistry in Organized and Constrained Media*; Ramamurthy, V., Ed.; VCH Publishers: New York, 1991.

(10) Breck, D. W. *Zeolite Molecular Sieves: Structure, Chemistry and Use*; John Wiley and Sons: New York, 1974.

(11) Dyer, A. *An Introduction to Zeolite Molecular Sieves*; John Wiley and Sons: Chischester, 1988.

(12) Meier, W. M.; Olson, D. H. *Atlas of Zeolite Structure Types*; Butterworths: London, 1992.

(13) Suib, S. L. *Chem. Rev.* **1993**, *93*, 803.

(14) van Bekkum, H.; Flanigen, E. M.; Jansen, J. C. *Introduction to Zeolite Science and Practice*; Elsevier: Amsterdam, 1991.

(15) Ramamurthy, V. In *Surface Photochemistry*; M. Anpo, Ed.1996; pp 65.

(16) Davis, M. E.; Saldarriaga, C.; Montes, C.; Garces, J.; Crowder, C. *Nature* **1988**, *331*, 698.

(17) Wilson, S. T.; Lok, B. M.; Messina, C. A.; Cannon, T. R.; Flanigen, E. M. *J. Am. Chem. Soc.* **1982**, *104*, 1146.

(18) Estermann, M.; McCusker, L. B.; Baerlocher, C.; Merrouche, A.; Kessler, H. *Nature* **1991**, *352*, 320.

(19) Beck, J. S.; Vartuli, J. C.; Roth, W. J.; Leonowicz, M. E.; Kresge, C. T.; Schmitt, K. D.; Chu, C. T. W.; Olson, D. H.; Sheppard, E. W.; McCullen, S. B.; Higgins, J. B.; Schlenker, J. L. *J. Am. Chem. Soc.* **1992**, *114*, 10834.

(20) Behrens, P.; Stucky, G. D. *Angew. Chem. Int. Ed. Engl.* **1993**, *32*, 696.

(21) Ramamurthy, V.; Turro, N. J. *J. Incl. Phenom. and Mol. Recogn. Chem.* **1995**, *21*, 239.

(22) Herron, N.; Corbin, D. R. *Inclusion Chemistry with Zeolites: Nanosecond Materials by Design*; Kluwer Academic Publishers: Boston, 1995; Vol. 6.

(23) Ramamurthy, V.; Eaton, D. F.; Caspar, J. V. *Acc. Chem. Res.* **1992**, *25*, 299.

(24) Scaiano, J. C.; García, H. *Acc. Chem. Res.* **1999**, *accepted*,

(25) Thomas, J. K. *Chem. Rev.* **1993**, *93*, 301.

(26) Fyfe, C. A.; Gies, H.; Kokotailo, G. T.; Pasztor, C.; Strobl, H.; Cox, D. E. *J. Am. Chem. Soc.* **1989**, *111*, 2470.

(27) Corbin, D. R.; Abrams, L.; Jones, G. A.; Eddy, M. M.; Harrison, W. T. A.; Stucky, G. D.; Cox, D. E. *J. Am. Chem. Soc.* **1990**, *112*, 4821.

(28) Sun, T.; Seff, K. *J. Phys. Chem.* **1993**, *97*, 5213.

(29) Müller, J. A.; Conner, W. C. *J. Phys. Chem.* **1993**, *97*, 1451.

(30) Klein, H.; Kirschhock, C.; Fuess, H. *J. Phys. Chem.* **1994**, *98*, 12345.

(31) Hoppe, R.; Schulz-Ekloff, G.; Woehrle, D.; Kirschhock, C.; Fuess, H. *Langmuir* **1994**, *10*, 1517.

(32) Cozens, F. L.; Régimbald, M.; García, H.; Scaiano, J. C. *J. Phys. Chem.* **1996**, *100*, 18165.

(33) Corma, A.; García, H.; Iborra, S.; Primo, J. *J. Catal.* **1989**, *120*, 78.

(34) Corma, A.; Fornes, V.; Rey, F. *Appl. Cat.* **1990**, *59*, 267.

(35) Ashton, A. G.; Batmanian, S.; Clark, D. M.; Dwyer, J.; Fitch, F. R.; Hinchliffe, A.; Machado, F. J. *Catalysis by Acids and Bases*; Elsevier: Amsterdam, 1985, pp 101.

(36) Pellet, R. J.; Blackwell, C. S.; Rabo, J. A. *J. Catal.* **1988**, *114*, 71.

(37) Bayerlein, R. A.; McVicker, G. B.; Yacullo, L. N.; Ziemak, J. J. *J. Phys. Chem.* **1988**, *92*, 1967.

(38) Herron, N. *Inorg. Chem.* **1986**, *25*, 4714.

(39) Cano, M. L.; Corma, A.; Fornés, V.; García, H.; Miranda, M. A.; Baerlocher, C.; Lengauer, C. *J. Am. Chem. Soc.* **1996**, *118*, 11006.

(40) Zhang, Z.; Turro, N. J.; Johnston, L.; Ramamurthy, V. *Tet. Lett.* **1996**, *37*, 4861.

(41) Dubin, M. M.; Isirikyan, A. A.; Rakhmatkariev, G. U.; Serpinskii, V. V. *Bull. Acad. USSR. Chem. Div.* **1973**, *4*, 900.

(42) Turro, N. J. *Modern Molecular Photochemistry*; Benjamin/Cummings Publishing Co.: Menlo Park, 1978, pp 628.

(43) Ramamurthy, V.; Sanderson, D. R.; Eaton, D. F. *J. Am. Chem. Soc.* **1993**, *115*, 10438.

(44) Ehrl, M.; Kinervater, H. W.; Deeg, F. W.; Bräuchle, C. *J. Phys. Chem.* **1994**, *98*, 11756.

(45) Ahn, S. W.; Kevan, L. *J. Chem. Soc. Faraday Trans.* **1998**, *94*, 3147.

(46) Bauer, R. K.; Borenstein, R.; de Mayo, P.; Okada, K.; Rafalska, M.; Ware, W. R.; Wu, K. C. *J. Am. Chem. Soc.* **1982**, *104*, 4635.

(47) Hasegawa, T.; Imida, M. *J. Phys. Org. Chem.* **1993**, *6*, 494.

(48) Lednev, I. K.; Mathivanan, N.; Johnston, L. J. *J. Phys. Chem.* **1994**, *98*, 11444.

(49) Ruetten, S. A.; Thomas, J. K. *J. Phys. Chem. B.* **1999**, *103*, 1278.

(50) Wilkinson, F.; Worrall, D. R.; Williams, S. L. *J. Phys. Chem.* **1995**, *99*, 6689.

(51) Climent, M. J.; Corma, A.; García, H.; Miranda, M. A.; Primo, J. *J. Photochem. Photobiol. A:Chem.* **1991**, *59*, 379.

(52) Cozens, F. L.; Gessner, F.; Scaiano, J. C. *Langmuir* **1993**, *9*, 874.

(53) Endo, T.; Nakada, N.; Sato, T.; Shimada, M. *J. Phys. Chem. Solids* **1988**, *12*, 1423.

(54) Liu, X.; Iu, K. K.; Thomas, J. K. *Langmuir* **1992**, *8*, 539.

(55) Mao, Y.; Thomas, J. K. *J. Org. Chem.* **1993**, *58*, 6641.

(56) Thomas, J. K. *Acc. Chem. Res.* **1988**, *21*, 275.

(57) Barrer, R. M. *Zeolites and Clay Minerals as Sorbents and Molecular Sieves*; Academic Press: London, 1978.

(58) Odom, I. E. *Phil. Trans. R. Soc. Lond. A* **1984**, *311*, 391.

(59) Weiss, R. G.; Ramamurthy, V.; Hammond, G. S. *Acc. Chem. Res.* **1993**, *26*, 530.

(60) *A Molecular View of Heterogeneous Catalysis*; Derouane, E. G., Ed.; De Boeck & Larcier: Paris, 1998.

(61) Derouane, E. G.; Gabelica, Z. *J. Catal.* **1980**, *65*, 486.

(62) Ramamurthy, V.; Corbin, D. R.; Eaton, D. F.; Turro, N. J. *Tet. Lett.* **1989**, *30*, 5833.

(63) Ramamurthy, V.; Corbin, D. R.; Turro, N. J.; Sato, Y. *Tet. Lett.* **1989**, *30*, 5829.

(64) Ramamurthy, V.; Caspar, J. V.; Corbin, D. R. *Tet. Lett.* **1990**, *31*, 1097.

(65) Engel, P. S. *J. Am. Chem. Soc.* **1970**, *92*, 6074.

(66) Turro, N. J. *Proc. Natl. Acad. Sci.* **1983**, *80*, 609.

(67) Turro, N. J.; Zimmt, M. B.; Gould, I. R. *J. Phys. Chem.* **1988**, *92*, 433.

(68) Wintgens, V.; Scaiano, J. C. *Can. J. Chem.* **1987**, *65*, 2131.

(69) Rao, V. P.; Zimmt, M. B.; Turro, N. J. *J. Photochem. Photobiol. A: Chem.* **1991**, *60*, 355.

(70) Turro, N. J.; Cheng, C.-C.; Lei, X.-G.; Flanigen, E. M. *J. Am. Chem. Soc.* **1985**, *107*, 3739.

(71) Turro, N. J.; Zhang, Z. *Tet. Lett.* **1987**, *28*, 5637.

(72) Garcia-Garibay, M. A.; Lei, X. G.; Turro, N. J. *J. Am. Chem. Soc.* **1992**, *114*, 2749.

(73) Garcia-Garibay, M. A.; Ottaviani, M. F.; Turro, N. J. *Mol. Cryst. Liq. Cryst.* **1992**, *211*, 199.

(74) García-Garibay, M. A.; Zhang, Z.; Turro, N. J. *J. Am. Chem. Soc.* **1991**, *113*, 6212.

(75) Turro, N. J.; Gould, I. R.; Baretz, B. H. *J. Phys. Chem.* **1983**, *87*, 531.

(76) Hashimoto, S.; Akimoto, H. *J. Phys. Chem.* **1986**, *90*, 529.

(77) Blatter, F.; Frei, H. *J. Am. Chem. Soc.* **1993**, *115*, 7501.

(78) Blatter, F.; Moreau, F.; Frei, H. *J. Phys. Chem.* **1994**, *98*, 13403.

(79) Blatter, F.; Frei, H. *J. Am. Chem. Soc.* **1994**, *116*, 1812.

(80) Sun, H.; Blatter, F.; Frei, H. *J. Am. Chem. Soc.* **1996**, *118*, 6873.

(81) Bezus, A. G.; Kiselev, A. V.; Lopatkin, A. A.; Du, P. Q. *J. Chem. Soc. Faraday Trans. 2* **1978**, *74*, 367.

(82) Tolman, C. A.; Druliner, J. D.; Nappa, M. J.; Herron, N. *Activation and Functionalization of Alkanes*; Wiley: New York, 1989.

(83) Yoon, K. B.; Kochi, J. K. *J. Phys. Chem.* **1991**, *95*, 3780.

(84) Sankararaman, S.; Yoon, K. B.; Yabe, T.; Kochi, J. K. *J. Am. Chem. Soc.* **1991**, *113*, 1419.

(85) Scurlock, R. D.; Ogilby, P. R. *J. Phys. Chem.* **1989**, *93*, 5493.

(86) Joy, A.; Robbins, R. J.; Pitchumani, K.; Ramamurthy, V. *Tet. Lett.* **1997**, *38*, 8825.

(87) Joy, A.; Scheffer, J. R.; Corbin, D. R.; Ramamurthy, V. *Chem. Commun.* **1998**, 1379.

(88) Kaprinidis, N. A.; Landis, M. S.; Turro, N. J. *Tet. Lett.* **1997**, *38*, 2609.

(89) Leibovitch, M.; Olovsson, G.; Sundarababu, G.; Ramamurthy, V.; Scheffer, J. R.; Trotter, J. *J. Am. Chem. Soc.* **1996**, *118*, 1219.

(90) Sundarababu, G.; Leibovitch, M.; Corbin, D. R.; Scheffer, J. R.; Ramamurthy, V. *Chem. Commun.* **1996**, 2159.

(91) Yoon, B. Y. *Chem. Rev.* **1993**, *93*, 321.

(92) Yoon, K. B.; Hubig, S. M.; Kochi, J. K. *J. Phys. Chem.* **1994**, *98*, 3865.

(93) Yoon, K. B.; Huh, T. J.; Kochi, J. K. *J. Phys. Chem.* **1995**, *99*, 7042.

(94) Gould, I. R.; Young, R. H.; Moody, R. E.; Farid, S. *J. Phys. Chem.* **1991**, *95*, 2068.

(95) Gould, I. R.; Ege, D.; Moser, J. E.; Farid, S. *J. Am. Chem. Soc.* **1990**, *112*, 4290.

(96) Corma, A.; Fornes, V.; Garcia, H.; Miranda, M. A.; Primo, J.; Sabater, M. J. *J. Am. Chem. Soc.* **1994**, *116*, 2276.

(97) Sanjuán, A.; Alvaro, M.; Aguirre, G.; García, H.; Scaiano, J. C. *J. Am. Chem. Soc.* **1998**, *120*, 7351.

(98) Yoon, K. B.; Park, Y. S.; Kochi, J. K. *J. Am. Chem. Soc.* **1996**, *118*, 12710.

(99) Iu, K.; Liu, X.; Thomas, J. K. *J. Phys. Chem.* **1993**, *97*, 8165.

(100) Liu, X.; Iu, K.; Thomas, J. K. *J. Phys. Chem.* **1994**, *98*, 13720.

(101) Liu, X.; Zhang, G.; Thomas, J. K. *J. Phys. Chem.* **1995**, *99*, 10024.

(102) Liu, X.; Thomas, J. K. *J. Chem. Soc. Faraday Trans.* **1995**, *91*, 759.

(103) Zhang, G.; Liu, X.; Thomas, J. K. *Radiat. Phys. Chem.* **1998**, *51*, 135.

(104) Gould, I. R.; Ege, D.; Mattes, S. L.; Farid, S. *J. Am. Chem. Soc.* **1987**, *109*, 3794.

2. Diffuse Reflectance Laser Flash Photolysis

2.1 Overview of Laser Flash Photolysis

Early work on the technique of laser flash photolysis (LFP), which is used to examine transients formed upon laser excitation of a suitable precursor, was reported by the groups of Kosonocky,[1] Lindqvist[2] and Porter.[3] Though several groups were designing similar systems, the system in use today is similar in architecture to the one reported by Lindqvist in 1966. This LFP system was originally developed for transparent samples, and is invaluable for mechanistic and kinetic studies of organic reactions. The development of picosecond and femtosecond pulsed lasers has dramatically increased the number of processes that can be studied.

The increasing interest in studying the photochemical properties of heterogeneous systems, many of which are opaque, has led to a modification of the setup of LFP for transmission studies in order to accommodate these opaque samples. Subjecting opaque samples to LFP requires diffuse reflected light instead of transmitted light as the analyzing source. This has led to the technique known as diffuse-reflectance laser flash photolysis (DR LFP), developed mainly by the Wilkinson group.[4-7]

The advent of DR LFP has allowed for the observation of transient spectra and decay kinetics for a variety of opaque materials such as semiconductor powders,[8] dyes bound to polymers[9] and zeolites.[6]

This chapter examines the technique of DR LFP along with the manner in which decay kinetics are interpreted for heterogeneous systems such as zeolites.

2.2 Principles of Diffuse Reflectance

Reflectance from opaque surfaces contains two components: specular reflection and diffuse reflectance. Diffusely reflected light, unlike specularly reflected light, is unpolarized and symmetrically distributed, regardless of the angle of incidence or polarization of the incident beam. Diffusely reflected light is a result of light that has penetrated below the surface, ultimately returning to the surface through multiple scattering events with individual particles making up the sample, and being attenuated by absorption within the particles. For fine powders, much of the reflected light is diffuse. Specularly or normal type reflection is a result of light that has bounced off the sample surface. This type of reflection occurs at an angle that is equal to the angle of the incident beam with respect to the surface normal. The detection of this type of reflection is avoided in the DR LFP setup.

The approach that is used to describe the interaction of light with opaque samples is the Kubelka-Munk approach:[10]

$$F(R) = \frac{K}{S} = \frac{(1-R)^2}{2R} \qquad \textbf{Equation 2-1}$$

where $K = 2\varepsilon C$, ε is the extinction coefficient, R and S are the reflecting and scattering coefficients, respectively, and C is the concentration. When looking at

small to moderate changes in reflectance, as occurs with the zeolite samples used for this thesis, the Kubelka-Munk function is linear with concentration. Under these conditions, Equation 2.1 then simplifies to the transient concentration being proportional to $\Delta J/J$, where ΔJ is the change in reflectance after excitation and J is the pre-laser flash voltage level. This is used to calculate the change in reflectance values used for DR work.

2.3 Diffuse Reflectance LFP Setup

Laser flash photolysis uses a pulsed laser to generate excited states or transients from an appropriate precursor and a monitoring light source in order to analyze the absorption of the transient. Typically, the laser pulse duration must be shorter than the processes being monitored and of high enough intensity to generate a detectable amount of transient. The setup can be thought of as a fast spectrophotometer, using a laser as the excitation source. A detailed account of the technique is given by Wilkinson.[11]

As mentioned in the previous section, diffusely reflected light from the sample is analyzed when examining opaque samples such as zeolites. The diffuse reflected light from the sample is measured by the photomultiplier tube (PMT) detector as a function of time in order to extract spectral and kinetic information.

There are a variety of lasers available at the University of Ottawa laser lab that cover wavelengths ranging from 248 nm to 1064 nm. The laser wavelengths used in this study are the 308 nm EX 530 Lumonics excimer laser and the 355 nm

Surelite Nd:YAG laser with pulse durations typically ≤ 10 ns and energies of < 100 and 30 mJ, respectively. The laser pulses were directed towards and concentrated on the sample at 90°C with respect to the monitoring beam, using a series of prisms and lenses. The experimental setup of a DR LFP is shown in Figure 2.1. The lasers are usually operated at 1 Hz and shutters control exposure of the sample to either the monitoring or laser light sources.

Solid powder zeolite samples to be studied by DR LFP were placed in a 3 x 7 mm^2 Suprasil quartz cell, which were either degassed with nitrogen or sealed under vacuum. To avoid product buildup or sample depletion, the sample is moved after every laser shot.

The monitoring / detection system consists of a pulsed 75 Watt xenon lamp, a high intensity monochromator and a PMT detector operating on six dynodes. The monochromator / PMT is located at an angle in between the laser and monitoring beams, to maximize the collection of DR light and minimize specular reflectance pick up. The monitoring beam is pulsed so that the intensity of the beam is increased by a factor of 5 - 20 during a few ms.

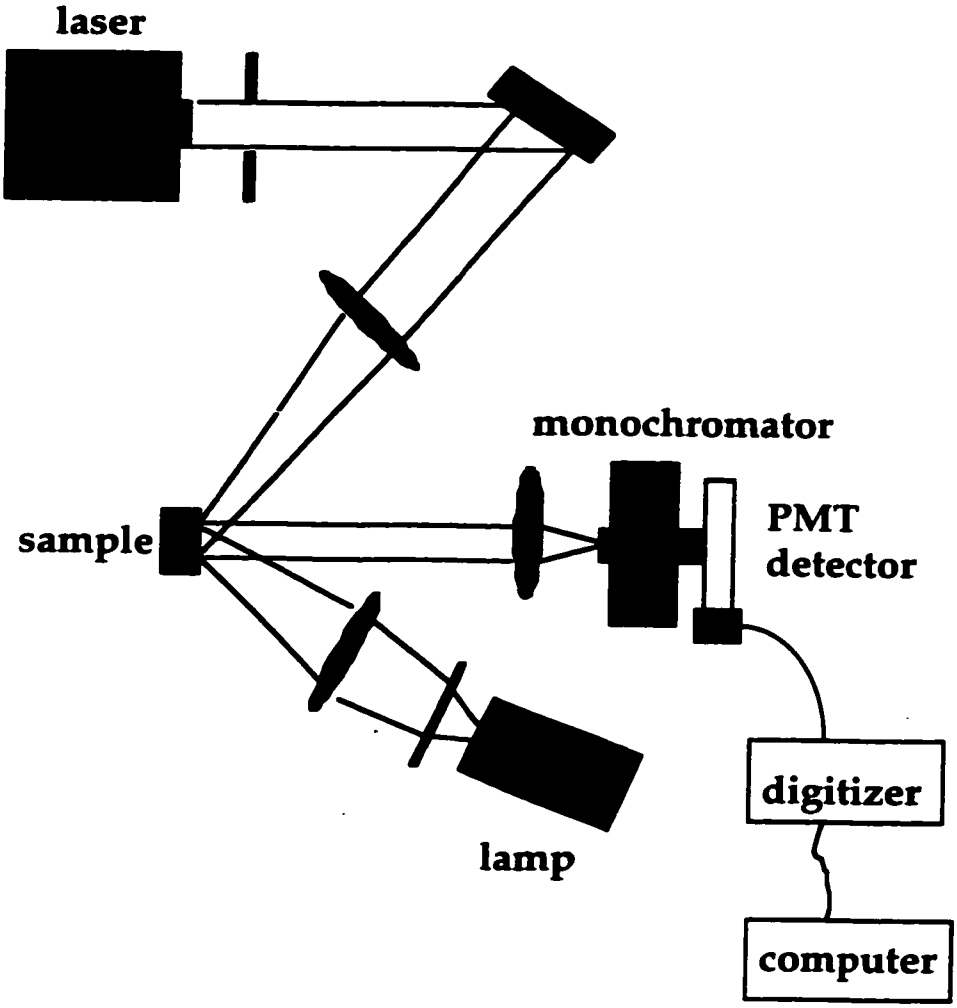

Figure 2-1: Diagram showing the setup for a diffuse reflectance laser flash photolysis system.

This enhances the signal to noise ratio which is especially important for studying short-lived transients (< 100 ns) or small signals. The monitoring beam is focussed onto the sample, and into the monochromator which selects the wavelength of light to be monitored. It is important to ensure that the analyzing light is only reflected from the area of the surface which has been excited by the laser beam. Any specular type reflection of the laser pulse from the quartz cell

must not reach the entrance slit of the analyzing monochromator. This is accomplished by positioning the monochromator as shown in Figure 2.1 and by using weakly absorbing materials. The selected wavelengths of light are detected by the PMT detector located at the exit slit of the monochromator. This yields a current which is terminated into an appropriate load resistor (typically 93 Ohms) giving a voltage signal. This signal, which changes with time is captured by a Tektronix 2440 digital storage oscilloscope equipped with pre-trigger capabilities which is interfaced to a Macintosh computer that controls the experiment with software developed in the LabVIEW 3.1 environment from National Instruments. A line synchronizer coordinates the various components of the LFP system including the lasers, lamp pulser and shutters through a series of transistor-transistor linked (TTL) pulses that originate at the same point on a 60 Hz AC sine wave so that proper time sequences of events are maintained.

Figure 2.2 shows a plot of PMT output versus time for a period from one second before to one second after a particular laser pulse. At the beginning of the experiment, light from the monitoring beam is recorded before it is pulsed which causes a sharp increase in the PMT output. The laser then fires and subsequently strikes a fiber optic cable which triggers the transient digitizer to start saving data points. The signal that results is shown in the small box in the figure. The intensity of the monitoring beam, J, is measured on a second channel and represents the baseline from which changes in PMT voltage are measured.

A kinetic trace is obtained by averaging the data collected from multiple laser shots. The $\Delta J/J$ is then plotted against time to provide a kinetic decay trace.

Transient absorption spectra are acquired by obtaining kinetic traces at several wavelengths and plotting $\Delta J/J$ of each kinetic trace against wavelength. For signals at different wavelengths to be comparable, the intensity of the monitoring beam must be similar over the wavelength range measured. This is achieved by using a programmable power supply that can set the PMT output to any desirable level and maintain it throughout the experiment.

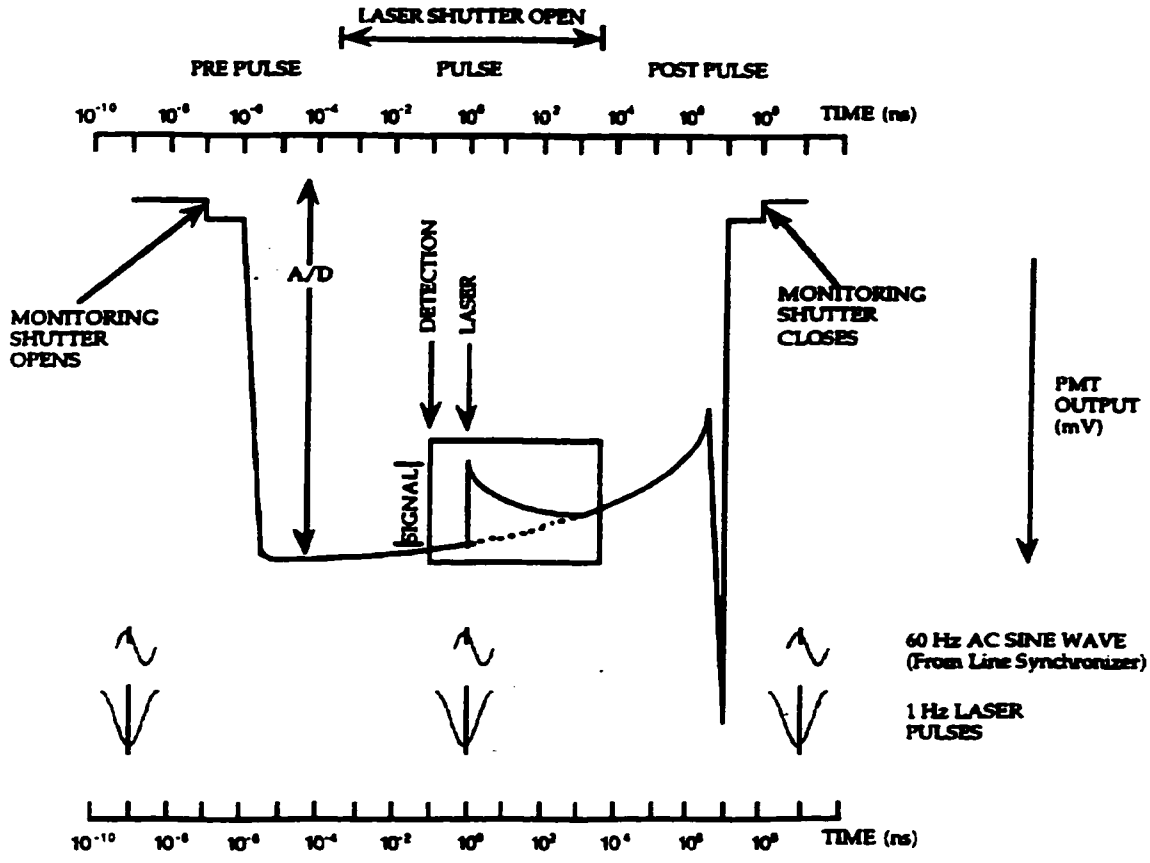

Figure 2-2: The sequence of timed events in the kinetic laser flash photolysis experiment.

2.4 Kinetic Treatment for Heterogeneous Systems

Analysis of kinetic data in heterogeneous systems such as zeolites is more difficult than in homogeneous media due to the location and distribution of the guest molecules in the cavities or channels of the zeolites. The nonhomogeneous distribution of guest molecules leads to decay traces which often do not fit well to single-exponential decay kinetics, especially if sufficiently long time periods are monitored. Lifetimes that are obtained using simple monoexponential or biexponential kinetics are frequently dependent upon the time scale used, with longer lifetimes recorded at longer time scales.[12] A more accurate way of handling the kinetics of guest molecules in zeolites that reflects the multiplicity of sites available is to employ a distribution analysis. The optimal method is to record decay traces in different instrumental time scales and subsequently combine them. This produces a composite decay with closely spaced data points at short times and larger values of point-to-point separation at the long time scales. This composite decay is then evaluated using a fitting function that contains 100 exponential terms, with fixed logarithmically spaced lifetimes from 10 ns to 10 ms and variable pre-exponentials. The fitting procedure gives rise to data which can be plotted as abundance vs. time (i.e., the distribution plot). The general outline for fitting kinetic traces is shown in Scheme 2.1.

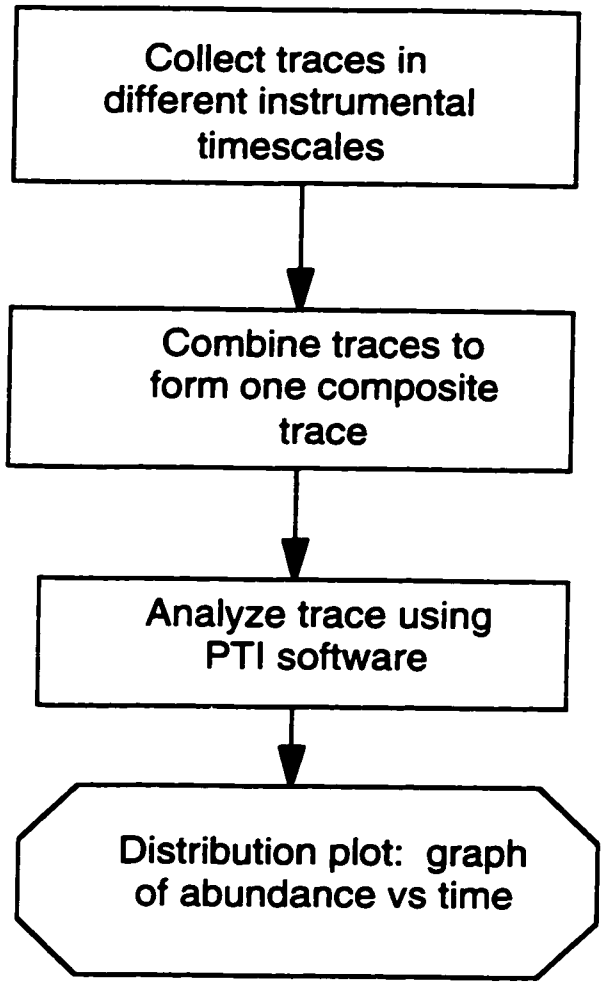

Scheme 2-1: Method of obtaining a distribution plot from kinetic decay traces for species in heterogeneous systems

A more detailed example of how a distribution analysis is determined is given below. For a sample of xanthone in NaY, a series of decay traces monitored at 600 nm were recorded using different instrumental time scales, in this case, 0.2, 0.5, 1 and 2 μs per division, with data collected for 20 divisions. Figure 2.3 shows the decay traces recorded at 0.2 and 2 μs. These decay traces are combined and plotted as $\Delta J/J$ vs log time, which is shown in Figure 2.4. The data

from this plot is read into the exponential series method (ESM) software from Photon Technology International (PTI) that has been customized to handle diffuse reflectance data. The trace is then fitted using a fitting function that consists of 100 exponential terms, rather than the one or two typically employed for true 1st order or 2nd order decay processes. The output of the fitting procedure can be plotted as abundance vs log time (see Figure 2.5). As illustrated in Figure 2.5, the sample of xanthone in NaY contains two distinct sites of xanthone. The first site contains a triplet lifetime distribution of 1.3 μs, which is twice as abundant as the other site, which has a longer lived triplet of 8.5 μs. It is clear that this method of distribution analysis gives a more accurate picture of the number of sites of the organic guest molecule within the zeolite, along with the transient lifetime. Determining a transient lifetime using only one kinetic trace does not reflect the inhomogeneity of the guest molecule location in the zeolite cavities.

A detailed kinetic analysis may not be desirable or necessary for all systems studied. In some cases, only a simple qualitative comparison in transient lifetimes is needed for a series of samples. When this occurs, the transient lifetime is calculated from a single decay trace, with the instrumental time scale of the decay kept constant for all samples. This is useful when an indication of how a transient lifetime is affected by changing certain parameters is required.

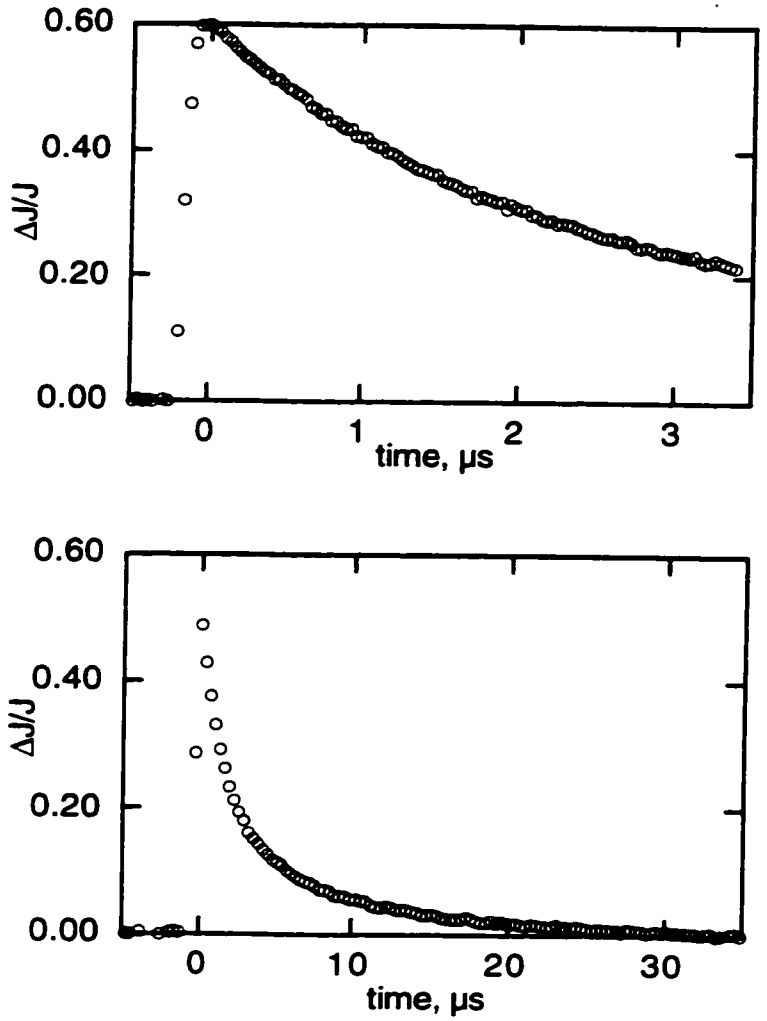

Figure 2-3: Kinetic decay traces of xanthone included in NaY, monitored at 600 nm using an excitation wavelength of 355 nm. Top trace was recorded using a 0.2 μs instrumental time scale, while the bottom trace was recorded using a 2 μs time scale.

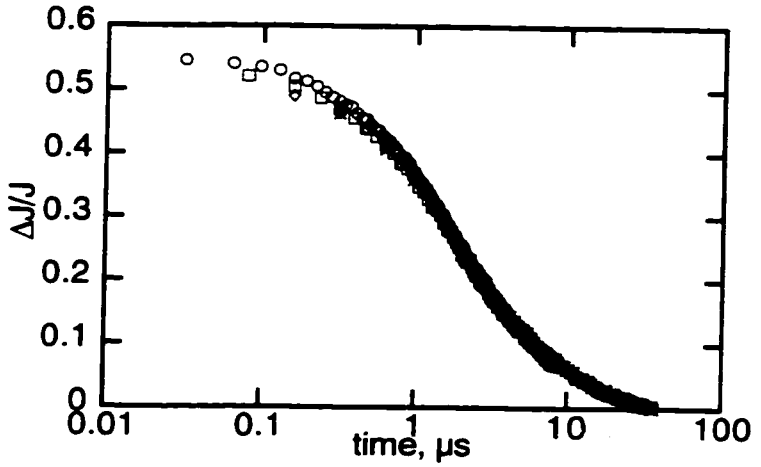

Figure 2-4: Composite decay trace of triplet xanthone included in NaY, using 0.2, 0.5, 1 and 2 μs instrumental time scales. Note the logarithmic scale used for the x-axis.

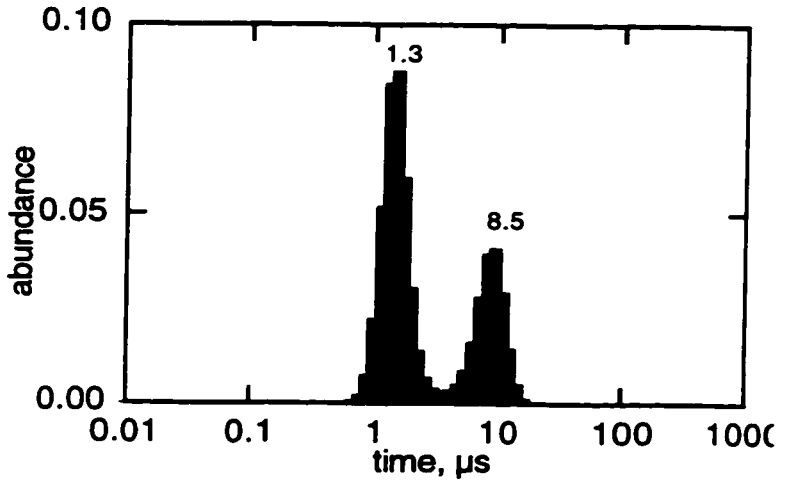

Figure 2-5: Triplet lifetime distribution analysis for xanthone included in NaY. Note the logarithmic scale used for the x-axis.

2.5 Experimental Section

The zeolite samples described in this section were prepared in a manner similar to that described in Chapter 1. Zeolite NaY (1 g) was activated at 550°C for 14 hours. This was added to a solution of hexane (~35 ml) containing xanthone (Aldrich product, recrystallized from ethanol, 5 mg). The mixture was stirred for 3 hours, filtered and was washed with fresh hexane. The zeolite complex was dried under vacuum (70 mTorr) and sealed.

2.6 References

(1) Kosonocky, W. F.; Harrison, S. E.; Stander, R. *J. Chem. Phys.* **1965**, *43*, 831.

(2) Lindqvist, L. *Hebd. Seances Acad. Sci., Ser. C* **1966**, *263*, 852.

(3) Porter, G. *Flash Photolysis and Primary Processes in the Excited State*; Almqvist and Wiksell: Stockholm, 1967, pp 141.

(4) Kessler, R. W.; Wilkinson, F. *J. Chem. Soc., Faraday Trans. 1* **1981**, *77*, 309.

(5) Wilkinson, F.; Willsher, C. J. *Appl. Spectrosc.* **1984**, *38*, 897901.

(6) Wilkinson, F.; Willsher, C. J.; Casal, H. L.; Johnston, L. J.; Scaiano, J. C. *Can. J. Chem.* **1986**, *64*, 539.

(7) Wilkinson, F.; McGarvey, D. J.; Worrall, D. R. *Proc. - Indian Acad. Sci., Chem. Sci.* **1992**, *104*, 739.

(8) Wilkinson, F.; Willsher, C. J.; Pouliquen, J.; Fichou, D.; Valet, P.; Kossanyi, J. *J. Photochem.* **1986**, *35*, 381.

(9) Wilkinson, F.; Willsher, C. J.; Pritchard, R. B. *Eur. Polym. J.* **1985**, *21*, 333.

(10) Kubelka, P. *J. Opt. Soc. Am.* **1948**, *38*, 448.

(11) Wilkinson, F.; Kelly, G. In *Handbook of Organic Photochemistry*; J. C. Scaiano, Ed.; CRC Press: Boca Raton, Florida, 1989; Vol. I; pp 293.

(12) Kelly, G.; Willsher, C. J.; Wilkinson, F.; Netto-Ferreira, J. C.; Olea, A.; Weir, D.; Johnston, L. J.; Scaiano, J. C. *Can. J. Chem.* **1990**, *68*, 812.

3. Role of Spectators on the Photobehaviour of Encapsulated Ketones in Faujasite Zeolite NaY

3.1 Introduction

The study of the transient spectroscopy of molecules included in zeolite pores is well established. These studies have provided a great deal of information about the behaviour of encapsulated molecules in a confined environment. Other work has focussed on the photoproducts that are obtained upon irradiating a substrate included in zeolite pores. These studies have demonstrated how the restricted zeolite environment influences the formation of products, which can often be different from those obtained in solution. Both transient spectroscopy and product studies have yielded important information on the influence of the zeolite interior on photophysical and photochemical properties of encapsulated organic molecules.

How do these properties change when an additional molecule is added to the pores of the zeolite? If a spectator molecule, which is defined as a molecule that does not participate directly in the photochemical reaction, is added to the zeolite cavities, can we 'tune' the photophysics and photochemistry of the included substrate molecule? To answer these questions, we use both transient spectroscopy and product studies.

The first part of this chapter will focus on the transient spectroscopy of three probe molecules, xanthone (I), p-methoxy-β-phenylpropiophenone (II) and benzophenone (III). The decay kinetics of the transients will be monitored as a

function of spectator loading. The latter half of this chapter will examine the change in the product ratios that are obtained from irradiating cis-2,6-diphenylcyclohexanone (IV) when various amounts of spectator molecules are included. Figure 3.1 contains the structure of the four molecules presented in this chapter.

The role of the spectator is very important. By modifying the characteristics of the zeolite cages, the spectator molecule can have an influence on the behaviour of the included organic molecule. Reports in the literature of spectator or additive molecules added to zeolite cavities have examined the changes in product formation or product yields. Work by Turro et al.[1] has shown that the inclusion of spectators such as benzene, cyclohexane and hexane restricts the diffusional motion of radical pairs produced upon photolysis of dibenzyl ketones.

The transient spectroscopy of the probe molecules (I) - (III) has previously been studied, both in solution[2,3] and in heterogeneous environments such as zeolites,[4] micelles[5] and cyclodextrins.[6-9] The transient spectroscopy of these probes in various zeolites[4,10-12] has yielded information on the polarity of the zeolite interior, as well as the conformation that the probe must adopt in the constricted environment.[4,12,13] These three probes were chosen to illustrate the modifications that the spectator may have on the acid-base properties of the zeolite interior, the reduction in diffusional behaviour of the probe and on spatial restrictions.

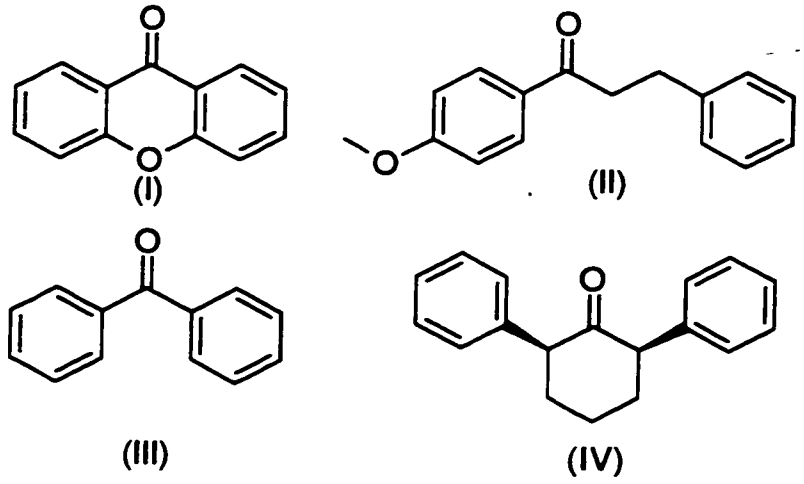

Figure 3-1: Structure of probe molecules (I)-(IV)

The photochemistry of xanthone in solution is very well known.[3,14] The triplet - triplet absorption of xanthone shifts depending upon the polarity of the medium, with shorter wavelengths reflecting a more polar environment. For example, triplet xanthone absorbs at 615 nm in 2-propanol and at 655 nm in carbon tetrachloride.[3] In polar media, the low lying triplet of xanthone has π, π^* character, and a fairly long lifetime due to the lower reactivity associated with π, π^* states. Xanthone in non-polar media has a low lying triplet of n, π^* character, rendering it fairly reactive towards hydrogen abstraction reactions. The triplet - triplet absorption of xanthone in zeolites silicalite[4] and NaY[10] are 605 and 595 nm, respectively, are indicative of a polar environment and corresponding to the λ_{max} of triplet xanthone in water.

p-Methoxy-β-phenylpropiophenone (II) has been used as a triplet probe in supramolecular systems such as silicalite[4] and cyclodextrins.[8,12,15] This ketone is an n, π^* triplet that is in thermal equilibrium with the low lying π, π^* state. Its mode of deactivation involves intramolecular β-phenyl quenching, which requires a

conformation in which the π system is in close proximity to the excited carbonyl, as shown in Figure 3.2. It is believed that the movement of the β-phenyl ring into the correct orientation for quenching is the rate-determining step of the reaction, rather than the dynamics of the charge transfer interaction.[9]

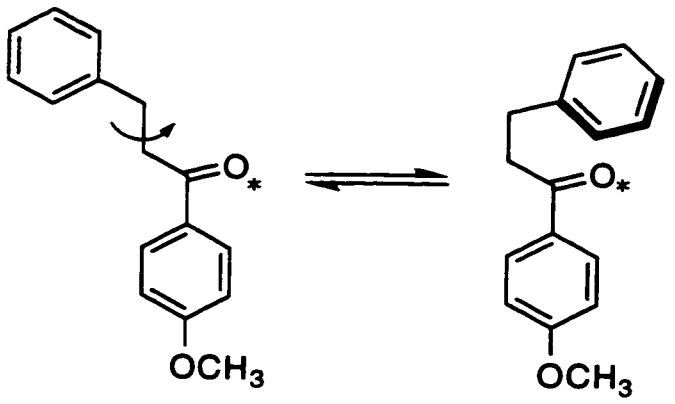

Figure 3-2: Mechanism of β-phenyl quenching upon irradiation of probe molecule (II)

The triplet τ of (II) in de-aerated methanol solution is 200 ns,[16] which increases to 8 μs in the solid state.[16] This increase in triplet lifetime occurs because the molecule crystallizes in a stretched conformation, making quenching through the β-phenyl mechanism less efficient compared to solution where the molecule can readily explore many conformations. The inclusion of (II) in silicalite causes an even greater enhancement of the triplet lifetime, because of the restrictions that the zeolite channels impose upon the organic guest. The triplet τ in silicalite is reported as 0.18 ms, an enhancement of approximately 5 orders of magnitude compared to solution values.[13] The channels of silicalite do not allow

for the β-phenyl ring to rotate and subsequently, the deactivation mechanism for β-phenyl quenching is severely impeded.

By incorporating (II) in a large pore zeolite such as NaY, and comparing the kinetics of deactivation with varying amounts of spectator will indicate the location of the spectator and the mobility of (II) in the zeolite cavities.

Benzophenone (III) was chosen as a control probe molecule, because its photochemistry is not sensitive to environmental polarity, as with (I), or space restrictions, as in (II). In the absence of hydrogen donors, the excitation of (III) leads to exclusive formation of the n, π^* triplet, whether in solution or hetergeneous systems such as zeolites. Benzophenone phosphoresces readily in zeolites in the absence of hydrogen donors.[12,17]

Distribution analysis of the triplet decay of probe molecules (I) - (III) was performed for both fresh and aged samples of the zeolite complexes. The changes in the distribution analysis for samples containing different amounts of spectator as well as differences occurring between fresh and aged samples will aid in understanding the behaviour of the guest molecules.

Probe molecule (IV) undergoes a Norrish Type I photoreaction and forms diradical (V), which undergoes decarbonylation to form the 1,5-diradical (VI). Diradical (VI) has a fairly long lifetime of approximately 900 ns.[18] This long lifetime ensures complete equilibration between the conformers of (VI). Diradical (VI) can either cyclize to form the combination products, cis- and trans-1,5-diphenylcyclopentane (VII) or it can disproportionate, yielding cis- and trans-1,5-diphenyl-1-pentene (VIII). (See Scheme 3.1). The chemoselectivity and

stereoselectivity of the reaction is indicated by the combination / disproportionation ratio and the cis / trans cyclopentane product ratio, respectively. The ratio of cis / trans cyclopentene products is not reported since these products are not stable to the photolysis conditions and react further.[19]

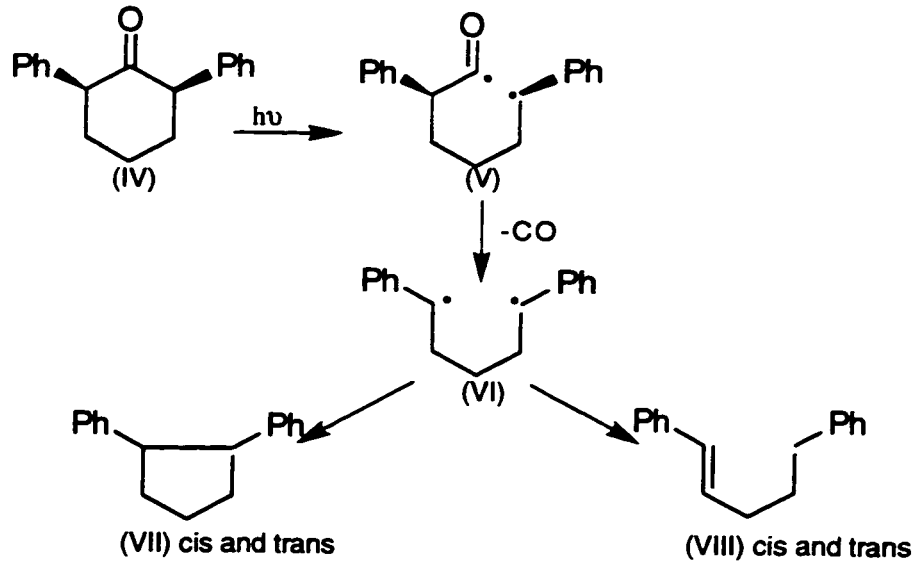

Scheme 3-1: Photolysis of probe molecule (IV)

Substrate (IV) was chosen for product studies for several reasons. First, it undergoes an intramolecular reaction upon photolysis, therefore only rotational restrictions need to be considered. In addition, the relative amounts of photoproducts formed can be used as a measure of both the stereo- and chemoselectivity of the reaction as a function of spectator loading.

Substrate (IV) was included in both NaY and KY, and two spectators, ammonia and pyridine were used. The two faujasite zeolites, NaY and KY, both have the same internal structure and Si/Al ratio and were chosen for this study to determine the effect of the counterion on the product ratios.

3.2 Effect of the Spectator Pyridine on Probe Molecules (I) - (III)

3.2.1 *Results*

Laser flash photolysis using an excitation wavelength of 355 nm of xanthone included in NaY is shown in Figure 3.3. The triplet - triplet absorption maximum of xanthone is at 600 nm, indicative of a polar environment, as reported previously.[10] When pyridine is added to the supercages of NaY containing xanthone, the triplet - triplet absorption spectrum shifts to longer wavelengths (see Figure 3.3). This red - shift of ~ 15 nm is also accompanied by a narrowing of the absorbance peak, which largely occurs on the short wavelength side.

The triplet decays of xanthone included in NaY with and without pyridine present were also monitored. We found that the triplet lifetime of xanthone in NaY is highly dependent upon the amount of pyridine that is present in the supercages. This effect is illustrated in Figure 3.4. It is important to note that the traces presented in Figure 3.4 are taken from samples that have been purged with dry nitrogen. We also prepared samples which were vacuum - sealed prior to laser irradiation; although the lifetimes of triplet xanthone varied according to preparation procedure, the trends that were observed upon addition of various amounts of pyridine were similar.

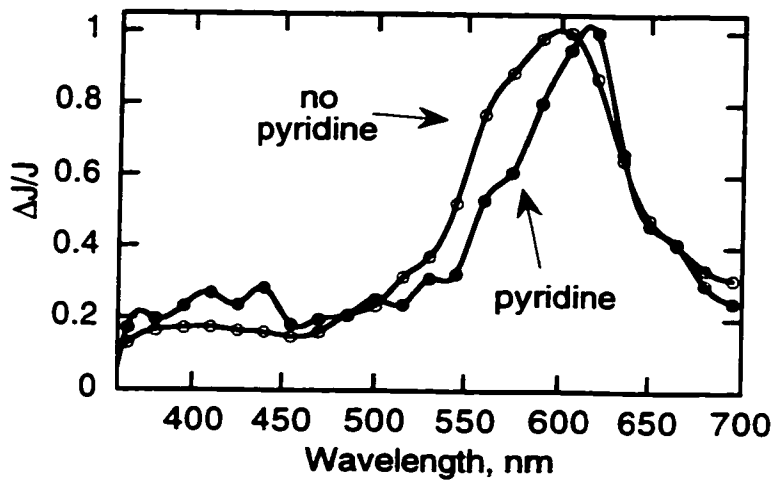

Figure 3-3: Transient absorption spectra obtained by 355 nm excitation of xanthone in NaY without pyridine and with a pyridine exposure time of 4 hours. ΔJ/J is the change in the reflectance signal.

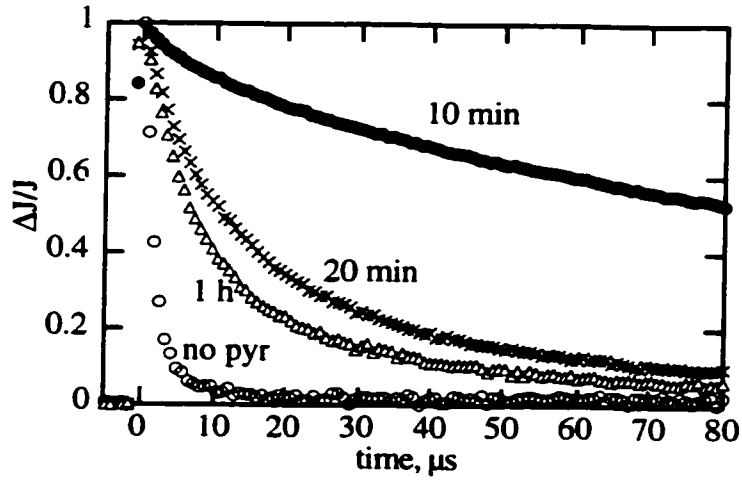

Figure 3-4: Normalized transient decay traces of xanthone triplet in NaY with different pyridine inclusion times (i.e. different pyridine amounts) for nitrogen-purged samples. The traces were recorded at 600 nm using a 5 μs time scale setting in the digitizer.

A remarkable observation is the dramatic increase in triplet lifetime upon addition of a small amount of pyridine. This effect diminishes when more pyridine

is added, but the triplet lifetime of xanthone is always larger when pyridine is present compared to a sample containing no pyridine. Distribution analysis (see Chapter 2) were obtained for these samples (vacuum - sealed ones as well as those purged with dry nitrogen). Figure 3.5 illustrates a composite trace obtained for a sample that has not been exposed to pyridine. Analysis of this trace leads to the distribution analysis shown in Figure 3.6. This distribution analysis indicates a fairly broad distribution of xanthone in the cavities of NaY, with predominantly a single lifetime of 11 μs. Also shown in Figure 3.6 is the distribution analysis obtained for a sample containing pyridine, <S> = 0.7, which illustrates a bimodal decay with a component that has a longer lifetime than the sample without pyridine. The lifetimes that were determined from the distribution analysis for both the vacuum - sealed and nitrogen purged samples are summarized in Table 3.1.

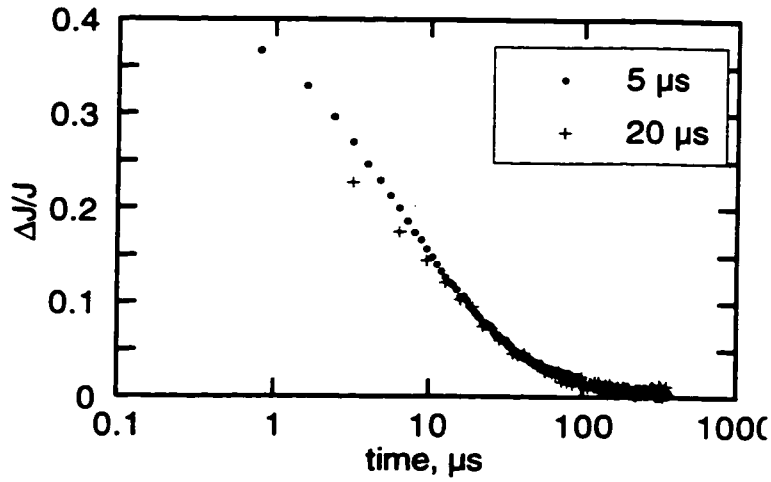

Figure 3-5: Transient decay trace in different time domains for triplet xanthone in NaY with no pyridine. The two independent traces were monitored at 600 nm. Note the logarithmic time scale.

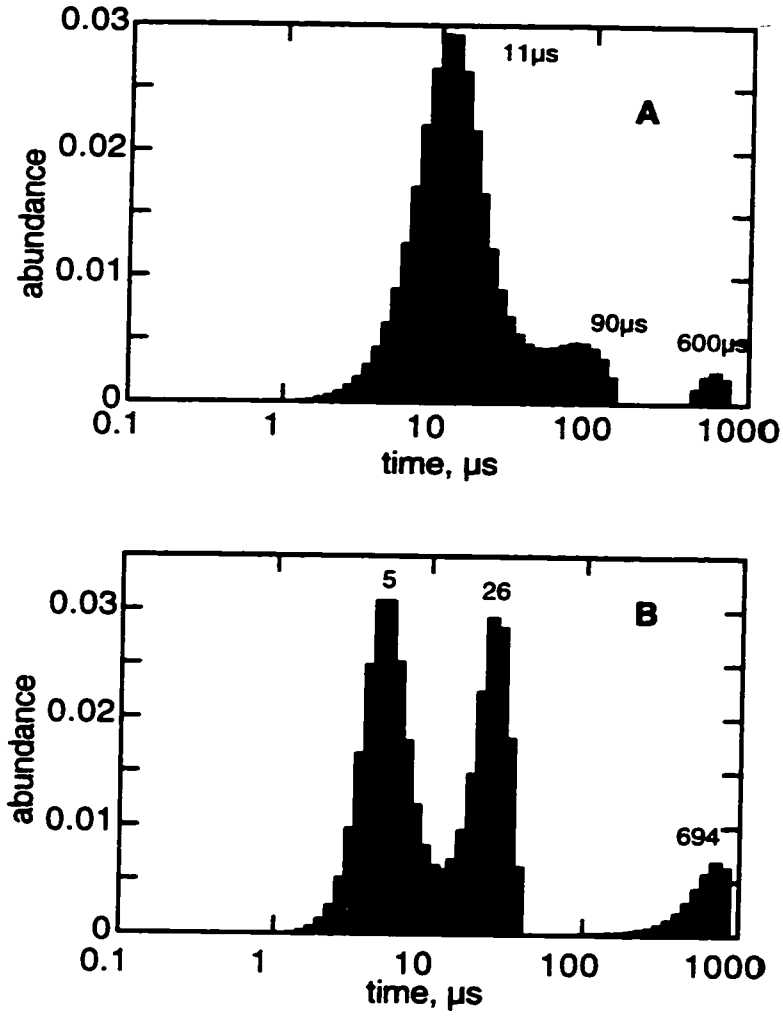

Figure 3-6: Triplet lifetime distribution analysis for xanthone included in NaY (top) and xanthone included in NaY (bottom) with pyridine exposure time of 2 hours; N_2 purged samples

In order to acquire an understanding of the processes occurring in the zeolite samples, we examined the effect of pyridine and a representative acid on the triplet decay of xanthone in homogeneous solution. The acid that we chose for this study was trifluoroacetic acid, and the quenching experiments were performed in acetonitrile. Figure 3.7 shows the quenching plots obtained, which from the

calculation of the slopes leads to triplet quenching rate constants of 6.6×10^{6} and $2.4 \times 10^{9}\ M^{-1}\ s^{-1}$ for pyridine and trifluoroacetic acid, respectively.

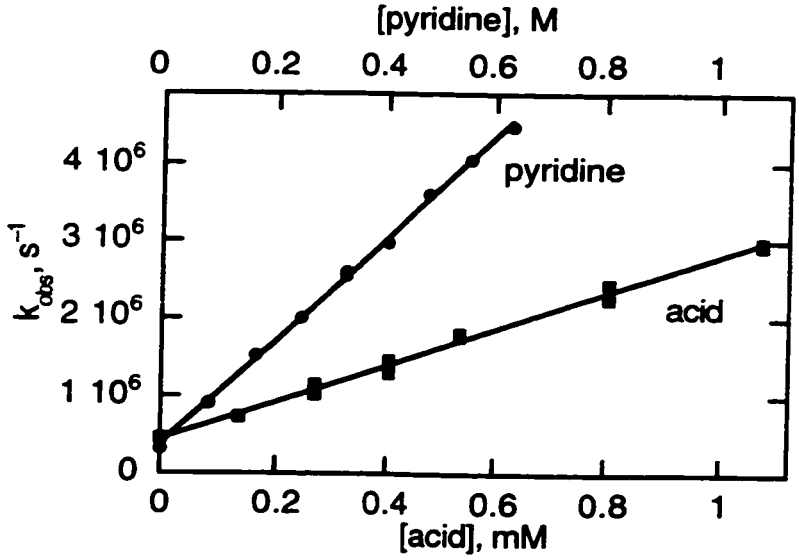

Figure 3-7: Quenching of xanthone triplet (monitored at 600 nm) in acetonitrile by pyridine (top scale) and by trifluoroacetic acid (bottom scale)

A sample was prepared in which water was absorbed into the cavities of a vacuum - dried NaY containing xanthone. The amount of water absorbed was similar to the amount of pyridine that was included in the sample containing the lowest amount of pyridine, <S> = 0.2, which corresponds to a exposure time of ten minutes. The effect of water on the triplet decay of xanthone was monitored, and no significant changes in lifetime between the wet and dry samples were observed.

The second ketone probe molecule that was used, p-methoxy-β-phenylpropiophenone (II), has a triplet - triplet absorption maximum at 400 nm upon excitation at 308 nm. The effect of pyridine addition on the triplet lifetime was

monitored, and the triplet decay traces obtained using a 1 μs instrumental time scale are shown in Figure 3.8. From this figure, it is clear that the amount of pyridine added to NaY has an influence on the behaviour of the triplet lifetime for ketone (II). Distribution analysis was also performed for these samples, and the lifetimes obtained are summarized in Table 3.2.

Table 3-1: Lifetime distribution analysis of NaY/xanthone samples with different pyridine exposure times for (a) vacuum sealed samples and (b) nitrogen purged samples.

Pyridine diffusion time, minutes	Molecules pyridine/ supercage	Triplet lifetime: largest component, μs	Triplet lifetime: 2nd largest component, μs
(a)	vacuum sealed samples		
0	0	0.9	---
10	0.20	115	---
20	0.46	18.7	2.6
120	0.82	18.8	---
480	1.14	2.3	14
(b)	nitrogen purged samples		
0	0	11	90
10	0.05	180	13
20	0.10	10	---
120	0.71	5	26

Table 3-2: Lifetime distribution analysis of NaY/MPP samples with different pyridine exposure times for (a) fresh samples and (b) aged samples.

Pyridine diffusion time, minutes	Molecules pyridine/ supercage	Triplet lifetime: largest component, μs	Triplet lifetime: 2nd largest component, μs
(a)		fresh samples	
0	0	3.8	0.4
10	0.11	0.7	0.1
60	0.73	9.6	---
120	1.80	13.6	3
240	2.52	19.2	2
(b)		aged samples	
0	0	9	0.3
10	0.11	2.2	0.2
60	0.73	15.3	---
120	1.80	17.8	0.4
240	2.52	19	0.6

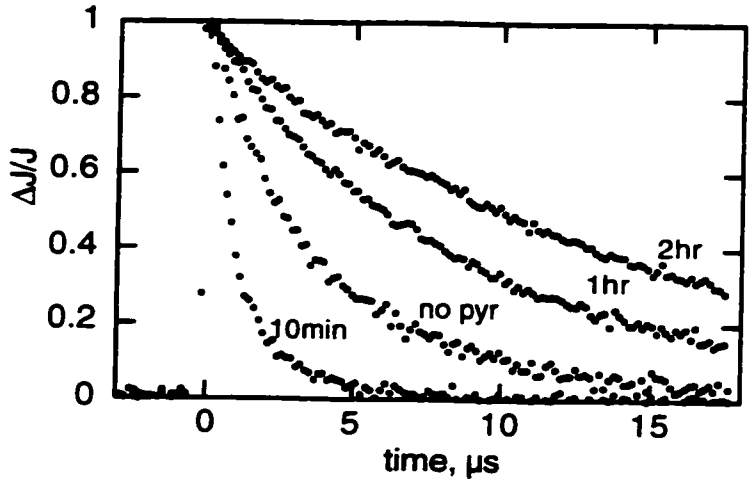

Figure 3-8: Normalized triplet decay traces of p-methoxy-β-phenylpropiophenone (II) in NaY with different pyridine inclusion times. The traces were recorded at 400 nm using a 1 μs instrumental time scale

Figure 3.9 illustrates the distribution analysis acquired when various amounts of pyridine are added.

We also looked at the effect that sample aging has on the triplet lifetime of (II), and these lifetimes are also presented in Table 3.2. The trends that were originally observed are conserved in the aged samples, with a small change in triplet lifetime occurring for all the samples except for the pyridine free sample, in which the triplet lifetime increases by 5 μs. An aged xanthone sample displayed a similar increase.

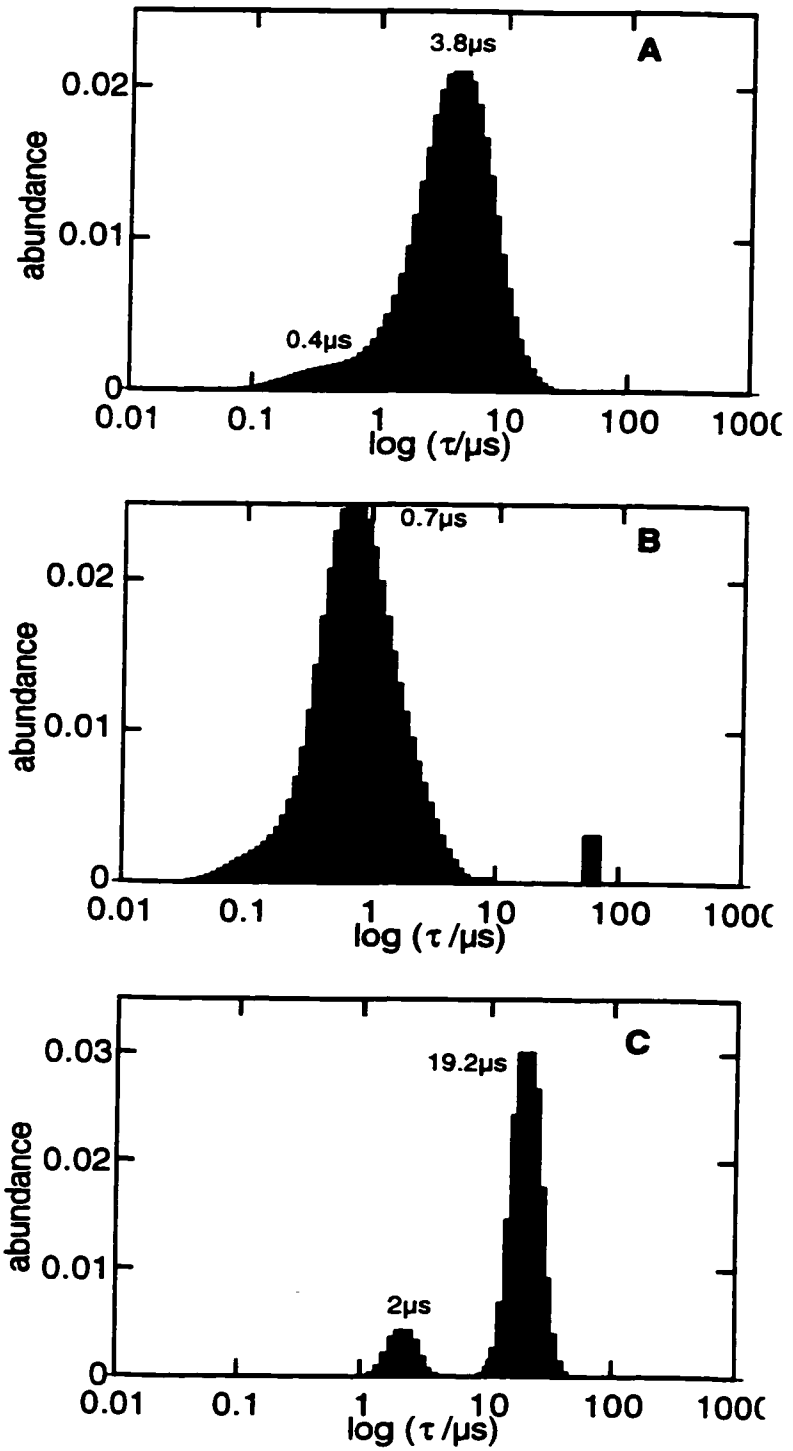

Figure 3-9: Triplet lifetime distribution analysis of NaY/p-methoxy-β-phenylpropiophenone **(A)** and NaY/p-methoxy-β-phenylpropiophenone with pyridine diffused in for 10 minutes **(B)** and 4 hours **(C)**

Benzophenone (III), was also included in NaY, and the effect of spectator molecule pyridine was monitored. Triplet - triplet absorption of benzophenone occurs at 520 nm, and the lifetime obtained for benzophenone included in NaY was around 2 μs. The triplet decay traces obtained when various amounts of pyridine were added did not show any significant changes. There was a minor reduction in the triplet lifetime, but the effects are very small when compared with guest ketones (I) and (II).

3.2.2 *Discussion*

Xanthone has been incorporated into heterogeneous systems such as cyclodextrins[6,7] and zeolites.[4,13] In fact, it was one of the first molecules studied in zeolite systems using time-resolved diffuse-reflectance techniques. Previous studies using xanthone have shown that the zeolite interior is very polar, which is also confirmed in the present experiment.

Studies of pyridine included in zeolites using FT-Raman and DRIFT spectroscopies[20,21] have provided information as to the location and interaction of pyridine in the supercages of NaY. From these studies, it was determined that the adsorption of pyridine causes not only a redistribution of water but also of the sodium cations in the zeolite. Other studies[22] have looked at the thermal desorption of pyridine from the zeolite, a widely used technique which gives information on the number and on the strength of acid sites in zeolites. From this work, it is apparent that pyridine included in the zeolite will first neutralize the stronger acid sites that are present. Based on these results, the dramatic

increase in triplet lifetime that occurs for xanthone when a small amount of pyridine is coincluded in the supercages becomes clear. The pyridine acts as a base, neutralizing the acid sites in the zeolite which can quench the triplet of xanthone; this results in the increase in triplet lifetime. That the acid sites in the zeolite can quench the xanthone triplet is confirmed by the quenching of xanthone in acetonitrile by trifluoroacetic acid. Consistent with the acid quenching observed in the case of xanthone, the pK_a for triplet xanthone is 3.0,[23] compared to 0.3 and 1.5 for triplet benzophenone,[24] depending upon the solvent system. Therefore, the short triplet lifetime that is seen for xanthone included in NaY is due to the interactions of this ketone with the acid sites in the zeolite. This lifetime increases by a significant amount when small amounts of a basic molecule neutralizes the acid sites. The possibility that a change in the local microviscocity of the zeolite upon addition of a small amount of pyridine explains the increase in triplet lifetime is ruled out by the experiment with coabsorbed water. The fact that the sample of xanthone in NaY containing similar amounts of water had no effect on the triplet lifetime of xanthone reaffirms the fact that it is the interaction of pyridine with acid sites that causes the increase in lifetime, and not microviscocity effects. The acidity of different types of zeolites is addressed in Chapter 4.

As the sample of xanthone in NaY absorbs more and more pyridine, we see a gradual decrease in the triplet lifetime of xanthone, although in our samples, the smallest triplet lifetime of xanthone observed occurs in a sample containing no spectator molecule. The decrease in the lifetime of triplet xanthone upon an increase in loading of pyridine reflects a quenching process; triplet xanthone is

quenched by pyridine, which is paralleled by the quenching determined in acetonitrile. The nature of the quenching of xanthone by pyridine is not known, but it is likely due to a charge transfer interaction between the π system of the quencher and the excited carbonyl. Similar quenchings by aromatics such as benzene (although less effective) and other alkylbenzenes are well established.[25,26] Thus, the effect of pyridine loading on the excited carbonyl is two-fold. At small pyridine loadings (0.05 - 0.2 molecules per supercage), the increase in xanthone triplet lifetime is due to the effect of the environment provided by the host zeolite, whereas at higher loadings, the moderate quenching of xanthone reflects an interaction with the guest.

The interaction of the acid sites with the triplet state of benzophenone is less pronounced, and the effect of pyridine quenching is less important since the triplet lifetimes are always much shorter, and therefore less sensitive in the case of benzophenone.

p-Methoxy-β-phenylpropiophenone (II) has also been included in heterogeneous systems such as cyclodextrins[8,12,15] and silicalite zeolite.[4] The inclusion of (II) in the constrained systems results in the β-phenyl quenching being impeded and hence a longer triplet lifetime. The triplet lifetime of (II) in NaY ranges from ~ 4 - 9 μs, depending on sample age, which is much larger than the triplet lifetime reported in solution. Initial additions of pyridine to a sample of NaY containing (II) resulted in a decrease in triplet lifetime; this is opposite to what is seen for xanthone. As in the case of xanthone, the absorption of a small amount of pyridine results in neutralization of acid sites. The strong affinity of pyridine to the

acid sites displaces (II), which was also bound to the acid sites, and causes it to adopt a tighter conformation. Thus, small amounts of pyridine displace (II), resulting in access to a conformation in which intramolecular quenching can more easily occur. It should be kept in mind, however, that the triplet lifetime of (II) with small amounts of pyridine present in the supercages is still much longer lived compared to solution.

The absorption of larger amounts of pyridine results in an enhancement of the triplet lifetime. This is clearly indicative of the reduced mobility of (II) as the cages become crowded, and hence the inability of (II) to readily access the conformation required for deactivation. The lifetime of (II) in the zeolite cages with large amounts of pyridine is even greater than the lifetime of 8 μs reported in the solid state, which reveals the extent of the compact environment that ketone (II) finds itself in.

The increase in the triplet lifetime of (II) in NaY upon aging reflects its mobility within the zeolite cages. This mobility leads to more molecules that adopt a conformation that makes intramolecular quenching more difficult. Transient absorption spectra and decay kinetics of molecules included in zeolites are known to vary somewhat with sample age, which is dependent upon the size of the guest molecule and the free space available in the zeolite pores. For a guest molecule to achieve equilibrium within the zeolite pores may take a few hours or weeks, or sometimes even months.[11] Thus the increase in triplet lifetime for (II) with sample age is not surprising, and the observation that the samples of (II) in NaY containing pyridine do not undergo such large changes in triplet lifetime is a result

of the increasing crowding in the zeolite cages. The mobility of (II) in cages containing pyridine is more hindered compared to cages that do not contain any spectator molecule.

3.2.3 *Conclusions*

Spectators have a large influence on the photochemistry of included guest molecules in zeolite supercages. They influence the photochemistry by at least three different mechanisms. The first is through modifying the acid-base properties of the zeolite cages, the second is by direct interaction with the excited state of the guest and the third is by hindering the mobility of the excited guest. The first two mechanisms were seen in the case of xanthone at both low and high loadings of pyridine, respectively, and the third mechanism was evident in the case of probe molecule (II).

3.3 Effect of Spectators Pyridine and Ammonia on the Photoproducts of Probe (IV)

3.3.1 *Results*

The product distribution obtained upon the photolysis of (IV) in either zeolite NaY or KY, or with the addition of ammonia or pyridine is altered compared to isotropic solvents. In solution, the photolysis of (IV) results in a 1:1 mixture of cis-(VII) and trans-(VII), whereas the photolysis of (IV) included in zeolites results in

preferential formation of trans-(VII) compared to cis-(VII). This stereoselective photocyclization is greater in the KY complex than in NaY, where the trans-(VII) product is formed four times as much compared to solution irradiations. For NaY, the amount of trans-(VII) produced is doubled compared to solution irradiations. The amount of cis and trans-(VII) produced changes as spectator molecules, pyridine or ammonia, are introduced into the cavities. Tables 3.3 and 3.4 list the product ratios that are obtained upon photolysis of probe (IV) in zeolites NaY and KY, respectively, with and without the addition of added spectator molecules. As is illustrated in the tables, the addition of spectator molecules in the zeolite cavities results in an increase in the formation of the cis-(VII) product upon photolysis as compared to the zeolite sample containing no spectators. The changes in the photocyclization ratios as a function of spectator loading for both zeolites NaY and KY are shown in Figures 3.10 and 3.11 for spectators pyridine and ammonia, respectively. For any given spectator loading, there is always more trans-(VII) photocyclization product formed in KY than in NaY.

Table 3-3: Product distribution upon photolysis of (IV) in NaY

	<S> spectator	medium[a]	cyclopentane products, cis / trans[b]	cyclization / disproportionation[b]
pyridine	0	slurry	0.39	1.6
	0.2	slurry	0.31	1.9
	0.9	slurry	0.37	1.3
	2.2	slurry	0.64	2.1
pyridine	0	solid	0.51	6.5
	0.2	solid	0.55	3.8
	0.9	solid	0.76	2.8
	2.1	solid	1.01	2.1
ammonia	0	solid	0.51	6.5
	0.5	solid	0.64	4.4
	1.6	solid	0.71	4.7
	1.9	solid	0.72	3.3
	6.3	solid	0.98	1.8

[a] Samples were irradiated as a hexane slurry for 4 hours or as a solid for 24 hours.
[b] Ratios were determined by GC analysis

Table 3-4: Product distribution upon photolysis of (IV) in KY

	<S> spectator	medium[a]	cyclopentane products, cis / trans[b]	cyclization / disproportionation [b]
pyridine	0	solid	0.29	47.7
	0.2	solid	0.31	8.0
	1.0	solid	0.58	4.5
	1.3	solid	0.44	7.5
	1.5	solid	0.48	8.3
ammonia	0	solid	0.24	28.1
	0.5	solid	0.26	4.6
	1.3	solid	0.36	3.4
	1.7	solid	0.45	2.7
	2.3	solid	0.35	3.5

[a] Samples were irradiated as a hexane slurry for 4 hours or as a solid for 24 hours.
[b] Ratios were determined by GC analysis

The regioselectivity of the reaction was also measured, that is, the ratio of combination products (VII) to disproportionation products (VIII). We measured the combination/disproportionation ratio for the photolysis of (IV) in dichloromethane to be 2.3, a value which does not change upon addition of pyridine or ammonia. By performing the reaction in zeolite cavities without spectator molecules, the combination products are preferentially formed over the disproportionation products (VIII), with combination to disproportionation ratios ranging from 6.5 in NaY to greater than 25 for KY.

When spectator molecules are added to the zeolite cavities, the combination/disproportionation ratio changes, eventually leading to values that are similar to those obtained in solution as more and more spectator is added. These ratios are listed in Tables 3.3 and 3.4.

Dihedral driving calculations were performed on the 1, 5-biradical (VI) using the Spartan program with AM1 parameters. As is shown in Figure 3.12, the local minima occur at 180°, corresponding to a stretched or transoid conformation, and 283°, corresponding to a compact or cisoid conformation.

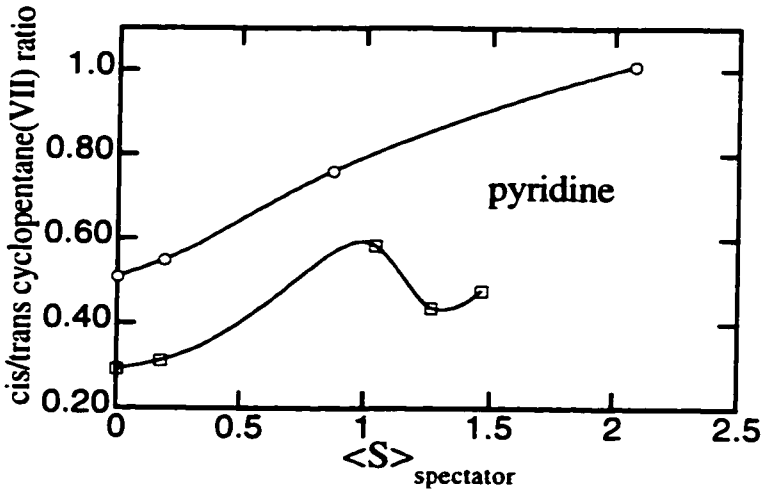

Figure 3-10: Comparison of the cis/trans cyclopentane ratio as a function of pyridine occupancy in zeolites NaY and KY. Circles = irradiation in NaY, squares = KY irradiation

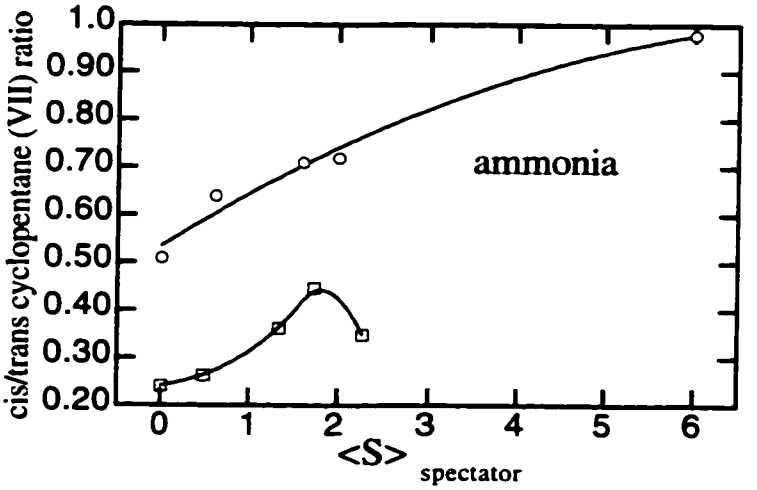

Figure 3-11: Comparison of the cis/trans cyclopentane ratio as a function of ammonia occupancy in zeolites NaY and KY. Circles represent values obtained upon irradiation in NaY, squares represent values obtained upon irradiation in KY.

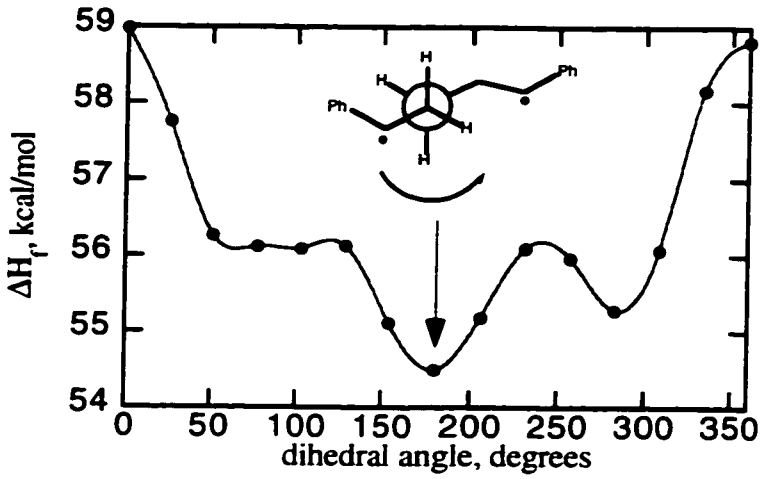

Figure 3-12: Dihedral driving calculation performed using Spartan program with AM1 parameters for biradical (VI). Calculation was performed by optimizing geometry at 15° interval rotations of the chosen dihedral from 0-360°

3.3.2 Discussion

Zeolites can act as 'passive' hosts or 'active' hosts,[27] thereby influencing an intrazeolite photoreaction. They act as passive hosts by providing a rigid environment for the guest organic substrate as it undergoes photolysis, which may lead to preferential formation of one photoproduct over another. Zeolites can act as active hosts by directly influencing the photochemical reaction through the high electrostatic field in the zeolite interior, largely due to the charge-balancing cations that are present. These two effects may have a significant influence on the outcome of the reaction taking place that would otherwise not occur in isotropic solution. This was seen in the case of probe molecule (IV) that had very different

product ratios compared to solution. Other examples have been reported in the literature.[1,28-30]

The increase in cis-(VII) photoproduct that occurs upon addition of spectator pyridine or ammonia can be understood in terms of the location of the included substrate molecule. Probe molecule (IV) is expected to interact with the walls of the supercages, which is where many of the cations are located. This leads to favourable interactions of the π rings with the countercation of the zeolite. Upon photolysis, the 1,5-biradical (VI) is formed, with a measured lifetime of 900 ns in solution,[19] and is not rotationally restricted in the 'empty' zeolite to form the trans-(VII) cyclopentane product. We speculate that the stereoselective formation of trans-(VII) over cis-(VII) as compared to solution may perhaps be due to an additional cation-π interaction with the second phenyl ring that could not be achieved in the cis conformation of the starting ketone. This favourable conformation is readily explored during the long lifetime of the 1,5-biradical, which is most probably longer-lived in the zeolite cavities than in solution. Other factors contributing to this selectivity cannot be ruled out at this time.

The spectator molecules, which also have a strong affinity for these sites, displaces the starting ketone (IV), which now has less mobility through the cages. Large amounts of spectators leads to a crowding of the supercages, along with an increase in the local microviscocity of the system, which in turn reduces the amount of free volume in the cages. This leads to the formation of the product that requires the least motion, cis-(VII). Naturally, this effect becomes greater as the loading level of the spectator increases. This is reflected in Tables 3.3 and 3.4,

where an increasing amount of spectators results in a larger amount of cis-(VII) compared to spectator-free samples.

The nature of the countercation also has a profound effect on the stereoselectivity. The greater amount of trans-(VII) formed in KY compared to NaY is again reflected in the supercage free volume, which is 827 Å for NaY and only 807 Å for KY. Furthermore, Na^+ ions interact more strongly than the larger K^+ ions with substrates that have π bonds or polar functional groups.[31] Therefore, not only the cage free volume but also the cation-π interactions between the countercation and the substrate must be taken into consideration when comparing results from NaY and KY.

The chemoselectivity of this reaction is also greatly influenced upon irradiation in the zeolite cavities. The changes in the chemoselectivity may be due to the conformation that the 1,5-biradical (VI) adopts most of the time. The results indicate that the biradical prefers to be in a cisoid geometry, a geometry that leads to the formation of products (VII) and (VIII), rather than adopting the transoid geometry, which cannot cyclize, but can form the disproportionation product (VIII). The preference for one conformation over another, is due to the restrictions that the zeolite framework imposes upon the reaction intermediates. This leads to an accentuation of the cisoid-transoid interconversion which does not occur in solution. As the cages become crowded with spectator molecules, probe (IV) is probably displaced from the cationic sites. Some of the molecules may be located in-between supercages, such that upon irradiation, biradical (VI) may then be

more likely to adopt a transoid conformation and provide once again the additional route to forming disproportionation products (VIII) as occurs in solution.

3.3.3 *Conclusions*

The regioselectivity and the stereoselectivity of the irradiation of probe molecule (IV) is altered as spectator molecules are included in the supercages of faujasite zeolites NaY and KY. As was seen in the previous section, the addition of spectator molecules influences the photochemistry of zeolite inclusion compounds, and can be used to 'tune' the photochemistry to obtain the desired product.

3.4 Experimental Section

Benzophenone and xanthone were purchased from Aldrich and were recrystallized from methanol prior to use. p-Methoxy-β-phenylpropiophenone was prepared as described previously.[9] Cis-2,6-diphenylcyclohexanone was also purchased from Aldrich and sublimed. Pyridine (Aldrich) and ammonia (Matheson Gas) were used as received.

Preparation of zeolite samples containing probes (I)-(III)

Zeolite NaY (from Aldrich, molecular sieves ZY52, Si/Al = 2.4) was activated by heating overnight at 550°C. The dry zeolite was stirred for 5 hours in a solution of the guest ketone in hexane. The zeolite was then separated and washed with hexane to minimize the amount of guest on the external surface of the zeolite

particles. The samples were then dried under vacuum (P < 20 mTorr) or by blowing dry nitrogen. Pyridine was diffused into the dry zeolite samples by placing the zeolite in an uncapped vial which was then exposed to pyridine vapours by placing it in a closed container with pyridine at room temperature. Several experiments were carried out to determine the amount of pyridine absorbed by the samples by monitoring the weight increase following different exposure periods. On average, it took 59, 132 and 240 minutes to achieve an average occupancy of 1, 2 and 3 molecules per supercage for the treatment of 'empty' zeolite. The occupancy leveled off eventually at around 3.7 pyridine molecules per cavity. Pyridine incorporation was slower when a guest molecule was already included in the supercages.

Preparation of samples incorporating probe (IV)

Sample preparation is similar to that described in the previous section, with the exception that the zeolite complex containing (IV) was vacuum dried only, using a pressure of 10 mTorr at room temperature overnight, prior to pyridine or ammonia absorption.

Laser flash photolysis

The laser flash photolysis setup and a description of how to perform distribution analysis is described in detail in Chapter 2.

Steady state irradiations

Irradiations were performed in the solid state or in a hexane slurry. The samples were placed in pyrex tubes which were continuously rotated in the irradiation chamber to ensure homogeneous light exposure. The samples were irradiated with eight 300 nm Rayonet lamps. Slurry samples were irradiated for 4 hours, and solid samples were irradiated for 24 hours. Irradiations were conducted to < 20% conversion. The products were extracted from the zeolite using dichloromethane. Product ratios were determined by GC analysis.

Molecular modeling

The dihedral driving calculation was performed using the Spartan program with AM1 parameters. The calculation was performed by optimizing the geometry at 15° rotations of the chosen dihedral from 0 - 360°.

3.5 References

(1) Turro, N. J.; Cheng, C.-C.; Lei, X.-G.; Flanigen, E. M. *J. Am. Chem. Soc.* **1985**, *107*, 3739.

(2) Encinas, M. V.; Scaiano, J. C. *J. Am. Chem. Soc.* **1981**, *103*, 6393.

(3) Scaiano, J. C. *J. Am. Chem. Soc.* **1980**, *102*, 7747.

(4) Wilkinson, F.; Willsher, C. J.; Casal, H. L.; Johnston, L. J.; Scaiano, J. C. *Can. J. Chem.* **1986**, *64*, 539.

(5) Scaiano, J. C.; Abuin, E. B.; Stewart, L. C. *J. Am. Chem. Soc.* **1982**, *104*, 5673.

(6) Barra, M.; Bohne, C.; Scaiano, J. C. *J. Am. Chem. Soc.* **1990**, *112*, 8075.

(7) Barra, M.; Bohne, C.; Scaiano, J. C. *Photochem. Photobiol.* **1991**, *54*, 1.

(8) Bohne, C.; Barra, M.; Boch, R.; Abuin, E. B.; Scaiano, J. C. *J. Photochem. Photobiol. A: Chem* **1992**, *65*, 249.

(9) Netto-Ferreira, J. C.; Leigh, W. J.; Scaiano, J. C. *J. Am. Chem. Soc.* **1985**, *107*, 2617.

(10) Scaiano, J. C.; Camara de Lucas, N.; Andraos, J.; García, H. *Chem. Phys. Lett.* **1995**, *233*, 5.

(11) Cozens, F. L.; Régimbald, M.; García, H.; Scaiano, J. C. *J. Phys. Chem.* **1996**, *100*, 18165.

(12) Casal, H. L.; Scaiano, J. C. *Can. J. Chem.* **1985**, *63*, 1308.

(13) Casal, H. L.; Scaiano, J. C. *Can. J. Chem.* **1984**, *62*, 628.

(14) Pownall, H. J.; Huber, J. R. *J. Am. Chem. Soc.* **1971**, *93*, 6429.

(15) Barra, M.; Scaiano, J. C. *Photochem. Photobiol.* **1995**, *62*, 60.

(16) Boch, R.; Bohne, C.; Scaiano, J. C. *J. Org. Chem.* **1996**, *61*, 1423.

(17) Okamoto, S.; Nishiguchi, H.; Anpo, M. *Chem. Lett.* **1992**, *6*, 1009.

(18) Zimmt, M. B.; Doubleday, C. J.; Gould, I. R.; Turro, N. J. *J. Am. Chem. Soc.* **1985**, *107*, 6724.

(19) Peyman, A.; Beckhaus, H. D.; Rüchardt, C. *Chem. Ber.* **1988**, *121*, 1027.

(20) Ferwerda, R.; van der Maas, J. H.; Hendra, P. J. *J. Phys. Chem.* **1993**, *97*, 7331.

(21) Ferwerda, R.; van der Maas, J. H. *J.Phys. Chem.* **1995**, *99*, 14764.

(22) Ward, J. W. *J. Catal.* **1968**, *10*, 34.

(23) Ireland, J. F.; Wyatt, P. A. H. *J. Chem. Soc., Faraday Trans I* **1972**, *68*, 1053.

(24) Rayner, D. M.; Wyatt, P. A. H. *J.Chem. Soc. Faraday Trans II* **1974**, *70*, 945.

(25) Wagner, P. J.; Truman, R. J.; Puchalski, A. E.; Wake, R. *J. Am. Chem. Soc.* **1986**, *108*, 7727.

(26) Yamaji, M.; Okada, K.; Shizuka, H. In *54th Okazaki Conference; Dynamic Studies of Hydrogen Atom Transfer Reactions*; Institute of Molecular Science: Okazaki, Japan, 1996; pp P. 6.

(27) Weiss, R. G.; Ramamurthy, V.; Hammond, G. S. *Acc. Chem. Res.* **1993**, *26*, 530.

(28) Lem, G., Kaprinidis, N.A., Schuster, D.I., Ghatlia, N.D. and Turro, N.J. *J. Am. Chem. Soc.* **1993**, *115*, 7009.

(29) Pitchumani, K.; Warrier, M.; Ramamurthy, V. *J. Am. Chem. Soc.* **1996**, *118*, 9428.

(30) Sabater, M. J.; García, S.; Alvaro, M.; García, H.; Scaiano, J. C. *J. Am. Chem. Soc.* **1998**, *120*, 8521.

(31) Ramamurthy, V.; Corbin, D. R.; Turro, N. J.; Sato, Y. *Tet. Lett.* **1989**, *30*, 5829.

4. Acid-Base Properties of Coumarin 6 in Solution and in Zeolites

4.1 Introduction

Zeolite acidity, a topic which is important in terms of catalytic acitivity, has been investigated using a wide range of techniques. These techniques include temperature-programmed desorption of ammonia,[1-3] Raman[4-6] and IR spectroscopic studies of pyridine absorbed on zeolites,[7] solid state NMR,[8,9] calorimetric studies[10] and Raman studies of a dye included within a faujasite zeolite.[11] These techniques all have advantages and disadvantages associated with them, such as pyridine being too large a molecule to readily explore all acid sites. These techniques have been used to determine the number of Lewis and/or Brønsted acid sites.

Lewis sites in a zeolite are attributed to the presence of Si and Al atom acceptors, which are considered as mild Lewis acid sites. The number of Al atoms present in the framework of the zeolite also determines the degree of Lewis acidity. Generally, the greater the number of framework Al, the greater the Lewis acidity of the zeolite. Extra-framework Al species are also classed as Lewis acid sites, and are found in the form of AlO^+, $Al(OH)^{2+}$, $Al(OH)_2^+$, and oligomer polyoxoaluminates. These species, which are not part of the aluminosilicate framework of the zeolite, are produced when generating the H^+ form of the zeolite, which occurs upon calcination of the ammonium-exchanged zeolites.[12] This can enhance the acidity of the framework Brønsted site, due to a polarization effect.

Brønsted acid sites in a zeolite are due to the bridging OH located between Si and Al atoms in the framework for a zeolite where the exchangeable cation is H^+.

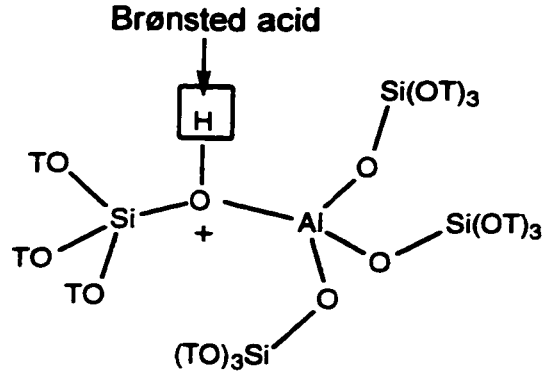

T = Si or Al atom

Since the number of exchangeable cations is directly related to the number of Al atoms in the framework (the introduction of each Al requires a counter cation to keep the framework neutral), the Si/Al ratio of the zeolite will also affect the Brønsted acidity of a H^+-exchanged zeolite. Compared to a silanol group which has a pK_a of 7.1 as measured for a surface silanol group in silica,[13] the acidity of the proton in the bridging hydroxyl group is much greater. For some sites, the pK_a is a negative value. This acidity can be thought of in terms of a silanol group that undergoes Lewis acid promotion by Al^{3+}.

In the previous chapter, we saw how the incorporation of a small amount of pyridine into the supercages of NaY resulted in significant changes in the triplet lifetime of included xanthone. This was concluded to be an acid-base interaction of pyridine with the acid sites present in NaY. To further investigate the acidity of

NaY in detail, we hypothesized that inclusion of a basic dye molecule, which is very sensitive to acidic environments, could provide more details. Some of the characteristics that the dye molecule must possess are: to be of such size that it is readily included in the zeolite cavities and that the spectral shifts in the absorption and fluorescence spectra that occur upon protonation of the dye in acidic environments must be significant. This is especially important when dealing with solid samples, since band broadening is common. The large spectral shifts make identification of the neutral and cationic forms of the dye molecule unambiguous.

This chapter will examine the acid-base properties of coumarin 6, a commercially available laser dye,[14-16] in a variety of zeolites with a wide range of zeolite acidities. The acid-base properties of coumarin 6 in solution and in the solid state will also be investigated, since we could find no previous reports on this subject; these results will help to identify the processes that are occurring in zeolites. The techniques that will be used to characterize the species formed upon zeolite inclusion are absorption, fluorescence and IR spectroscopies. The zeolites used in this study can be subdivided as follows:

(a) NaY, KY, CsY	(increase in basicity moving from NaY to CsY)
(b) NaY, CBV 720, CBV 740	(increase in Lewis acidity moving from NaY to CBV 740)
(c) NaY, HY21, HY100	(increase in Brønsted acidity moving from NaY to HY100)

Series (a) consists of faujasite Y zeolite in which the Na^+ counterion has been exchanged with other alkali metal ions. The vacant space within the supercages also decreases as larger cations are used. This results in a lower inclusion amount of guest molecule. The amount of vacant space within the supercages of NaY is calculated at 827 $Å^3$ compared to only 781 $Å^3$ for CsY.[17] Series (b) consists of Y zeolites that contain different Si/Al ratios. The Si/Al ratio for NaY is 2.6, 15 for CBV 720 and 20 for CBV 740. An increasing Si/Al ratio may suggest a decrease in the Lewis acidity of the zeolite. This is not the case. In fact, the Lewis acidity increases. Though there are fewer acid sites in a zeolite with a higher Si/Al ratio, the remaining acid sites are strongly acidic, resulting in a more acidic zeolite compared to one with a smaller Si/Al ratio. This increase in Lewis acidity occurs up to a certain Si/Al ratio and then levels off. Theoretical calculations indicate that the acid strength of the bridging hydroxyls depend not only on the number of nearby Al atoms, but also on the geometry of the bridge. Series (c) consists of faujasite Y zeolite where the Na^+ counterion has been exchanged with a proton. HY21 corresponds to a Y zeolite that has 21% of the exchangeable ions as H^+, and HY100 refers to a Y zeolite where all of the exchangeable cations are protons. A description about how proton-exchanged zeolites are obtained is given in Chapter 1.

While this method of coumarin 6 inclusion may not replace the other established techniques for determining the number and type of acid sites in solid zeolite complexes, it will prove to be useful in obtaining certain information about the properties of zeolites that was previously unattainable. This is especially true

in the case of NaY, a zeolite considered as non-acidic. The amount of water present in the zeolite cavities, as determined by the preparation method of the zeolite complexes, will also determine the effect on the resulting acidity. This is also an important property in terms of applications of solid acids to heterogeneous catalysis.

4.2 Results

4.2.1 *Properties of Coumarin 6 in Solution*

From the structure of coumarin 6 it is evident that there are two possible sites of protonation upon addition of acid. One site is at the ring nitrogen and the other at the amino nitrogen.

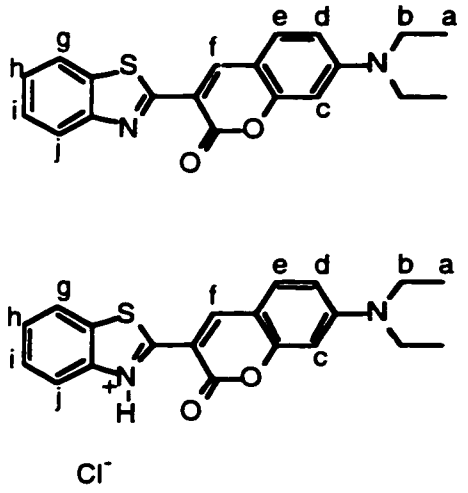

To answer the question of which site first becomes protonated to form the monocation, ^{1}H NMR spectroscopy was used, although other methods, such as X-ray crystallography, could also be applied.The determination was accomplished by

comparing the peak positions of the free base form of the dye to that of the HCl salt of coumarin 6 dissolved in $CDCl_3$. From these studies, it was determined that the protonation occurs on the ring nitrogen.

The peak assignments, which are listed in Table 4.1, were straightforward using a combination of 1D and 2D NMR. Protons Ha and Hb can be assigned directly from the ^1H NMR spectrum. Proton Hc at 500 MHz, is a doublet with a 2.5 Hz coupling constant, typical for meta coupling. The 2D NMR shows the connectivity to allow assignment to Hd, which subsequently shows the other connectivity to He. The assignment of Hf is also straightforward since it is the only singlet. The chemical shift is quite low field for an olefinic proton, but it is beta to two electron-withdrawing groups. Unambiguous assignment of Hj or Hg is not possible; 2D NMR shows the connectivity of the two peaks, thus the two possibilities are given. This also holds true for protons Hh and Hi. Regardless that the exact assignment of proton Hj could not be achieved, it is clearly evident that a change of 0.36-0.43 ppm (see Table 4.1) indicates that this proton is affected by the decreasing electron density of the ortho nitrogen. Protons Hf and He undergo a large chemical shift upon protonation, which can be rationalized in terms of resonance contributions, which is illustrated in Scheme 4.1. In contrast to the large changes in chemical shifts shown for protons e and f, protons b, c, and d exhibit negligible changes, which proves that the monocation formed is protonated exculsively at the ring nitrogen and not the amino nitrogen. The ^1H NMR spectrum of the free base is given in Figure 4.1.

Table 4-1: ^{1}H chemical shifts of the neutral compound and the HCl salt of coumarin 6. Assignments were based using a combination of 1D and 2D NMR. The benzothiazole protons for the neutral compound could not be determined unambiguously, thus both possibilities are listed.

Proton	chemical shift, ppm neutral compound	chemical shift, ppm HCl salt	δΔ
a	1.24	1.27	0.03
b	3.45	3.51	0.06
c	6.55	6.53	-0.02
d	6.65	6.70	0.05
e	7.47	7.91	0.44
f	8.90	10.02	1.12
g	7.95 or 8.02	7.70	-0.25 or -0.32
h	7.35 or 7.48	7.50	0.15 or 0.02
i	7.48 or 7.35	7.60	0.12 or 0.25
j	8.02 or 7.95	8.38	0.36 or 0.43

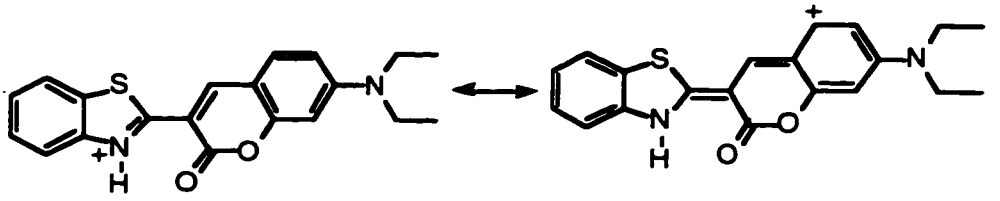

Scheme 4-1: Resonance contributions for protonated form of coumarin 6

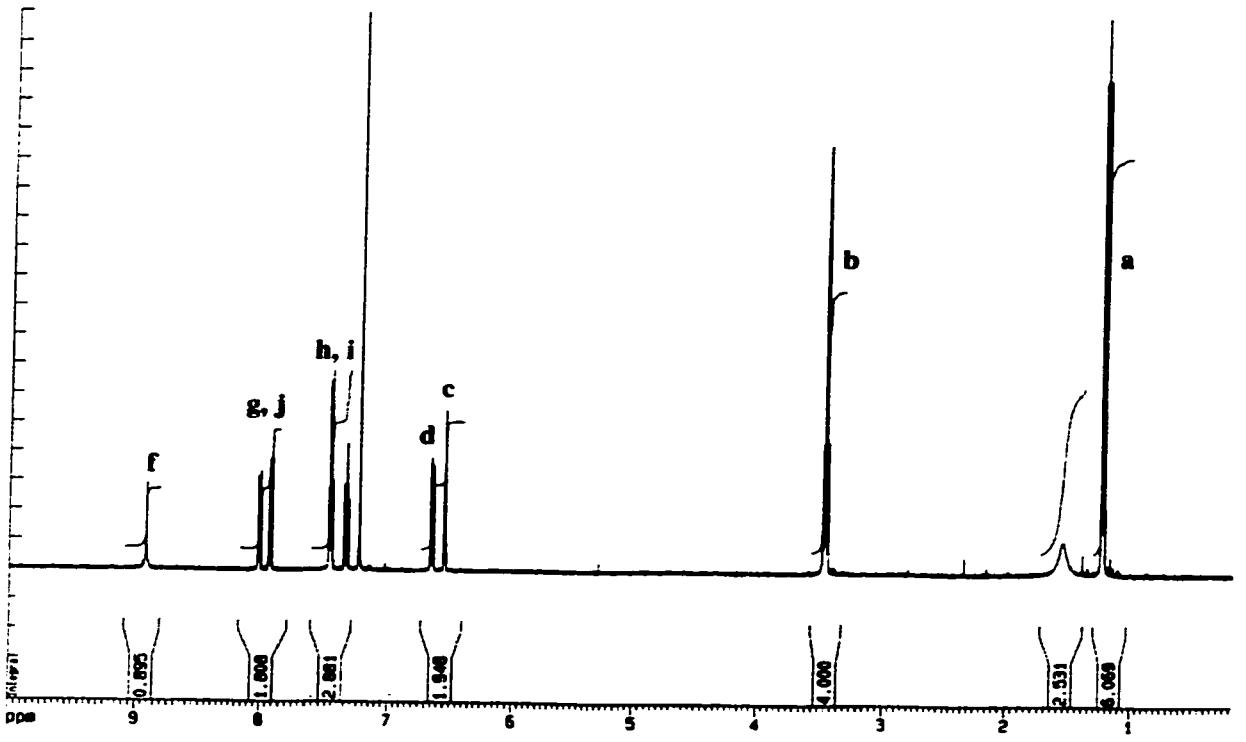

Figure 4-1: ^{1}H NMR spectrum of coumarin 6 in $CDCl_3$

In dichloromethane solution, the changes in the absorption and the fluorescence spectra of coumarin 6 upon addition of acid, resulting in formation of the monocation species, is very large (Figure 4.2). The red-shifts in both the fluorescence and absorption spectra of the monocation species compared to the neutral form range from 60-70 nm. As can be seen from Figure 4.2, the extinction coefficient of the monocation is much larger compared to the neutral species. The addition of larger amounts of acid, resulting in the formation of the dication, causes a blue shift in the λ_{max} of absorption to 375 nm, since the lone pair of electrons on the amino N are no longer available for resonance stabilization. The absorption values vary slightly with the solvent employed. Table 4.2 lists the

absorption and fluorescence λ_{max} in a non-polar solvent, CH_2Cl_2, and a polar solvent, 50% methanol solution.

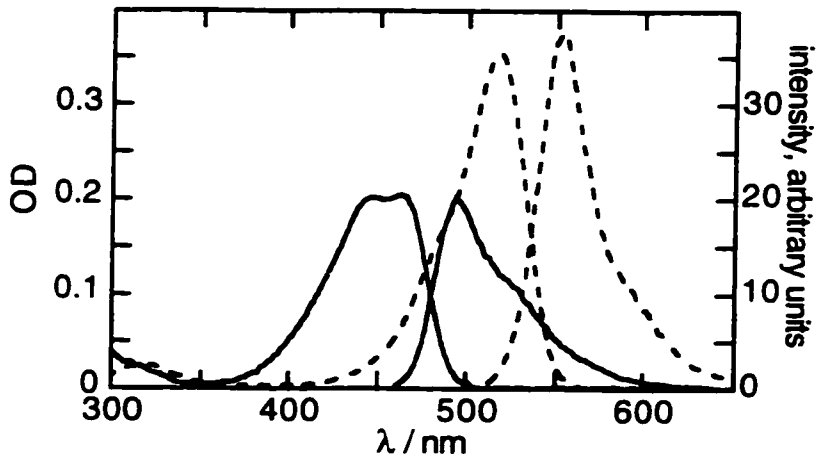

Figure 4-2: The absorption and fluorescence spectra of 4 x 10^{-6} M coumarin 6 in CH_2Cl_2 for the neutral species (— solid line) and for the monocation formed upon small addition of acid (---dashed line).

The change in the dipole moment between the ground and excited state of coumarin 6 was calculated through use of the Lippert[18] equation:

$$\nu_a - \nu_f(cm^{-1}) \sim \frac{2}{hc}\left(\frac{\varepsilon - 1}{2\varepsilon + 1} - \frac{n^2 - 1}{2n^2 + 1}\right)\frac{(\mu^* - \mu)}{a^3} + \text{constant}$$

where ν_a - ν_f = Stokes shift in cm^{-1}

1st quantity in brackets = Δf (known for a given solvent)

a = radius of cavity (obtained from calculation of geometry optimization)

μ^* - μ = change in dipole moment

n = refractive index of solvent

ε = dielectric constant of solvent

From a plot of the Stokes shift in various solvents against the polarizability function, Δf of the solvent, the change in the dipole moment was calculated as 12 D. Figure 4.3 illustrates the plot of the Stokes shift versus Δf for non-polar and polar solvents.

Table 4-2: Absorption and fluorescence λ_{max} of coumarin 6 in solution and the solid state

system	absorption λ_{max} (nm)	fluorescence λ_{max} (nm)
CH_2Cl_2	450 (neutral)	500
	520 (monocation)	560
	375 (dication)	
50% MeOH	468 (neutral)	510
	519 (monocation)	555
	384 (dication)	460
$AlCl_3$ in trichlorobenzene	520	535
solid coumarin 6	460 (br)	630
	570 (sh)	630
solid coumarin 6/HCl salt	350 (br)	485, 535
	525 (br)	570, 700

The pK_a for the neutral to monocation equilibrium was measured through absorption spectroscopy using buffered solutions of the dye at different pH's. Due to the low solubility of coumarin 6 in water, the buffer solutions were prepared in 50/50 water/methanol and the dye was dissolved in 0.2 vol % diglyme. A value of

1.6 was measured for the pK_a. This value was not corrected for the presence of the organic solvent. Figure 4.4 shows the plot used to determine the pKa value for the neutral to monocation equilibrium.

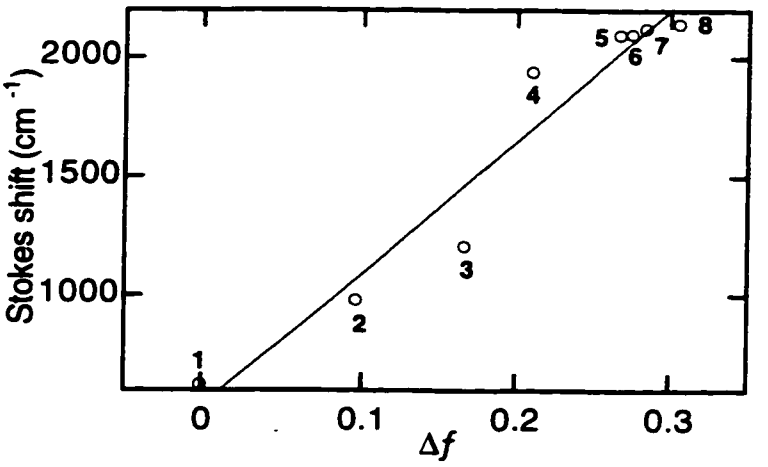

Figure 4-3: Determination of the excited state dipole moment of coumarin 6 using the slope of plot of Stokes shift vs Δf. The numbers correspond to different solvents: 1=cyclohexane, 2=dibutyl ether, 3=diethyl ether, 4=THF, 5=DMSO, 6=DMF, 7=acetone and 8=acetonitrile

Addition of a Lewis acid such as $AlCl_3$ to a solution of coumarin 6 in trichlorobenzene results in an absorption spectrum with a λ_{max} of 520 nm, which corresponds to the absorption of the monocation species. The fluorescence of this solution occurs at 535 nm.

IR spectroscopy can be used to distinguish the interaction of coumarin 6 with Brønsted and Lewis acid sites. This is accomplished by monitoring the shift of the carbonyl stretching frequency. For the neutral species, the carbonyl stretching vibration occurs at 1710 cm^{-1}; the characteristic peak at 1650 cm^{-1} corresponds to interaction with a Lewis acid, and the interaction with a Brønsted

acid results in a broad band at 1689 cm^{-1} with a shoulder at 1740 cm^{-1}. All of these spectroscopic changes that occur for coumarin 6 in solution upon protonation were used as a reference for the heterogeneous systems under study.

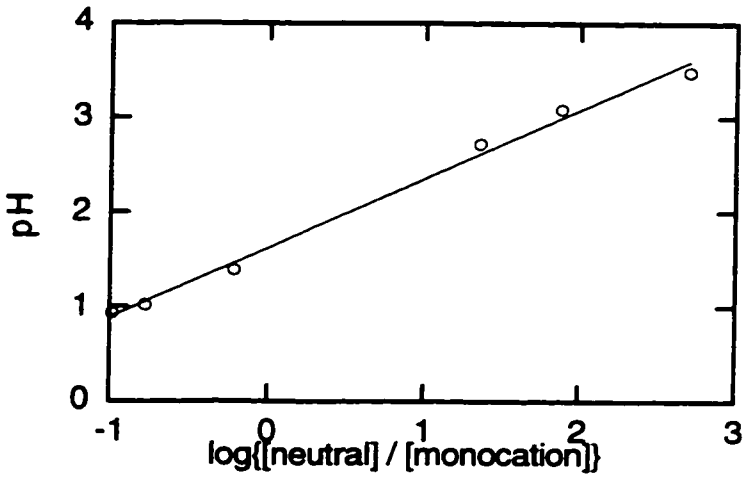

Figure 4-4: Determination of the pK_a for the neutral to monocation equilibrium of coumarin 6. The slope of the pH vs log {[neutral] / [monocation]} yields the pK_a value, which is 1.6.

4.2.2 *Coumarin 6 in the Solid State*

The absorption and the fluorescence spectra of the solid samples of coumarin 6, a bright orange sample and the hydrochloride salt of coumarin 6, a purple solid, were examined. Both solids show a significant Stokes shift, on the order of 180 nm, as well as significant band broadening when compared to solution spectra. This is clearly evident upon examination of Figure 4.5, which shows the absorption and fluorescence spectra of solid coumarin 6. The λ_{max} values for both samples are listed in Table 4.2.

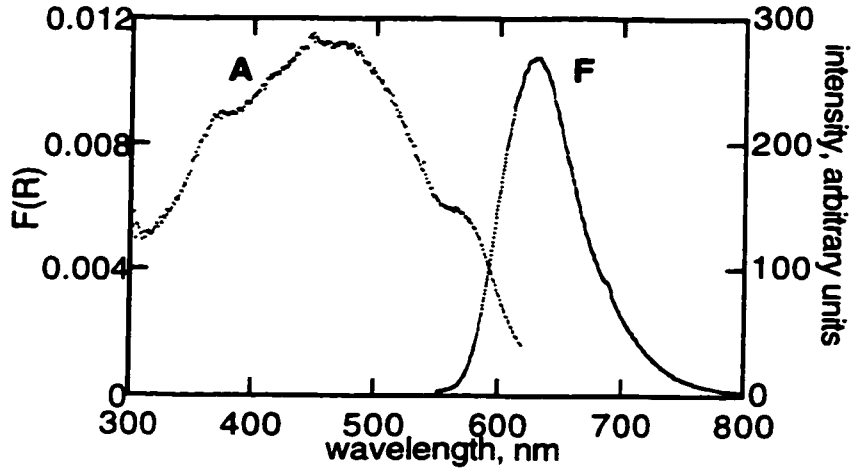

Figure 4-5: The absorption (**A**) and fluorescence (**F**), of solid coumarin 6. The excitation wavelength is 460 nm. Note the large Stokes shift for this sample.

For the sake of comparison, concentrated solutions of coumarin 6, which are also a deep orange colour, were prepared (1.6×10^{-2} M in CH_2Cl_2). The absorption spectrum for this concentration has a λ_{max} at 450 nm as well as at 550 nm. Using a λ_{ex} of 450 nm (where the neutral form absorbs) for the concentrated solution results in an emission spectrum having a λ_{max} of 510 nm as well as one at longer wavelengths (620 nm). The long wavelength band in both the absorption and emission spectra coincide well with that seen in solid coumarin 6. As the concentration of the dye decreases, the long wavelength emission band becomes blue-shifted and eventually disappears at low dye concentrations (1.6×10^{-4} M in CH_2Cl_2, yellow solution). The long wavelength absorption band also disappears at this low dye concentration. These results suggest the occurrence of some type of dye aggregation. Two fluorescence spectra of the concentrated solutions of

coumarin 6 in dichloromethane are shown in Figure 4.6, with λ_{ex} of 450 nm (neutral species absorbs) and 530 nm (monocation absorbs).

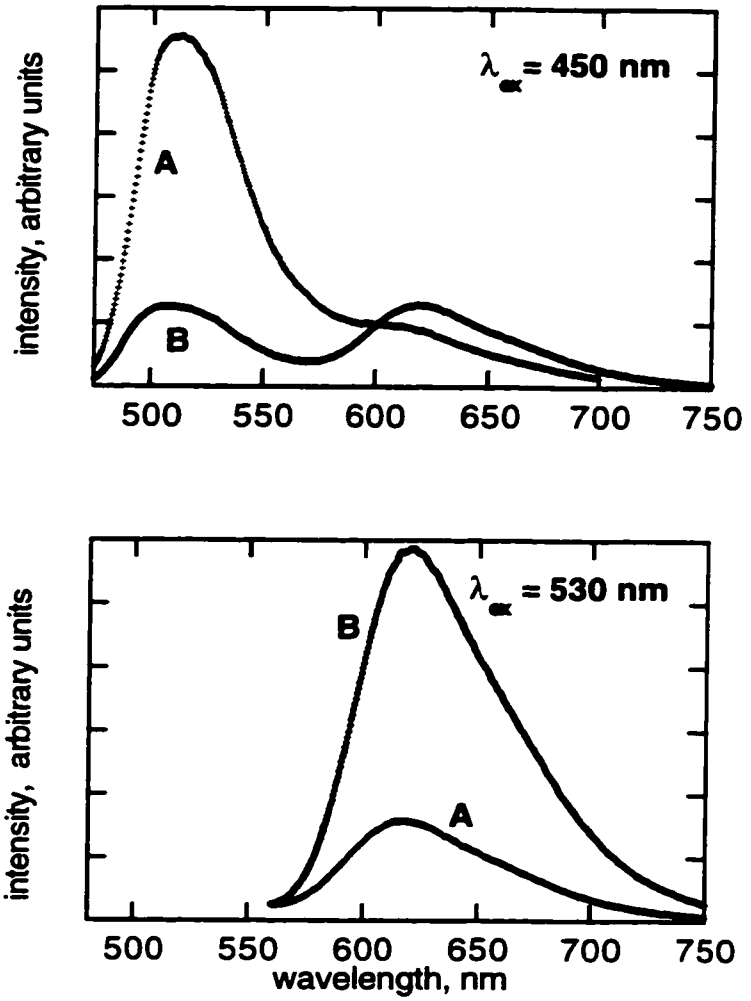

Figure 4-6: Fluorescence spectra of concentrated solutions of coumarin 6. **A** and **B** refer to concentrations of 1.6×10^{-3} M and 1.6×10^{-2} M, respectively. The top spectra has an λ_{ex} of 450 nm (where neutral coumarin 6 absorbs), while the bottom spectra has an λ_{ex} of 530 nm (where monocation of coumarin 6 absorbs). Note the decrease in intensity of the 620 nm band (assigned as aggregate of coumarin 6) as the concentration decreases.

4.2.3 *Coumarin 6 Included within Zeolites*

The amount of coumarin 6 included into the series of zeolites varied, from high loadings of coumarin 6 (10 mg coumarin 6 / g zeolite) to low loadings (0.02 mg coumarin 6 / g zeolite). This was done to test the effect of dye concentration within the voids of the zeolite cavities. The λ_{max} values of absorption and fluorescence for all the zeolites employed and the different coumarin 6 loadings are given in Table 4.3. To illustrate the different species of coumarin 6 formed upon inclusion in different zeolites, the absorption and fluorescence spectra of the dye in the series of zeolites NaY, HY21 and HY100 are illustrated in Figures 4.7 and 4.8. This series of zeolites increases in Brønsted acidity.

Upon examination of Table 4.3, one trend becomes apparent: for the sample with the low loading levels of coumarin 6, the λ_{max} of both absorption and fluorescence correspond well to values obtained in solution. Samples containing high loadings of coumarin 6 have their absorption and fluorescence λ_{max} values red-shifted, as large as 70 nm in the case of HY100. This indicates that there are interactions other than acid-base interactions dominating the spectra. This red-shift is illustrated in Figure 4.9 in the emission spectra of coumarin 6 in NaY as the loading increases from 0.4 mg of coumarin 6 / g zeolite to 6 mg of coumarin 6 / g zeolite.

Table 4-3: Absorption and fluorescence maxima of coumarin 6 in zeolites. The values reported are for vacuum dried (20 mTorr) samples. **Unless stated otherwise, the excitation wavelength corresponds to the absorption λ_{max}.**

n = neutral form, m = monocation, d = dication, a = aggregate

system	loading, mg guest/g host	absorption λ_{max}, nm	fluorescence λ_{max}, nm	assignt
NaY saturated with pyridine	0.02	460	515	n
NaY	10	520	585	a
	2	520	575	a
	0.4	520 (br)	550	m
			λ_{ex} 450 -- 510, 553	n + m
	0.02	520(br)	540	m
			λ_{ex} 450 -- 500 (sh), 540	n + m
HY 100	10	510	607	a
	0.4	370	440, 540	d + m
		520	550	m
	0.02	350	440, 540	d + m
		520	535	m
HY 21	10	520	585	a
	0.4	520 (br)	555	m
	0.02	520	540	m
silica gel BASF	0.03	520 (br)	560	m
CBV 720	10	505	600	a
	0.02	400	λ_{ex} 450--495 (br)	
		510	540 (w)	m
CBV 740	10	500	590	a
	0.02	370	450, 550	d + m
		520	540	m
KY	10	530	565, 600 (br)	a
CsY	<0.4	460	505	n

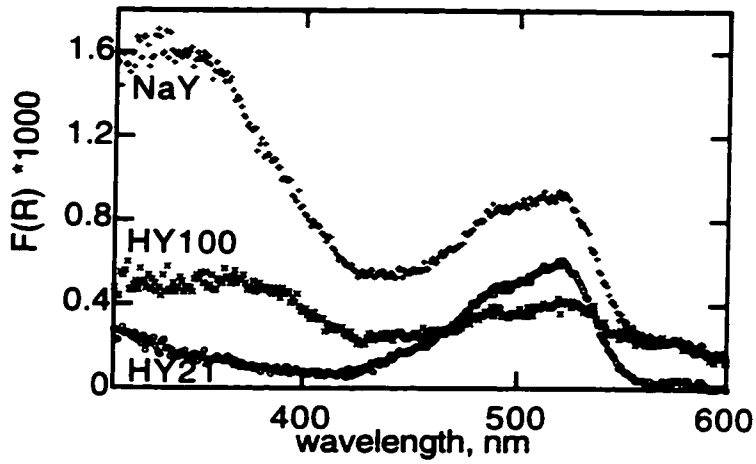

Figure 4-7: Absorption spectra of coumarin 6 included in zeolites NaY, HY21 and HY100. The samples contain 0.02 mg coumarin 6 / g zeolite, and were dried and sealed under vacuum.

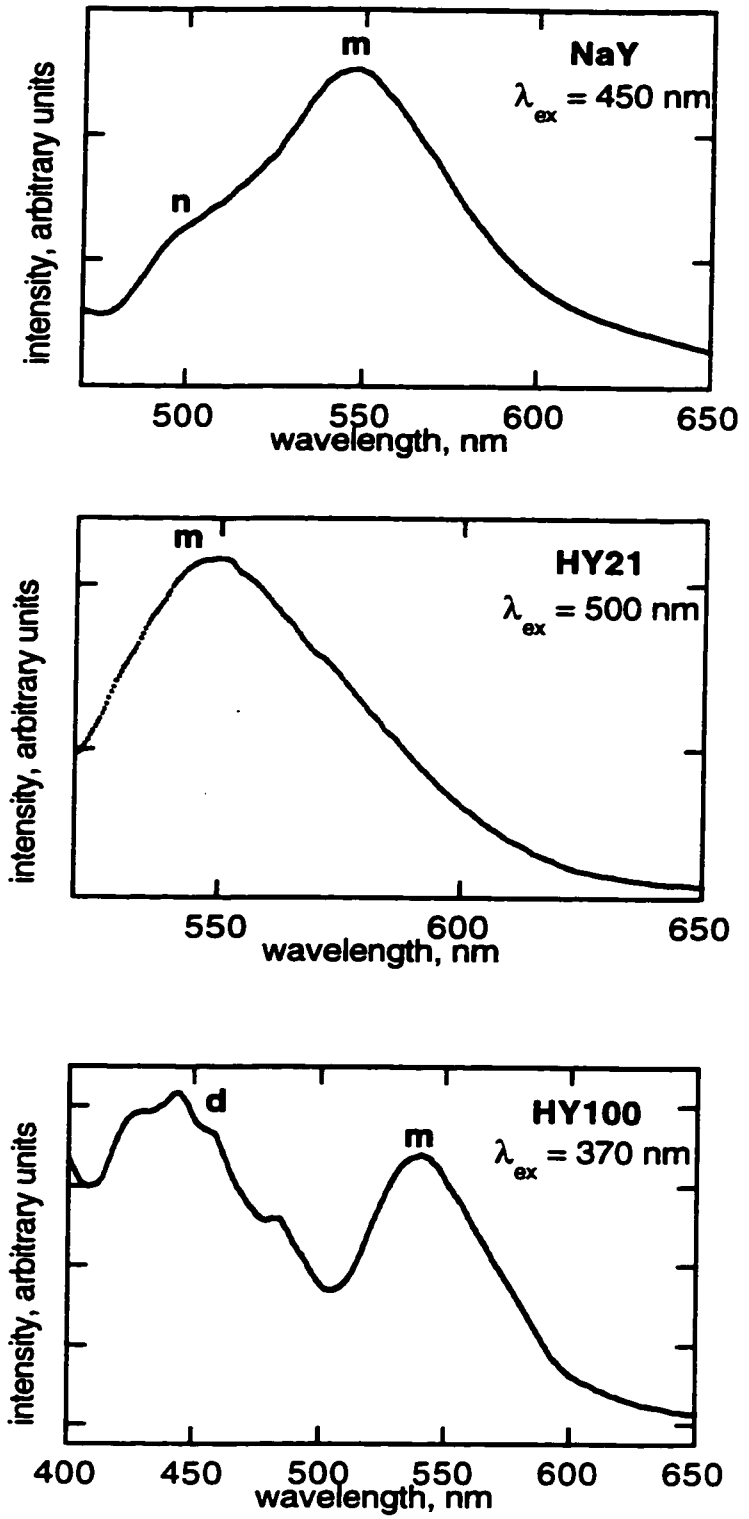

Figure 4-8: Fluorescence spectra of coumarin 6 included NaY, HY21 and HY100. Samples are as described in Figure 4.7. **n** = neutral species, **m** = monocation and **d** = dication species.

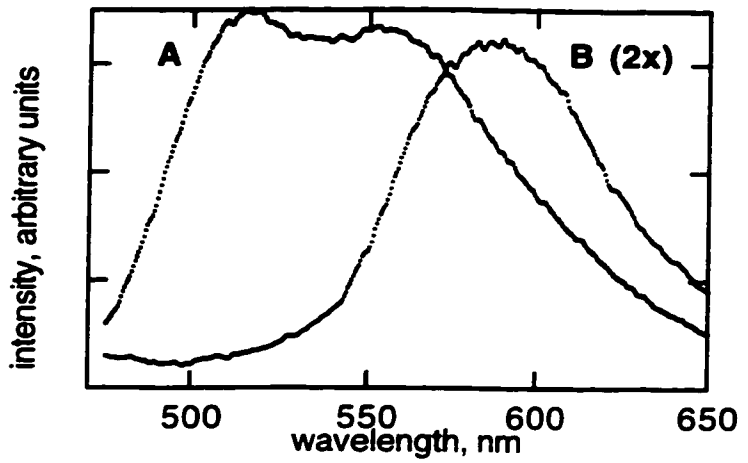

Figure 4-9: Fluorescence spectra of coumarin 6 included in NaY using an excitation wavelength of 450 nm. **A** = 0.4 mg coumarin 6/g NaY and **B** = 6 mg coumarin 6 / g NaY. The sample with the lower loading level of coumarin 6 displays emission from both the neutral and the monocation is observed, whereas the higher loading sample shows emission from the aggregate species only.

An additional experiment, in which zeolite NaY was treated with pyridine, was performed. The amount of pyridine added corresponded to an occupancy of 1.5 pyridine molecules per supercage. This occurred prior to inclusion of coumarin 6. The zeolite pretreated with pyridine did not cause the solution to turn red once coumarin 6 was added, unlike the sample of NaY that was not previously treated with pyridine. Rather, the sample of NaY containing both pyridine and coumarin 6 was yellow, with an absorption λ_{max} at 460 nm and an emission λ_{max} at 515 nm. This indicates that the species of the dye detected is the neutral form. Pyridine was also adsorbed in NaY after incorporation of coumarin 6. The exposure of a sample of NaY containing coumarin 6 to pyridine vapours causes the complex to change colour from red to yellow with a corresponding absorption

λ_{max} shift from 515 to 460 nm. A shift is also seen in the fluorescence spectra, which is illustrated in Figure 4.10. The fluorescence shows that the adsorption of pyridine results in more of the neutral species of coumarin 6, compared to a sample containing no pyridine. This suggests that pyridine alters the acidity of the zeolite environment.

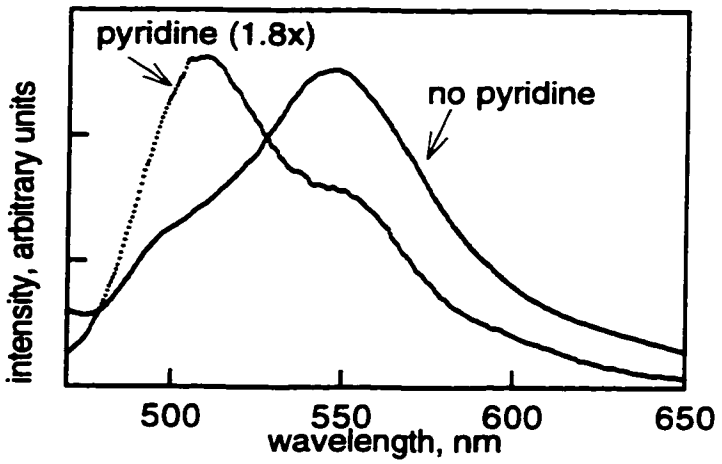

Figure 4-10: Fluorescence spectra of coumarin 6 in NaY (0.02 mg / g zeolite), with and without pyridine. λ_{ex} = 450 nm. Note the shift in the λ_{max} as pyridine (<S> = 5) is added to the sample. The sample with pyridine is the one in which pyridine was included after incorporation of coumarin 6 in NaY.

It is important to note that of all the zeolite samples used in this study, (except for NaY pretreated with pyridine), only CsY did not change the colour of the dichloromethane solution of coumarin 6 upon its addition. The absorption and fluorescence λ_{max} of coumarin 6 in CsY correlate very well to the neutral form of coumarin 6 measured in solution.

The presence of residual water in the supercages and its effect on the acid-base properties of coumarin 6 were also studied. This was accomplished by drying one set of the inclusion complexes under a stream of nitrogen and by drying the other set under reduced pressure (20-30 mTorr). The differences between the two sets of samples in terms of spectral features are very apparent. The vacuum-dried samples have better spectral resolution in both the absorption and fluorescence spectra while the nitrogen dried samples have much broader peaks. Residual solvent does appear to have some effect on the acid-base environment of the zeolite interior. This is best illustrated in Figure 4.11, which compares the absorption spectra for coumarin 6 included in HY21 for a vacuum dried and N_2 dried sample.

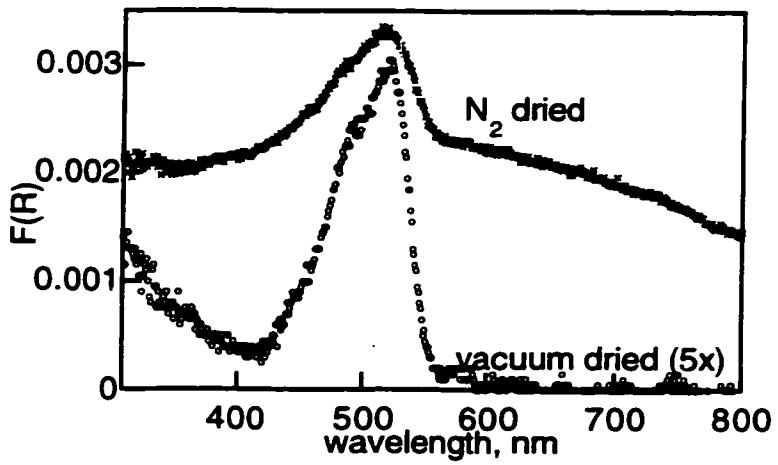

Figure 4-11: Absorption spectra of coumarin 6 included in zeolite HY21 (0.02 mg coumarin 6 / g zeolite). The first sample was dried under N_2, while the second sample was dried under vacuum.

The IR spectra of the higher loading levels of the dye incorporated in the alkali exchanged zeolites NaY and KY were recorded, as well as that obtained by adsorption of coumarin 6 onto silica gel. These spectra are shown in Figure 4.12. What is immediately apparent from these spectra is that the normally intense carbonyl stretching frequency which appears at 1710 cm^{-1} for the neutral dye is weak in these samples. There are very strong bands that appear at 1645 and 1653 cm^{-1} for the NaY and KY samples, respectively, and all three samples show a very strong band at 1517 cm^{-1}, indicative of a Lewis acid interaction with coumarin 6.

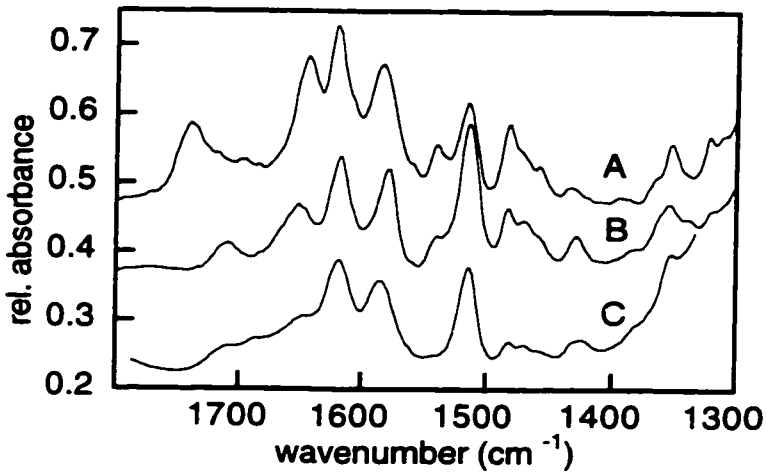

Figure 4-12: IR spectra of coumarin 6 included within the supercages of NaY, <S> = 0.04 (plot A); KY, <S> = 0.04 (plot B); BASF silica gel (plot C). Note the strong band at 1517 cm^{-1} present in all three samples, indicating a Lewis acid interaction with coumarin 6.

4.3 Discussion

4.3.1 *Properties of Coumarin 6 in Solution*

As previously mentioned, there is a large shift in the absorption and fluorescence spectra of coumarin 6 upon protonation to form the monocation. Differences of 70 and 60 nm were measured for the absorption and fluorescence, respectively, between the neutral and monocationic species of coumarin 6 in dichloromethane. This large shift is attributed to a charge-transfer interaction that occurs from the electron-rich diethylamino moiety to the ring protonated benzothiazole. A change in the dipole moment between the ground state and excited singlet state of coumarin 6 was calculated as 12 D, which is a significant difference. Such a large change in dipole moment is due to the charge-transfer interaction that occurs upon excitation, resulting in very different solvation of the ground and excited states, with more polar solvents stabilizing the excited state.

The addition of a Brønsted acid to coumarin 6 is known to protonate the benzothiazole ring (as proven by ^{1}H NMR spectroscopy), forming the monocation; dication formation occurs once enough acid has been added. The question then arises as to whether or not addition of a Lewis acid causes the same spectral shifts as occurs upon Brønsted acid addition. Examination of Table 4.2 reveals that the addition of $AlCl_3$ in trichlorobenzene to coumarin 6 results in an absorption and fluorescence λ_{max} of 520 and 535 nm, respectively. This correlates fairly well to the absorption and fluorescence spectra of the monocation of coumarin 6.

Thus, it is reasonable to conclude that coumarin 6 is sensitive not only to Brønsted acids, but to Lewis acids as well, most likely resulting in complexation.

Another interesting property of coumarin 6 was evident when looking at very concentrated solutions or at the solid samples. An additional long wavelength band was detected, which often dominated the spectra. This additional band is attributed to the formation of aggregates of the dye. Since the band is red-shifted compared to the monomer, it is a head-to-tail or J-aggregate of coumarin 6. Since high concentrations of the dye (> 10^{-3} M) are required in order to detect any aggregates, it is likely that the equilibrium constant for this process must be very low, on the order of 10^{1} M. The formation and characterization of coumarin 6 aggregates in concentrated solutions are important results with respect to dye inclusion in zeolites, since coumarin 6 molecules may be forced into close proximity in the confined zeolite environment.

4.3.2 *Properties of Coumarin 6 in Zeolites*

The loading level of coumarin 6 in the zeolite is an important parameter, since too high a loading will result in formation of dye aggregates and will mask the acid-base interactions. This is noted in Table 4.3 where the absorption and fluorescence λ_{max} of high loadings of coumarin 6 in zeolites were red-shifted compared to solution values. A loading of 0.02 mg coumarin 6 / g zeolite was low enough so that the interactions of the dye with acid sites in the zeolite could be monitored, keeping the probability of aggregate formation extremely low.

At low dye loadings in the zeolite, some interesting results were obtained. The incorporation of coumarin 6 in NaY yielded an absorption and fluorescence spectra that reveal the presence of mainly the monocationic species of coumarin 6. Some of the neutral form is detected as well; this is indicated by the shoulder at 510 nm in the fluorescence spectrum upon excitation at 450 nm, where the neutral form absorbs. A comparison of the absorption of coumarin 6 in dichloromethane and in NaY is shown in Figure 4.13. These results clearly show that in NaY, which has been considered a non-acidic zeolite, there are enough acidic sites to alter the photophysical properties of included organics. This was also seen in the previous chapter.

The adsorption of pyridine in NaY was done in order to quench the zeolite acid sites. Adsorption of pyridine, followed by coumarin 6 inclusion, resulted in the neutral species of the dye being detected. This is in contrast to what occurs when only coumarin 6 is included; both the monocation and neutral forms of the dye are detected. Thus, adsorption of pyridine in this case does not allow for the monocation of coumarin 6 to form.

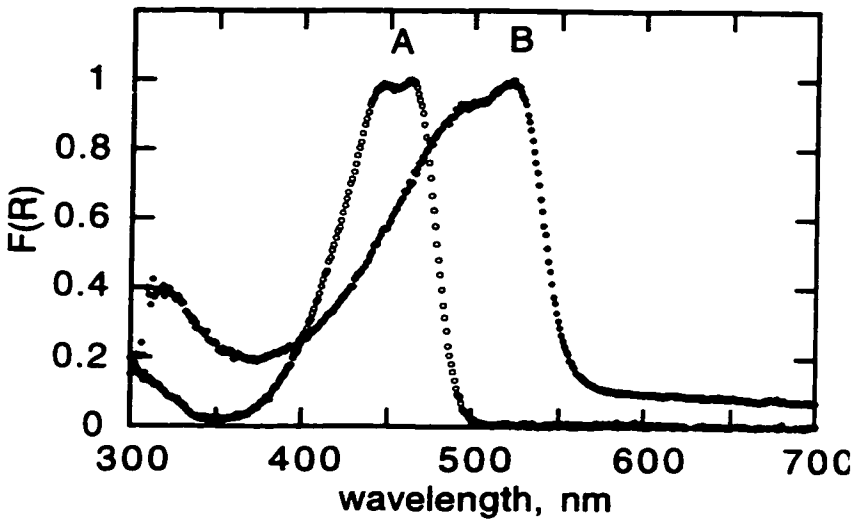

Figure 4-13: Normalized absorption spectra of coumarin 6. Curve A is the absorption spectrum in dichloromethane and curve B is the absorption spectrum in NaY.

The adsorption of pyridine following coumarin 6 inclusion results in a shift of both the absorption and fluorescence λ_{max}. In this case, however, the pyridine is unable to attack all the acid sites, due to the interference of coumarin 6. This is demonstrated in Figure 4.10, where some of the monocation is still present. These sets of experiments verify that pyridine does quench acid sites in NaY, as indicated in the previous chapter. This quenching influences the behaviour of included guest molecules.

For the series of zeolites NaY, HY21 and HY100, which increases in Brønsted acidity, the inclusion of coumarin 6 results in the following: the formation of the monocation, along with the neutral species in the case of NaY; the formation of only the monocation in the case of HY21; the formation of both the monocation

and dication in the case of HY100. The detection of the different species of coumarin 6 correlates well with the increasing acidity of the zeolites.

The series of zeolites NaY, CBV 720 and CBV 740 increases in Lewis acidity from NaY to CBV 740. This is reflected in the species of coumarin 6 formed upon inclusion. In the case of CBV 720, inclusion of coumarin 6 results in the detection of both the neutral and monocation forms of the dye, whereas inclusion in CBV 740 results in the formation of both the monocationic and dicationic forms of coumarin 6. In all of the zeolites studied, the dication of coumarin 6 was detected in only CBV 740 and HY100, which are the most Lewis acidic and Brønsted acidic zeolites, respectively, used in this study.

The series of zeolites, NaY and CsY, was used because of the increase in basicity from NaY to CsY. The inclusion of coumarin 6 in CsY resulted in absorption and fluorescence spectra corresponding to the neutral species only. No other form of the dye could be detected. Only small amounts of the dye could be included in CsY, because of size restraints. The IR spectrum of coumarin 6 included within NaY reveals that the acidity of these zeolites is due to the presence of Lewis sites, as indicated by the characteristic band at 1650 cm^{-1}, which represents the interaction of carbonyl with a Lewis acid. In both NaY and CsY, the neutral form of the dye is still detected. The presence of both neutral and monocationic forms of coumarin 6 in NaY indicates a mixture of both interacting and non-interacting coumarin 6 within the zeolite. No bands due to the presence of Brønsted sites were observed in the IR spectrum of the dye within NaY. Though NaY is not a strongly acidic zeolite, the acid sites within this zeolite are strong

enough to form the monocation of coumarin 6, but not the dication, and alter the triplet lifetime of included carbonyl compounds. The IR spectrum of coumarin 6 in CsY could not be recorded because of the low amount of the dye that was included in this zeolite.

The absorption and fluorescence spectra of coumarin 6 interacting with BASF silica gel indicated the presence of the monocation species. The BASF sample did not show any cracking activity at 300°C, and has been used as a standard for zero acidity in such tests.[19] The detection of the monocation form of courmarin 6 in this sample once again shows the remarkable sensitivity of the dye to very weakly acidic silanol groups. No evidence of the neutral species was recorded.

4.4 Conclusions

The acid-base properties of coumarin 6 in solution as well as the solid samples of coumarin 6 and its hydrochloride salt have been presented. This molecule has a large amount of charge-transfer character, which results in a fairly large difference in the dipole moments of the ground and excited singlet state of 12 D. The formation of the monocation occurs from protonation of the ring nitrogen, which was proven using NMR techniques of the free base and hydrochloride salt. In the solid state and concentrated solutions of coumarin 6, there is evidence for the formation of aggregates, which tend to dominate the absorption and fluorescence spectra.

The incorporation of coumarin 6 into zeolites with different ranges of Brønsted and Lewis acidities give some interesting results. Dye aggregation occurs in the zeolite cavities at a high loading level of coumarin 6, but at low loadings of coumarin 6 (< 0.02 mg coumarin 6 / g zeolite), acid-base interactions dominate the spectra. The dye included in NaY has absorption and fluorescence spectra corresponding to formation of the monocation, with some neutral species also being detected. The monocation was detected even for the sample of silica gel BASF, which is used as a standard for zero acidity.[19] The dication was formed in HY100 and CBV 740 which are the most highly Brønsted and Lewis acidic zeolites, respectively, used in this study. The sensitivity of coumarin 6 to its microenvironment as well as the large spectral shifts between the neutral, monocation and dication forms make it a good candidate for studying other heterogeneous systems as well.

4.5 Experimental Section

Materials

The zeolite LZ-Y52 molecular sieve (NaY zeolite, Si/Al ratio of 2.6) was obtained from Aldrich. Zeolites HY21, HY100, CBV 720 and CBV 740 were prepared at the Instituto Tecnología Química in Valencia, Spain. The procedure for the zeolite preparation is given in references 20 and 21. CsY was prepared from NaY using conventional exchange techniques.[22] Coumarin 6 was purchased from Aldrich and was recrystallized from ethanol prior to use.

Preparation of Dye-Zeolite Complexes

Zeolite inclusion compounds were prepared as described in Chapter 3. Upon addition of the zeolite, the mixture immediately changed colour for most of the zeolite samples studied, turning various intensities of orange-red, indicating interaction with acidic sites.

The zeolite NaY was saturated with pyridine by placing the activated zeolite in an uncapped vial which in turn was placed in a closed container of pyridine. The zeolite sample was left exposed to the pyridine vapour for a period of a few hours. The amount of pyridine included in the zeolite was determined by the resulting change in weight.

Instrumentation

UV-vis absorption spectra were recorded on a Shimadzu 2101 PC using a $BaSO_4$ standard for the solid samples, and a Cary 1E spectrophotometer was used for the solution measurements. Fluorescence spectra were recorded on a Perkin-Elmer LS-50 spectrofluorimeter using a front face attachment for solid samples and for very concentrated solutions (>1 x 10^{-3} M) in dichloromethane. IR spectra of the dye included zeolites were recorded on a Nicolet 710 FTIR spectrometer using self-supported wafers (10 mg).

^1H NMR spectra of the free base and of the hydrochloride salt were recorded on a Bruker AMX 500 in $CDCl_3$. All chemical shifts were referenced to residual $CHCl_3$ and are reported relative to TMS = 0.00 ppm.

4.6 References

(1) Guimon, C.; Zouiten, A.; Boreave, A.; Pfister-Guillouzo, G. *J. Chem. Soc. Faraday Trans.* **1994**, *90*, 3461.

(2) Karge, H. G.; Dondur, V.; Weitkamp, J. *J. Phys. Chem.* **1991**, *95*, 283.

(3) Katada, N.; Igi, H.; Kim, J.-H.; Niwa, M. *J. Phys. Chem. B* **1997**, *101*, 5969.

(4) Ferwerda, R.; van der Maas, J. H.; Hendra, P. J. *Vibr. Spec.* **1994**, *7*, 37.

(5) Egerton, T. A.; Hardin, A. H.; Sheppard, N. *Can. J. Chem.* **1976**, *54*, 586.

(6) Ferwerda, R.; van der Maas, J. H.; Hendra, P. J. *J. Phys. Chem.* **1993**, *97*, 7331.

(7) Ferwerda, R.; van der Maas, J. H. *J. Phys. Chem.* **1995**, *99*, 14764.

(8) Haw, J. F.; Nicholas, J. B.; Xu, T.; Beck, L. W.; Ferguson, D. B. *Acc. Chem. Res.* **1996**, *29*, 259.

(9) Gil, B.; Broclawik, E.; Datka, J.; Klinowski, J. *J. Phys. Chem.* **1994**, *98*, 930.

(10) Drago, R. S.; Dias, S. C.; Torrealba, M.; de Lima, L. *J. Am. Chem. Soc.* **1997**, *119*, 4444.

(11) Place, R. D.; Dutta, P. K. *Anal. Chem.* **1991**, *63*, 348.

(12) Corma, A.; Fornés, V.; Rey, F. *Appl. Catal.* **1990**, *59*, 267.

(13) Marshall, K.; Ridgewell, G. L.; Rochester, C. H.; Simpson, J. *Chem. Ind.* **1974**, *5*, 775.

(14) Abdel-Mottaleb, M. S. A.; Loutfy, R. O.; Lapouyade, R. *J. Photochem. Photobiol, A: Chem.* **1989**, *48*, 87.

(15) Abdel-Mottaleb, M. S. A.; Antonious, M. S.; Abo Ali, M. M.; Ismail, L. F. M.; El-Sayed, B. A.; Sherief, A. M. K. *Proc. Indian Acad. Sci.* **1992**, *104*, 185.

(16) Jones, G. I.; Jackson, W. R.; Choi, C. *J. Phys. Chem.* **1985**, *89*, 294.

(17) Ramamurthy, V.; Corbin, D. R.; Eaton, D. F.; Turro, N. J. *Tet. Lett.* **1989**, *30*, 5833.

(18) Lippert, E. *Z. Naturforsch* **1955**, *A10*, 541.

(19) García, H., personal comm.

(20) Corma, A.; García, H.; Iborra, S.; Primo, J. *J. Catal.* **1989**, *120*, 78.

(21) Beyer, H. K.; Belenkaya, I. *Catalysis by Zeolites*; Elsevier: Amsterdam, 1980.

(22) Breck, D. W. *Zeolite Molecular Sieves: Structure, Chemistry and Use*; Wiley and Sons: New York, 1974.

5. Use of 1-Azaxanthone as a Probe for Radical Reactions in Zeolite Y

5.1 Introduction

Probe molecules have been included in zeolite pores in an effort to obtain more information on properties of the zeolite interior or on the behaviour of certain molecules located in a confined microenvironment. In a previous chapter it was shown how probe molecules such as xanthone[1,2] and p-methoxy-β-phenylpropiophenone[1] have been used to determine the polarity of zeolites, and on the mobility and rotational abilities of molecules within zeolite cavities, respectively. Other probe molecules reported in the literature have examined the behaviour of geminate radical pairs in faujasite zeolites by photolyzing substituted dibenzylketones.[3] These studies have focussed on the competition between recombination and separation of the radical pairs in a confined environment, which determines the final outcome of the reaction. This leads to a product distribution that reflects confinement within the supercages, rather than the statistical distribution of products that has been measured in solution. There are many other examples in the literature[4-6] concerning the inclusion of guest molecules in zeolite cavities that have demonstrated the unique environment that zeolites provide in photochemical reactions, relative to solution.

The examples presented above illustrate how the incorporation and subsequent excitation of various substrates in zeolites provide valuable information on the zeolite in question or its influence on the outcome of a particular

photochemical reaction. To this end, we wanted to examine the effectiveness of generating radicals in the supercages of faujasite zeolites either by hydrogen abstraction or by electron transfer mechanisms. The substrate chosen for this purpose was 1-azaxanthone, which we postulated to be a potential probe for radical reactions in supramolecular systems such as micelles, cyclodextrins and zeolites.

Aromatic ketones, in general, can generate radical pairs upon photoreduction by adding hydrogen donors. This photoreduction leads to ketyl radical formation, as is depicted in Scheme 5.1.

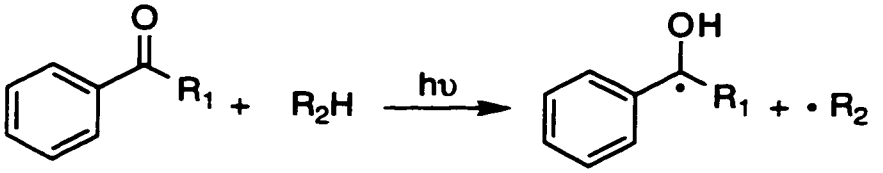

Scheme 5-1: Photoreduction of aromatic ketone by an added hydrogen donor

Xanthone, in a polar environment such as zeolites, photoreduces inefficiently owing to its low-lying π,π^* triplet character, which is fairly unreactive towards hydrogen abstraction. A desirable property of xanthone is that when it photoreduces efficiently in non-polar media, the differences in the transient spectrum between the n,π^* triplet and the ketyl radical that is formed upon photoreduction is significant. This contrasts what occurs for benzophenone, since its transient absorption spectrum upon photoreduction has a small difference between the maximum for the ketyl radical and the triplet, making unequivocal

detection of radicals more difficult. Upon examination of Figure 5.1, we see that 1-azaxanthone is structurally similar to xanthone, and hence may bear some of the convenient properties that characterize xanthone.

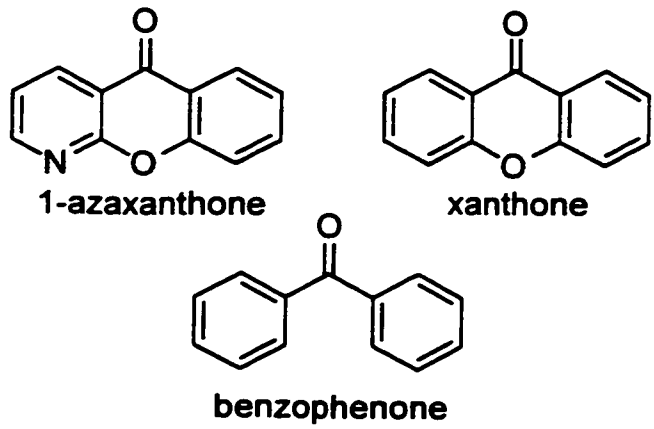

Figure 5-1: Structures of 1-azaxanthone, xanthone and benzophenone

Furthermore, previous studies have shown that replacing the phenyl ring on a molecule such as benzophenone with a pyridyl ring results in an enhancement of the rate of reaction towards radical-like reactions, such as H-abstraction.[7] This led to the idea that 1-azaxanthone would react faster than xanthone in H-abstraction reactions, and may offer the advantage of having significant differences in the absorption of ketyl reactions and the triplet state, as occurs with xanthone.[8] Thus, 1-azaxanthone may potentially be a useful probe in radical-radical reactions.

In this chapter, we will examine the photochemical properties of 1-azaxanthone included in faujasite zeolites NaY and HY, as well as the effect of coincluding increasing amounts of a good H-donor and an electron donor to the zeolite cages. Emission, IR and transient spectroscopy studies will be presented

and from these studies, the usefulness of 1-azaxanthone as a probe molecule for radical-radical reactions will be discussed.

5.2 Results

5.2.1 *Steady State Emission*

The emission spectrum of 1-azaxanthone included in NaY is presented in Figure 5.2. The emission is fairly broad and centered at ~ 440 nm. A comparison of the emission of 1-azaxanthone in NaY to the fluorescence of 1-azaxanthone in water and its phosphorescence in a MeOH/EtOH glass is also shown in Figure 5.2. The fluorescence of 1-azaxanthone in water[9] has a maximum at ~ 415 nm and overlaps with only part of the emission spectrum of 1-azaxanthone in NaY. The other region of the emission spectrum overlaps well with the phosphorescence of 1-azaxanthone in a MeOH/EtOH glass.[9]

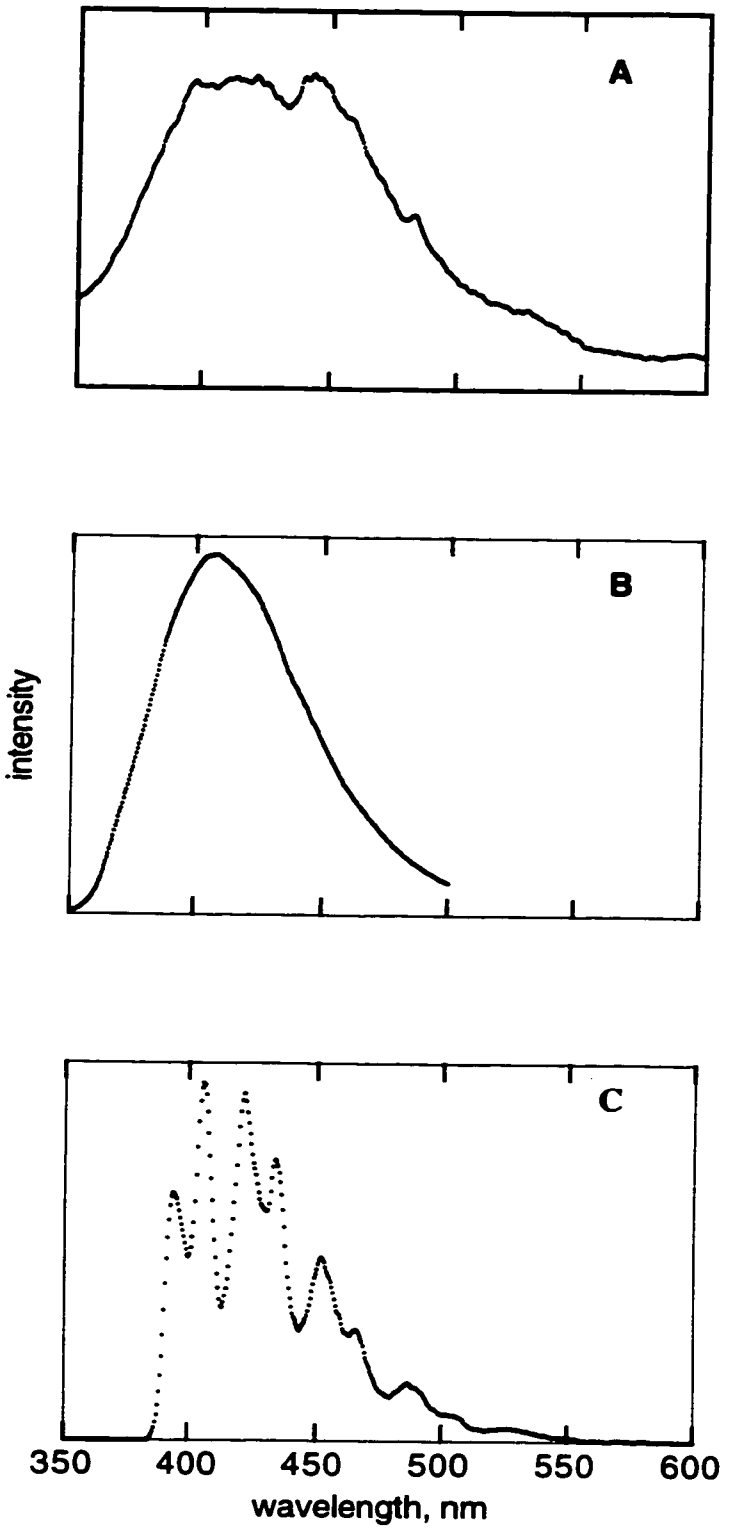

Figure 5-2: Emission of 1-azaxanthone: **(A)** included in NaY zeolite, **(B)** fluorescence in water, **(C)** phosphorescence from ethanol/methanol glass at 77K. Excitation at 330 nm.

This indicates that the emission from 1-azaxanthone in NaY may in fact be a combination of both fluorescence and room-temperature phosphorescence.

The emission of 1-azaxanthone included in HY is also broad and centered at ~ 420 nm. This emission correlates well with the fluorescence of 1-azaxanthone measured in 1N sulphuric acid.

5.2.2 *IR Spectroscopy*

The IR spectra obtained for 1-azaxanthone in a KBr pellet as well as included in NaY and HY are presented in Figure 5.3. The zeolite clearly has a pronounced effect on the position of the carbonyl stretching vibration. Inclusion of 1-azaxanthone in NaY causes the carbonyl stretching vibration mode to shift by over 20 cm^{-1} compared to 1-azaxanthone in a KBr pellet, from 1677 cm^{-1} (KBr) to 1655 cm^{-1} (in NaY). This suggests that the interaction of the probe molecule with the zeolite interior involves the carbonyl group rather than the pyridyl ring. For the sample of HY containing 1-azaxanthone, there are three carbonyl bands; the least intense band is positioned at ~ 1675 cm^{-1}, coinciding with the band in KBr. The other two bands, at 1688 cm^{-1} and 1702 cm^{-1}, (strong bands) indicate protonation of the pyridine ring by the strong Brønsted acid sites in HY. This results from a change in distribution of electrons in the molecule upon protonation, which causes a change in the carbonyl frequency through an inductive effect. The protonated 1-azaxanthone is ionically bound to the zeolite framework. The strength of this interaction is manifested by the fact that the IR spectrum remains essentially unchanged even upon outgassing the zeolite complex at 400°C under 10^{-2} Pa for

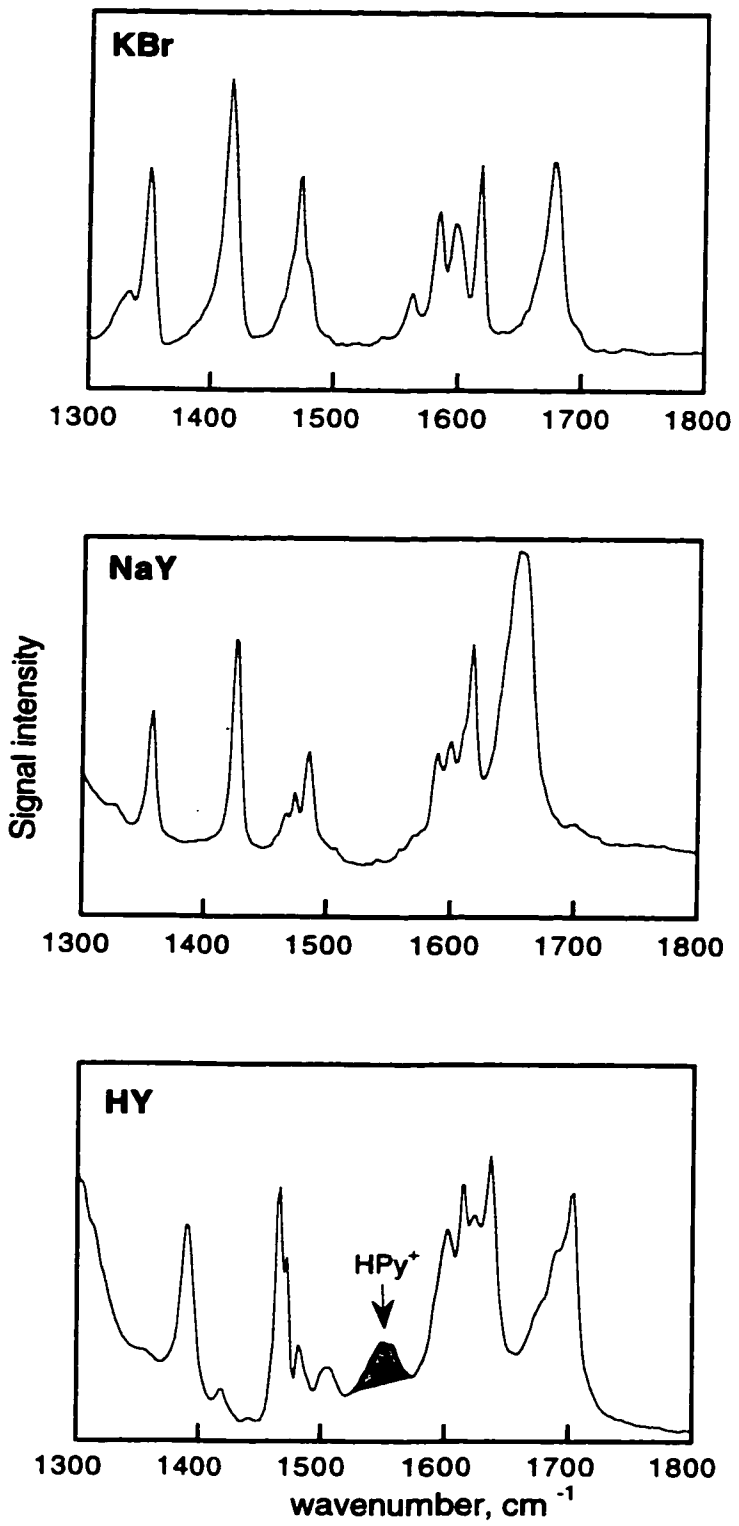

Figure 5-3: IR spectra of 1-azaxanthone in a KBr pellet (top), in NaY zeolite (middle) and in HY zeolite (bottom).

one hour, whereas for a majority of organic guests, the application of the above conditions leads to a total desorption from the zeolite host. A characteristic pyridinium band[10] at 1550 cm^{-1}, is observed for the complex of 1-azaxanthone in HY.

5.2.3 *Laser Flash Photolysis*

Excitation of the sample of 1-azaxanthone in NaY at 355 nm results in a broad absorption peak from 550 to 720 nm, with the maximum centered at ~ 650 nm (see Figure 5.4). This maximum corresponds to the triplet state of 1-azaxanthone, which correlates well with the triplet-triplet absorption of 1-azaxanthone in solution[11] and in micelles.[9]

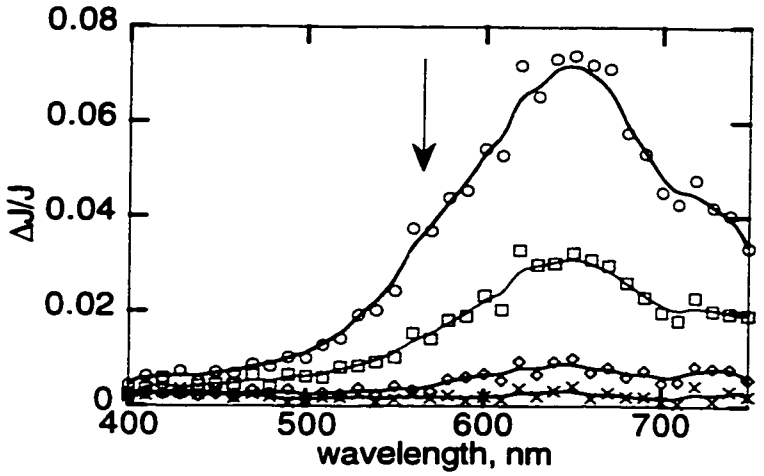

Figure 5-4: Transient absorption spectrum of 1-azaxanthone included in NaY (355 nm excitation), 0.72, 2.8, 7.92 and 15.7 μs after the laser pulse. The maximum at 650 nm corresponds to triplet 1-azaxanthone.

Distribution analysis of the triplet decay was performed on a fresh sample of 1-azaxanthone in NaY as well as an aged sample, to determine any changes in triplet lifetime that might occur upon aging. For the fresh sample, there are 3 components of the triplet lifetime, ranging from 0.24 μs, 1.2 μs and 6.0 μs. The band at 1.2 μs was the most intense. As the sample aged for ten days, the lifetime distribution changed. The main component of the triplet was then 0.26 μs, which is approximately five times shorter than the main component in the fresh sample. A second component occurs at 2.2 μs. The distribution plots for both samples are given in Figure 5.5. As illustrated in this figure, there is clearly a significant decrease in triplet lifetime that occurs upon sample aging. It should be noted that while the lifetimes between the fresh and the aged samples were different, the transient absorption spectra for the fresh and aged samples did not change.

The sample of 1-azaxanthone included in HY has a transient absorption spectrum with a λ_{max} that is red-shifted compared to the inclusion of 1-azaxanthone in NaY. The λ_{max} occurs at 740 nm, and this transient decays faster (~ 320 ns) than triplet 1-azaxanthone in NaY. A comparison of the transient spectra of 1-azaxanthone in HY and in an acid solution of 1N H_2SO_4 is given in Figure 5.6.

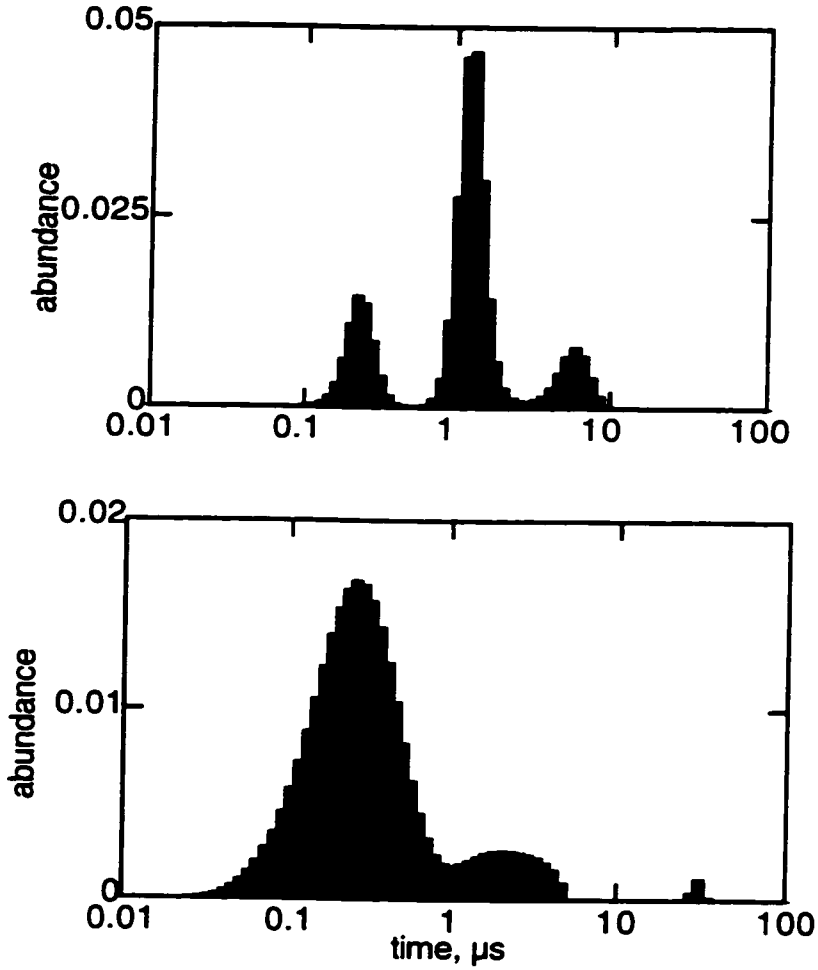

Figure 5-5: Triplet lifetime distribution plots for fresh (*top*) and aged (*bottom*) samples of 1-azaxanthone in NaY.

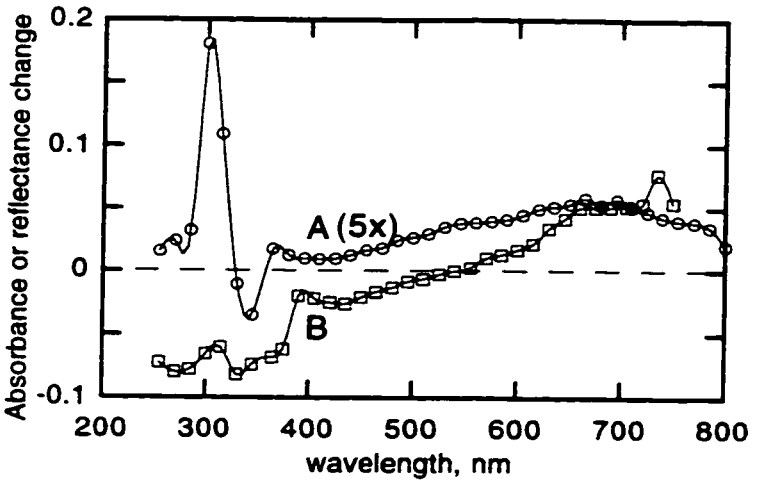

Figure 5-6: Transient absorption spectra of 1-azaxanthone in (A) a 1N H_2SO_4 solution (the absorbance has been magnified 5 times) and (B) in HY zeolite

5.2.4 *Inclusion of Hydrogen and Electron Donors into Cavities of NaY containing 1-Azaxanthone*

Triethylamine efficiently quenches triplet 1-azaxanthone in solution via an electron transfer mechanism with a rate constant of 1.1×10^{10} M^{-1} s^{-1}.[11] In water, the rate of triplet quenching by triethylamine is 7.4×10^{8} M^{-1} s^{-1}.[9] The transient absorption spectrum of 1-azaxanthone in water upon addition of triethylamine displays a red-shift in the λ_{max} (see Figure 5.7) which indicates the formation of the ketyl radical anion. In non-polar solvents, the species that is detected is the ketyl radical,[11] which has a maximum at 550 nm.

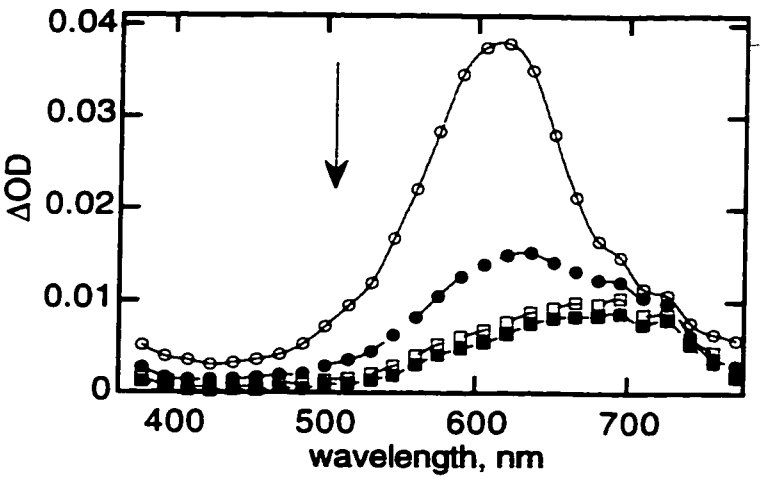

Figure 5-7: Transient absorption spectra of 1-azaxanthone in water with 3.22×10^{-4} M NEt_3. 0.72 μs, 2.88 μs, 8.48 μs and 15.8 μs after the laser pulse.

The addition of varying amounts of triethylamine to the supercages of NaY containing 1-azaxanthone (<S> ranging from 0 to 1.7 molecules of triethylamine) was performed. The decay traces of the samples were monitored at 660 nm, where triplet 1-azaxanthone absorbs. The decay traces for these samples are shown in Figure 5.8. As is depicted in the figure, a small amount of triethylamine results in a significant increase in the triplet lifetime with a kinetic trace that decays back to the pre-excitation level. As more triethylamine is added, there is a residual absorption in the decay trace (i.e., the kinetic trace does not decay back to the pre-excitation level), and a decrease in triplet lifetime. The transient spectra for these samples all have a broad absorption from 580 nm to 750 nm. The lifetime of triplet 1-azaxanthone as a function of triethylamine loading was determined by fitting the decay traces at 660 nm as two first order processes and reporting the main component. This process, in a qualitative manner, yields a definite pattern. The trend observed showed that upon addition of a small amount of triethylamine

(<S> = 0.6), there is a significant increase in the triplet lifetime, from 205 ns for a sample containing no triethylamine to ~ 795 ns. As more triethylamine is added, the triplet lifetime decreases to 260 ns and 315 ns for <S> = 1.3 and <S> = 1.7, respectively. It is important to note that the triplet lifetimes for 1-azaxanthone are always longer when triethylamine is present compared to a sample containing no electron donor.

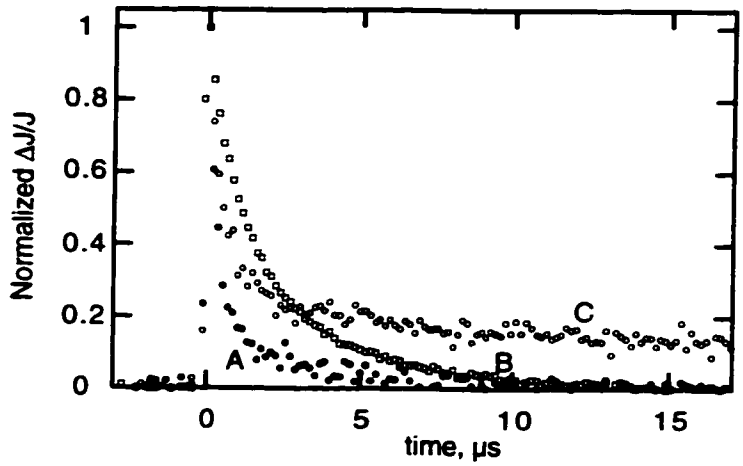

Figure 5-8: Normalized kinetic traces monitored at 660 nm using a 1 μs instrumental time scale for samples of 1-azaxanthone in NaY with (A) no triethylamine included, (B) 0.6 molecules of triethylamine per supercage and (C) 1.7 molecules of triethylamine per supercage.

Isopropanol, which is a good H donor, was also coincluded into the supercages of zeolite Y containing 1-azaxanthone. Varying amounts of isopropanol were added, with <S> ranging from 0 to 3 molecules of isopropanol per supercage. When a small amount of isopropanol is added (corresponding to 1 molecule per supercage), there is virtually no effect on the triplet lifetime of 1-

azaxanthone; the kinetic traces for the sample of NaY containing no isopropanol and 1 molecule of isopropanol per supercage are superimposable. As larger amounts of isopropanol are added to the cages (i.e. <S> = 2 to 3) there appears a small residual absorption in the kinetic trace monitored at 660 nm. The transient absorption spectra for these samples have an absorption peak which is blue-shifted compared to the sample containing no isopropanol, which persists after the triplet of 1-azaxanthone has decayed. Also present in the spectra is an absorption band at 390 nm. This trace at 390 nm contains a much larger residual absorption compared to the kinetic trace at 660 nm. Figure 5.9 has the two transient absorption spectra that are recorded at different delay times after the laser pulse for the sample of 1-azaxanthone in NaY that contains a large amount of isopropanol, to illustrate the different transients that are formed upon excitation. The decay traces corresponding to these two species are shown in Figure 5.10.

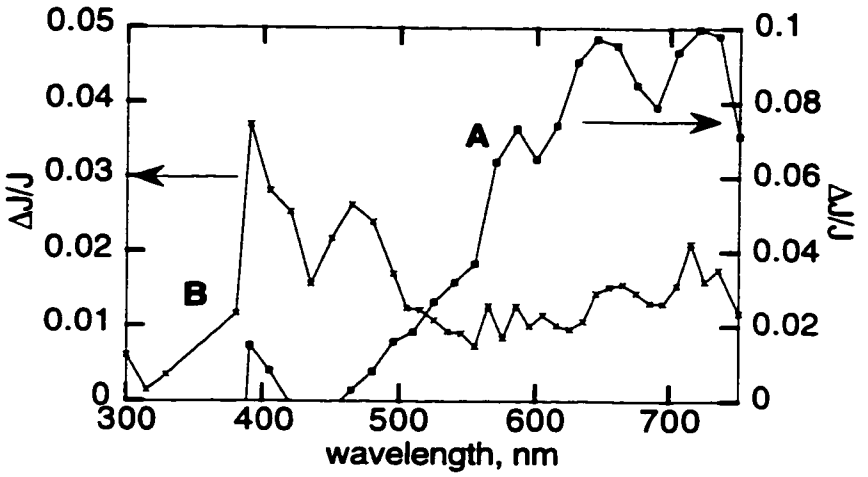

Figure 5-9: Transient absorption spectra of 1-azaxanthone included in NaY with large amount of isopropanol(<S> = 3). Spectrum A, 0.24 μs after the laser pulse; spectrum B, 158 μs after the laser pulse.

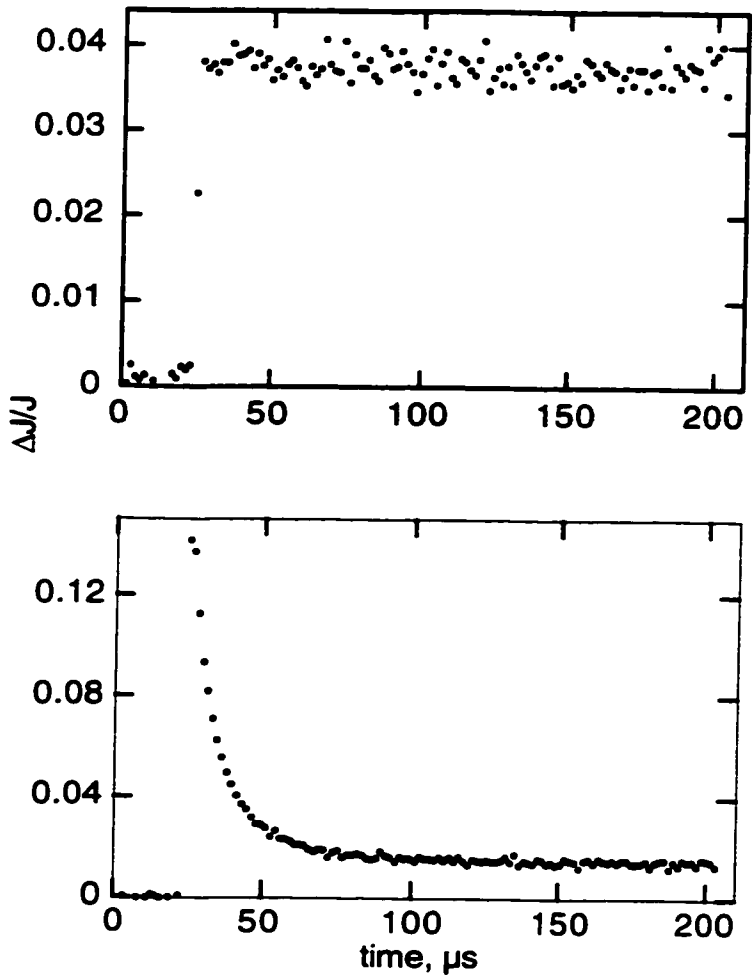

Figure 5-10: Decay traces monitored at (top) 390 nm and (bottom) 660 nm for a sample of 1-azaxanthone in NaY containing isopropanol (<S> =. 3). Note the differences in the residual absorption for the two decay traces.

5.3 Discussion

5.3.1 *Steady State Emission*

Based on previous studies on the photochemistry of 1-azaxanthone, it was determined that state switching from n,π* to π,π* occurs for the lowest lying triplet

state when the dielectric constant of the medium is greater than 60.[9] That is, excitation of 1-azaxanthone in acetonitrile results in a low lying triplet state having n,π^* character[11] whereas excitation in water leads to a low lying triplet state having predominantly π,π^* character.[9] The fact that state inversion occurs for 1-azaxanthone is also evident from low temperature phosphorescence studies. In an ethanol glass, the phosphorescence of 1-azaxanthone is very structured, with separation of bands occurring at ~ 30 cm^{-1}, corresponding to the carbonyl stretching vibration. This structured emisssion is indicative of an n,π^* triplet. Phosphorescence in a 2:1 ethylene glycol / water glass is not structured, suggesting that the lowest triplet state has significant π,π^* character.[9] Based on the onset of fluorescence emission and phosphorescence in aqueous media, the singlet-triplet energy gap is estimated at 6 kcal/mol.

Various studies have shown that the zeolite interior is very polar. The triplet-triplet absorption of xanthone in NaY occurs at ~ 600 nm,[2] the wavelength at which the triplet-triplet absorption of xanthone occurs in water. Other probes included in NaY, such as 1-pyrenealdehyde and p-dimethylaminobenzonitrile, have been used to show that the micropolarity of the zeolite cages is approximately 44D.[12,13] This is considered an average number, since the distribution of sites within the zeolite is expected to be non-uniform. The above argument indicates that the emission seen from 1-azaxanthone included in NaY is a combination of both n,π^* and π,π^* states. There is clearly also fluorescence and room temperature phosphorescence occurring, given the overlap between the emission in NaY and the fluorescence in water and low temperature phosphorescence in a MeOH/EtOH

glass. This is also supported by the small singlet-triplet energy gap of ~ 6 kcal/mol. Room temperature phosphorescence is not uncommon for solid state complexes; in fact, room temperature phosphorescence has been reported for benzophenone in solid cyclodextrin complexes[14] as well as in zeolites.[15,16]

5.3.2 *Effect of Aging on the Sample of 1-Azaxanthone included in NaY*

The triplet lifetime of 1-azaxanthone included in NaY decreases as the sample ages, from over 1 μs down to ~ 250 ns. This decrease in triplet lifetime must reflect migration of 1-azaxanthone through the supercages in order to reach a final equilibrium state. Molecules included in a zeolite are mobile, and movement throughout the cages occurs until a final equilibrium state is attained. Equilibration of a zeolite complex may take hours or even months,[17] depending on the substrate used. The inclusion of 1-azaxanthone in NaY, regardless of sample age, results in a triplet lifetime shorter than the lifetime of 6 μs reported in acetonitrile.[11] The triplet lifetime of 1-azaxanthone is also pH dependent, ranging from 154 ns at pH 2 to more than 11 μs at pH 7.[9] A list of the lifetimes of 1-azaxanthone in different media is given in Table 5.1. In light of the above facts, and what we have reported in Chapter 3 of the quenching of acid sites by pyridine, we conclude that the decrease in triplet lifetime of 1-azaxanthone upon inclusion in NaY and upon sample aging is due to quenching of the triplet by the zeolite acid sites. The shorter triplet lifetime of 1-azaxanthone upon sample aging reflects 1-azaxanthone experiencing a more acidic environment, due to migration of this

guest towards the acid sites. This correlates with the triplet lifetimes of 1-azaxanthone in different environments given in Table 5.1.

Table 5-1: Triplet lifetimes of 1-azaxanthone in different systems at room temperature

System	Triplet lifetime, μs
acetonitrile (a)	6.3
water, pH 2 (b)	0.154
water, pH 7 (b)	>11
NaY, fresh sample (c)	1.2 (main component), 0.24, 6
NaY, aged sample (c)	0.26 (main component). 2.2

(a) From reference[11]
(b) A phosphate buffer was used for these measurements.[9]
(c) Lifetimes were determined by distribution analysis. For a detailed description, see Chapter 2.

5.3.3 *Transients formed upon Addition of Hydrogen and Electron Donors*

Triethylamine is an efficient triplet quencher of aromatic ketones such as 1-azaxanthone, through an electron transfer mechanism. The quenching of 1-azaxanthone by triethylamine is somewhat reduced in water compared to organic solvents, by ~ 2 orders of magnitude.[9,11] The role of triethylamine in the supercages of NaY containing 1-azaxanthone is altered to some extent compared

to solution. This variation is dependent upon the loading level of triethylamine in the supercages. A small amount of triethylamine causes an increase in the triplet lifetime of 1-azaxanthone, with no other transient detected. This parallels what we have seen in Chapter 3 where a small amount of pyridine added to the supercages of NaY containing xanthone resulted in a significant increase in the triplet lifetime. To confirm this, pyridine was also included in a sample of NaY containing 1-azaxanthone, and the triplet lifetime of 1-azaxanthone was measured as a function of pyridine concentration. It was found that the triplet lifetime increases when a small amount of pyridine is present in the supercages. Therefore, small amounts of triethylamine in NaY acts as a Lewis base, interacting with the acid sites in the supercages. As a larger amount of triethylamine is added, there is a residual absorption and a broadening of the triplet-triplet absorption peak upon irradiation. The residual absorption indicates the presence of an additional species, which in this case is the formation of the ketyl radical anion of 1-azaxanthone. This occurs when triethylamine acts as an electron donor. (Note that the ketyl radical anion also has some absorbance at 660 nm, resulting in the residual absorption being detected in the triplet decay trace of 1-azaxanthone). Therefore, triethylamine acts as a base, quenching the acid sites in the zeolite; once the acid sites are quenched, triethylamine then takes on its role as electron donor.

The addition of a small amount of isopropanol does not have any significant effect on the triplet lifetime of 1-azaxanthone. There is not enough isopropanol present in close proximity to the 1-azaxanthone triplet

to undergo photoreduction, and isopropanol is not a basic molecule. Therefore, there is no quenching of the zeolite acid sites, as occurred with triethylamine. This result illustrates that changes in the local environment or microviscosity of the zeolite supercage do not play a major role in determining the carbonyl excited state lifetime of a guest molecule when a basic spectator is added. Higher loadings of isopropanol results in a small residual absorption at 660 nm, which is assigned to the formation of the ketyl radical (Scheme 5.1). The small residual absorption is surprising and indicates a small yield of ketyl radical being formed from the triplet. This was an unexpected result in view of the fact that 1-azaxanthone in organic solvents photoreduces quite efficiently, even more so than benzophenone.[11] The reason for the small amount of ketyl radical formation is seen in the transient absorption spectrum. The absorbance peak at 390 nm, which persists after the triplet has decayed, is assigned to the cyclohexadienyl radical of 1-azaxanthone. The kinetic trace at 390 nm is virtually non-decaying, and this extremely long lifetime is consistent with the assignment of a cyclohexadienyl radical, since these species are highly unreactive. This transient dominates the absorption spectrum, and has been observed when 1-azaxanthone was included in micelles.[9] The formation of either the ketyl radical or the cyclohexadienyl radical is dependent upon the lowest triplet character of 1-azaxanthone. For ketyl radical formation, the lowest triplet state of 1-azaxanthone must have n,π^* character, whereas π,π^* character is required for formation of the cyclohexadienyl radical. Scheme

5.2 summarizes the process that occur upon high loadings of triethylamine and isopropanol to the cages of NaY containing 1-azaxanthone.

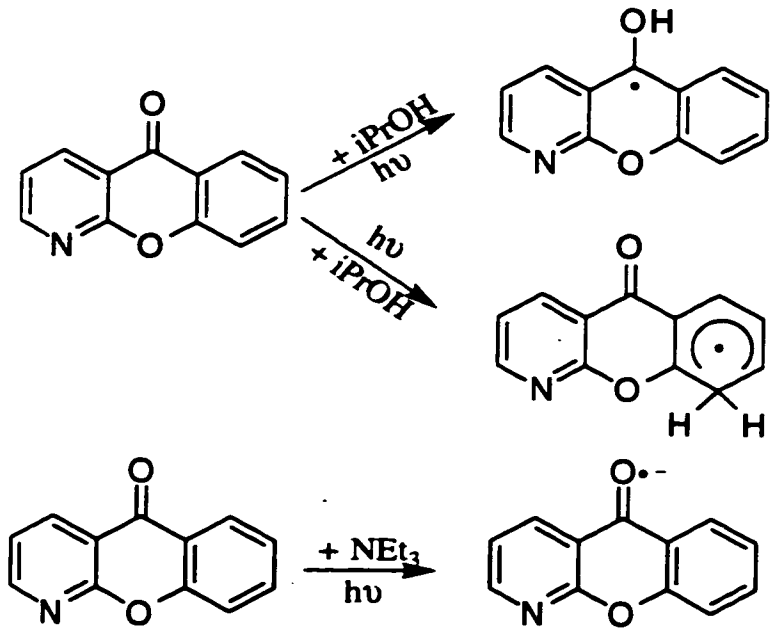

Scheme 5-2: Processes that occur upon excitation of 1-azaxanthone in the presence of electron or H-donors.

5.3.4 *Transient Formed Upon Inclusion in HY*

The transient that is formed upon inclusion of 1-azaxanthone in the acidic zeolite HY is the pyridinium cation species. It has previously been reported that in the case of 1-azaxanthone as well as for phenyl-3-pyridyl ketone,[7] the pyridinium cation species is characterized by its red-shift in the transient absorption spectrum relative to the triplet, and also by its shorter lifetime, which is seen for 1-azaxanthone in HY. This is also confirmed by the similarity in the fluorescence and

the transient absorption spectrum of 1-azaxanthone in 1N H_2SO_4, as well as by IR spectroscopic studies.

5.4 Conclusions

Free radical reactivity of 1-azaxanthone in zeolites proved to be more moderate than originally anticipated. The mixing of n,π^* and π,π^* states of 1-azaxanthone that occurs in very polar environments, such as NaY, results in photochemical reactions stemming from both states, i.e. formation of ketyl radical and cyclohexadienyl radical when a good H-donor, such as isopropanol, is present in the supercages. The domination of the transient absorption spectrum by the cyclohexadienyl radical indicates, in a qualitative manner at least, that the formation of the transient from the π,π^* triplet state is the predominant pathway in the H-abstraction reaction. Addition of small amounts of base, such as triethylamine, results in a significant increase in the triplet lifetime for 1-azaxanthone, due to initial neutralization of acid sites in the zeolite. This does not occur when isopropanol is added, since it is not a basic molecule.

The inclusion of 1-azaxanthone in HY results in formation of the pyridinium cation upon excitation at 355 nm. This was confirmed by both LFP, fluorescence and IR spectroscopies. The formation of this transient stems from the π,π^* triplet state.

5.5 Experimental

Zeolite NaY (Linde molecular sieves LY-52) and triethylamine were obtained from Aldrich and used as received. Isopropanol (HPLC grade)

was obtained from VWR Scientific. HY was a gift from the Instituto de Tecnología Química in Valencia, Spain. 1-Azaxanthone was purchased from Lancaster and recrystallized twice from ethanol prior to use.

Preparation of zeolite inclusion compounds

Zeolite inclusion compounds were prepared as described in Chapter 3. Triethylamine and isopropanol inclusion into the zeolite containing the ketone was accomplished by placing the dry zeolite complex into a closed container containing a small amount of the respective liquid and allowing the free diffusion into the supercages. The amount of triethylamine or isopropanol included was determined by the resulting change in weight of the inclusion compound. From the amount of guest included, the occupancy number, <S> can be determined.

Instrumentation

UV-Visible absorption spectra were recorded on a Cary 1E spectrometer. Steady-state emission spectra were recorded on a Perkin Elmer LS-50 luminescence spectrometer. IR spectra were obtained at room temperature using greaseless quartz cells fitted with CaF_2 windows in a Nicolet model 710 FTIR spectrophotometer controlled by a work station. Wafers (10 mg) were pressed into disks and typically outgassed under 10^{-2} Pa at 200°C for about one hour before recording the spectra.

Laser Flash Photolysis and Lifetime Distribution Analysis

Details of the setup and how to perform distribution analysis are given in Chapter 2.

5.6 References

(1) Wilkinson, F.; Willsher, C. J.; Casal, H. L.; Johnston, L. J.; Scaiano, J. C. *Can. J. Chem.* **1986**, *64*, 539.

(2) Scaiano, J. C.; Kaila, M.; Corrent, S. *J. Phys. Chem. B* **1997**, *101*, 8564.

(3) Turro, N. J. *Pure Appl. Chem.* **1986**, *58*, 1219.

(4) Consuelo Jimenez, M.; Miranda, M. A.; Tormos, R. *J. Photochem. Photobiol. A: Chem.* **1995**, *86*, 225.

(5) Joy, A.; Scheffer, J. R.; Corbin, D. R.; Ramamurthy, V. *Chem. Commun.* **1998**, 1379.

(6) Pitchumani, K.; Warrier, M.; Cui, C.; Weiss, R. G.; Ramamurthy, V. *Tet. Lett.* **1996**, *37*, 6251.

(7) Elisei, F.; Favaro, G.; Ortica, F. *J. Chem. Soc. Faraday Trans.* **1994**, *90*, 279.

(8) Scaiano, J. C. *J. Am. Chem. Soc.* **1980**, *102*, 7747.

(9) Martinez, L. J.; Scaiano, J. C. *J. Phys. Chem., B.*, **1998**, *103*, 203.

(10) Parry, E. P. *J. Catal.* **1963**, *2*, 371.

(11) Scaiano, J. C.; Weldon, D.; Pliva, C. N.; Martinez, L. J. *J. Phys. Chem., A* **1998**, *102*, 6898.

(12) Ramamurthy, V.; Sanderson, D. R.; Eaton, D. F. *Photochem. Photobiol.* **1992**, *56*, 297.

(13) Ramamurthy, V.; Eaton, D. F. *Proceedings of the 9th International Zeolite Conference*; Butterworth-Heinemann: Boston, 1992, pp 587.

(14) Barra, M.; Bohne, C.; Scaiano, J. C. *Photochem. Photobiol.* **1991**, *54*, 1.

(15) Ramamurthy, V.; Caspar, J. V.; Corbin, D. R. *Tet. Lett.* **1990**, *31*, 1097.

(16) *Photochemistry in Organized and Constrained Media*; Ramamurthy, V., Ed.; VCH Publishers Inc.: New York, 1991.

(17) Cozens, F. L.; Régimbald, M.; García, H.; Scaiano, J. C. *J. Phys. Chem.* **1996**, *100*, 18165.

6. Photophysical Properties of Transparent PDMS-Zeolite Films

6.1 Introduction

Diffuse reflectance techniques have provided a great deal of information on the characterization of solid opaque materials. The basis for diffuse reflectance techniques is the monitoring of diffusely reflected light, instead of transmitted light as is required for transmission techniques. The development of diffuse reflectance laser flash photolysis was a significant breakthrough in terms of the ability to study time-resolved phenomena of solid, opaque materials such as clays, cyclodextrins and zeolites. This allowed for the characterization of transients formed upon excitation of solid materials, along with their decay kinetics. As highly informative and effective as this technique is, there are a few drawbacks, as with any diffuse reflectance technique. Some molecular properties are either unattainable or significantly less quantitative using diffuse reflectance laser flash photolysis, such as quantum yields. Quantification in this mode is difficult, because of the non-linear relationship between concentration and response intensities. This also leads to the inability to quantify ground state extinction coefficients when measuring ground state absorption spectra.

There are fairly recent literature reports on the dispersing of zeolites (containing no guest molecules) into polydimethylsiloxane[10,8] (PDMS) or polyimide[9] (PI) polymers. This has led to the formation of transparent zeolite films. These reports have focussed on the passage of hydrocarbons and

ethanol/water vapours across the membrane, to determine the flux and selectivities of the vapours for various zeolites incorporated into the films. In all cases, the incorporation of zeolites into the PDMS polymer leads to a reduced swelling of the membrane, due to the cross-linking action of the zeolite.[10,9] Incorporation of zeolites into the PI polymer resulted in weaker membranes (less cross-linking) being produced.[9]

Other reports in the literature have examined the growth of zeolite films onto metal[7] or glass substrates.[12] The type of metal used, or the roughness of the glass surface, as well as the preparation conditions, have an effect on the resulting film thickness and density.

The examples mentioned above look solely at 'empty' zeolite films (i.e. zeolites containing no guest molecules). While these materials may have many applications, the use of organic molecules embedded into the zeolites as the doping materials for the polymer may in fact lead to other new potential applications.

We have prepared zeolite films using a PDMS membrane, with the zeolite containing an organic cationic guest molecule. These materials are attractive candidates to study using laser flash photolysis techniques because the PDMS backbone does not contain any chromophores that will interfere in the UV-Vis region of the spectrum. In addition, these films are transparent, resulting in characterization of the transients formed upon excitation, as well as decay kinetics, using transmission techniques. The apolar nature of the PDMS backbone may also provide a highly apolar surrounding for the dispersed zeolite complexes,

which may further protect the encapsulated organic molecule from oxygen. The ability to use transmission techniques on these new materials allows for the quantification of certain photophysical properties that were unattainable using diffuse reflectance techniques, such as extinction coefficients and quantum yields. This will also allow for the first direct comparison between the properties of organic dye molecules in solution and included within zeolites. This novel material may also contain new possibilities for further applications that have been limited up to this point by the lack of transparency of the opaque zeolite solid complexes and the low mechanical resistance of self-supported wafers.

We could only find one report of using transmission techniques on a zeolite. This involved single layers of 40 μm NaY crystals on a CaF_2 support, and was used to study the absorption profile of an alkene/O_2 charge transfer contact complex.[11] This has a limited application because the usual crystal size of zeolites synthesized by common hydrothermal techniques is smaller than 1 μm. We could find no reports, however, on the characterization of photophysical properties of organic guest molecules included in zeolite films using time-resolved transmission techniques.

This chapter will examine the photophysical properties of organic-embedded zeolite films using transmission spectroscopies. The films that will be discussed contain the cations shown below; xanthylium cation (X^+) in HZSM-5, 1,5-diphenylpentadienylium cation (DPP^+) in HZSM-5, (trimethoxy phenyl)tritylium cation (TMT^+) in HY and malachite green (MG^+) in HY. These cations were generated in the zeolite by using functional group transformation of a precursor

molecule (X^+ in HZSM-5 and DPP^+ in HZSM-5) or through a synthetic route that involves new C-C bond formation (ship in a bottle synthesis) when the size of the cation is larger than the window diameter of the zeolite (TMT^+ in HY and MG^+ in HY).

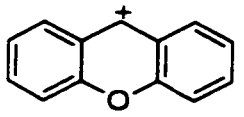

X^+

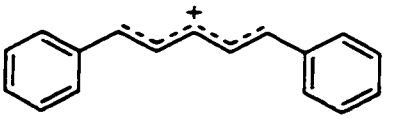

1,5-DPP^+

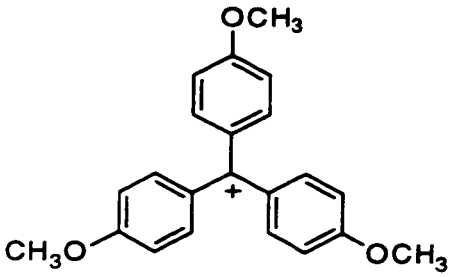

TMT^+

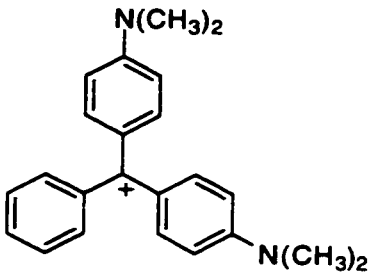

MG^+

The zeolites containing these organic cations have previously been studied using diffuse reflectance techniques. It was demonstrated that the organic cations included in the zeolite pores are persistent cations, and are very stable due to the electrostatic field of the zeolite interior as well as by the geometrical restraints imposed by the zeolite cavities. The fluorescence, ground state and transient absorption spectra of the zeolite films will be compared to the values that have been reported for the corresponding opaque powders. The extinction coefficients

of the organic cations included in the zeolite will be measured in the zeolite films, and compared to solution values where possible. For quantum yield determination, a zeolite film of xanthone in NaY was prepared in order to determine the quantum yield of triplet formation.

6.2 Results

6.2.1 *Measurement of Extinction Coefficients*

The extinction coefficients of the organic cation included in the zeolite dispersed in a PDMS membrane were measured using the ground state absorption spectra obtained by transmission spectroscopy. Illustrative examples of the ground state absorption spectra obtained are shown in Figure 6.1. The measurements were carried out as follows: from the Beer-Lambert equation, the path length, l, is equal to the film thickness (which was measured and found to be uniform). The concentration of the dye in the film, which is equal to the number of moles divided by the film volume (area of film x thickness) is substitued into the Beer-Lambert equation. This yields an expression where a plot of the absorbance versus the number of moles of guest divided by the area of the film yields a slope of ε. The linearity of these plots, in accordance with the Beer-Lambert law, are seen in Figure 6.2 for MG^+/HY and X^+/HZSM-5. A linear relationship between the thickness of the film and the absorption in the UV-Vis spectrum has also been observed. What is truly remarkable is that a comparison of the log ε values

obtained for the organic cations in solution and the organic cations embedded in the zeolite film are equal, within experimental error.

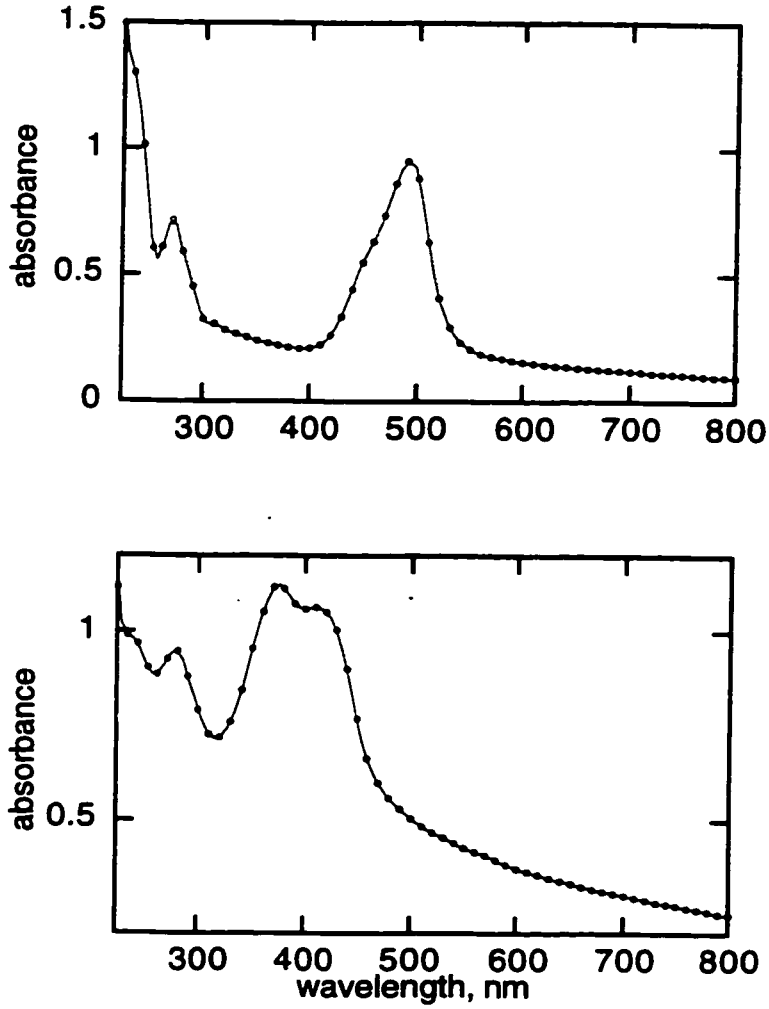

Figure 6-1: Ground state absorption spectra of PDMS film containing TMT^+/HY. Composition of film: 30 mg of TMT^+/HY (5% TMT^+ loading) in 1 g of polymer (*top spectrum*) and X^+/HZSM-5, film composition is 40 mg of X^+/HZSM-5 (5% X^+ loading) in 1 g of polymer (*bottom spectrum*).

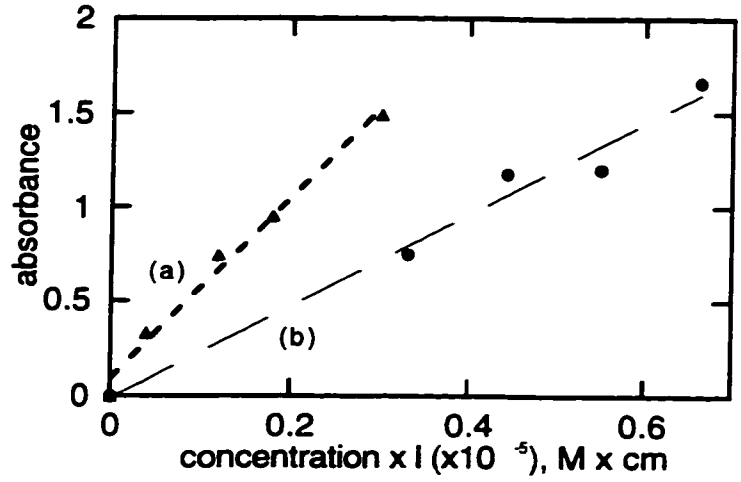

Figure 6-2: Determination of ε for organic cation included zeolites dispersed within a PDMS film. (a) MG^+/HY and (b) X^+/HZSM-5. See text for description of method used to obtain ε values.

6.2.2 *Fluorescence Spectroscopy*

The steady state fluorescence spectra of the zeolite films were also recorded and compared to the spectra of the solid zeolite complex. These values matched very well, and are reported in Table 6.1 for both the film samples and the opaque zeolite complexes. Representative fluorescence spectra for the films of DPP^+ in HZSM-5 and MG^+ in HY are given in Figure 6.3.

Table 6-1: Fluorescence data for solid zeolite[a] and zeolite film samples. For the film samples, the loading of the dye is 5% and the zeolite loading in the polymer is 15%.

	solid λ_{max} (nm)	film λ_{max} (nm)
DPP^+/HZSM-5	575, 615 (sh)	575, 615 (sh)
TMT^+/HY	570	570
MG^+/HY	620	640
X^+/HZSM-5	495 520	495 520

[a] Data taken from previous work[1,4,5]

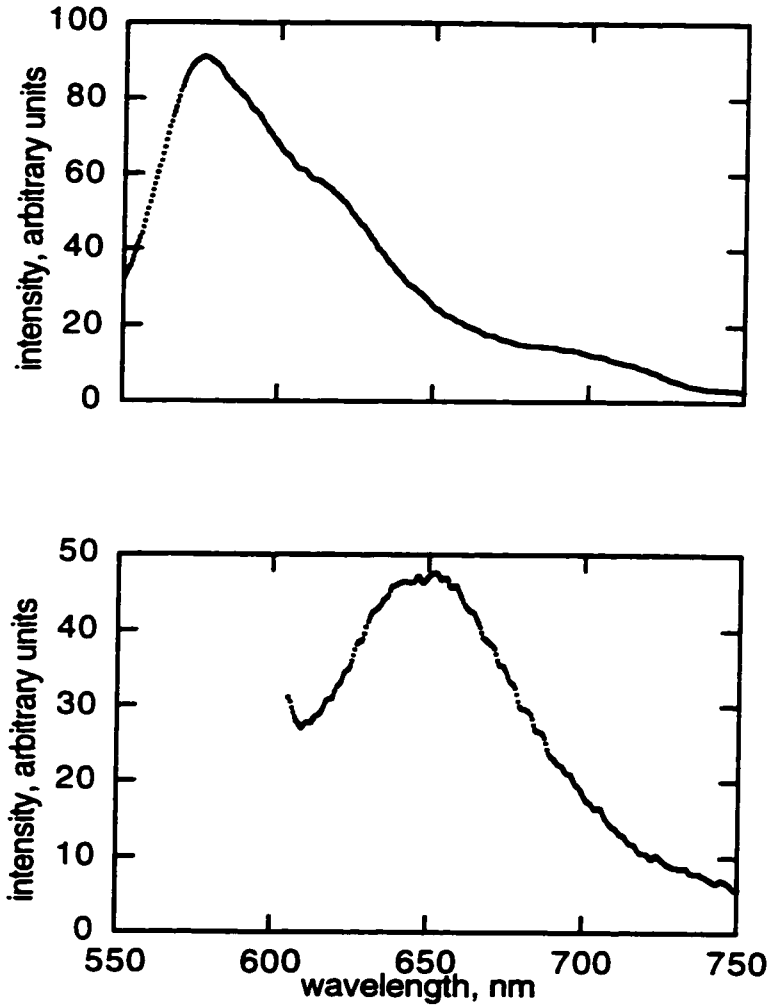

Figure 6-3: Fluorescence spectra of PDMS films containing DPP^+/HZSM-5 using a λ_{ex} of 515 nm (*top*) and MG^+/HY using a λ_{ex} of 590 nm (*bottom*). For both films, the loading of the organic in the zeolite is 5%, and the zeolite loading in the polymer is 15%.

6.2.3 *Laser Flash Photolysis*

6.2.3.1 Films of xanthone included in NaY

A zeolite film containing xanthone included in the supercages of NaY was also prepared, for the purposes of measuring the quantum yield of triplet formation. The transient absorption spectrum, measured using transmission laser flash photolysis, displays the triplet-triplet absorption peak at 600 nm, which is the same as the λ_{max} for the solid opaque sample of xanthone in NaY (see Chapter 3). In order to determine the quantum yield of triplet formation, two samples of a xanthone-zeolite film were prepared. In the first film sample prepared, the zeolite NaY was calcined to remove all water, while in the second film sample prepared, the zeolite was not calcined prior to use, and thus its supercages are filled with water. This leads to film samples such that in the first case, xanthone is included inside the supercages of NaY, whereas in the second case, xanthone is located on the exterior surface of the zeolite. Both film samples contain an equal amount of xanthone and zeolite. The triplet decay of xanthone was monitored at 600 nm, and the decay traces for these two film samples are shown in Figure 6.4. The signal to noise ratio is poorer in these samples compared to the other film samples used. The difference lies in the sample preparation. In this case, the film was prepared in the interior of a 3x7 mm^2 laser cell, to ensure that the film thicknesses were identical for both samples. This leads to much thicker films, resulting in more scattering than is encountered when

thinner film samples are used. In any event, it is evident from Figure 6.4 that the two xanthone film samples yield superimposable decay traces.

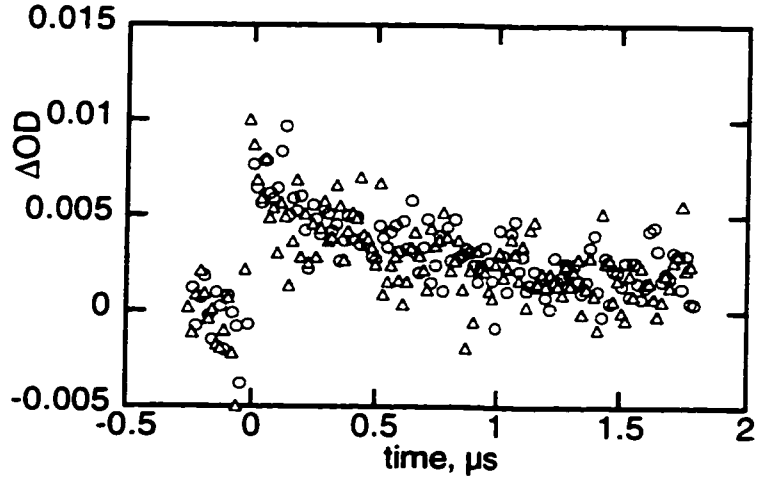

Figure 6-4: Transient decay trace monitored at 600 nm for a film of xanthone and NaY. Open circles corresponds to xanthone included in NaY and open triangles corresponds to xanthone located on the exterior surface of NaY. The amount of xanthone with respect to zeolite for these film samples is 2%, with a 1% loading of zeolite in the polymer.

To test the permeability of gases across the membrane into the zeolite cavities, a film sample of xanthone in NaY was purged with N_2 in a quartz cell for one hour. Excitation of this sample led to detection of the long lived triplet of xanthone ($t_{1/2}$ > 50 μs) and a λ_{max} indicative of zeolite inclusion (see Figure 6.5). This sample was then purged with O_2 for different periods of time, ranging from 0.5 to 3 hours. This led to partial quenching, with a minor reduction in triplet lifetime. This is illustrated in Figure 6.6.

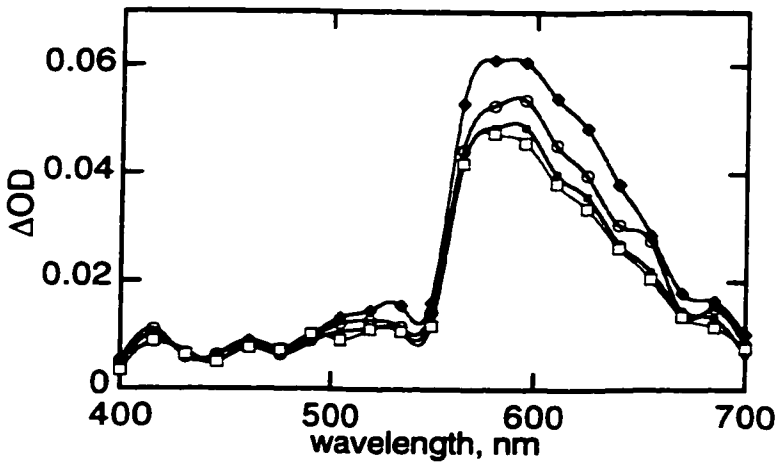

Figure 6-5: Transient absorption spectra of film sample of xanthone in NaY that has been purged with N_2. Excitation wavelength is 355 nm. The time windows were taken 7.2, 28, 81.6 and 157 μs after the laser pulse.

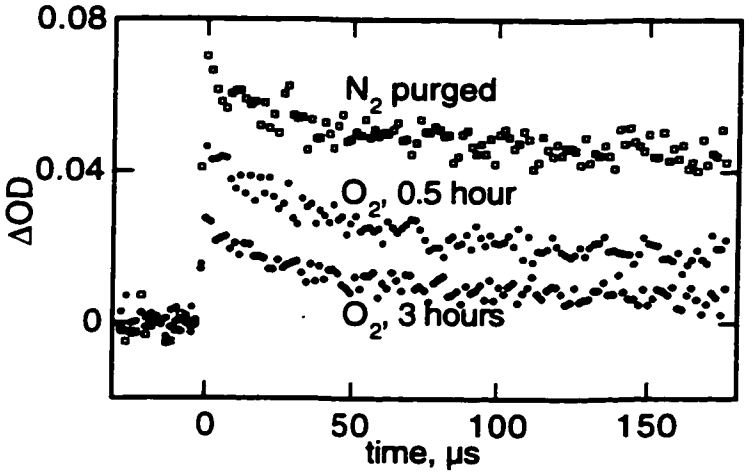

Figure 6-6: Triplet decay traces for film samples of xanthone in NaY upon purging with N_2 or O_2. The time scale used was 10 μs per division.

These experiments were repeated over the course of several days and were reproducible. These films of xanthone in NaY were reexamined after a period of a few months, and it was found that the xanthone triplet was almost completely quenched upon purging with O_2 for 20 minutes (see Figure 6.7). Upon purging the

sample with N_2, the λ_{max} of the triplet of xanthone shifted to 610 nm, indicative of a less polar environment. For this particular film sample, the included organic molecule is not fully protected from gaseous molecules that permeate the membrane.

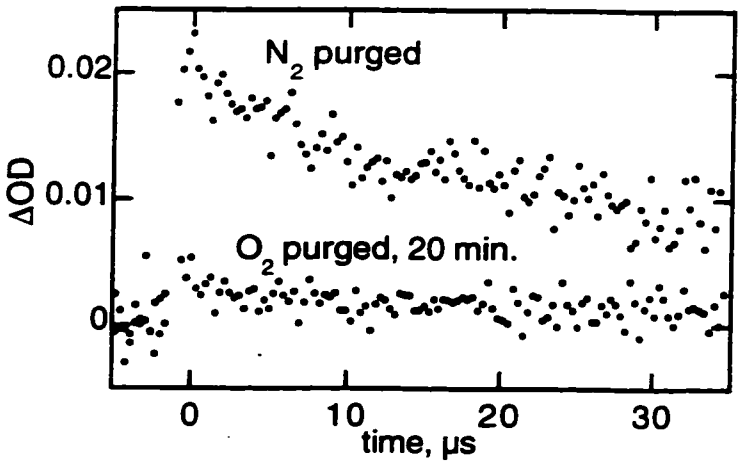

Figure 6-7: Triplet decay traces for aged film samples of xanthone in NaY upon purging with N_2 or O_2. The time scale used was 2 μs per division.

6.2.3.2 Film Samples of Organic Cations included in Zeolites

Laser flash photolysis was performed on all the cation-included zeolite film samples. The λ_{max} values obtained for the film samples are compared to those obtained using diffuse reflectance laser flash photolysis on the opaque solid samples. These values, along with the assignment of the transient, are given in Table 6.2. As is seen in the table, there is a very good correlation between the λ_{max} values taken in diffuse reflectance and transmission modes. The transient

absorption spectra for the film and opaque solid samples containing HZSM-5 zeolites are shown in Figure 6.8, while the transient spectra for the samples containing the HY zeolites are shown in Figure 6.9. While the λ_{max} values correlate very well between the film samples and the opaque solid samples, there are some noticeable differences in the transient absorption spectra. These include changes in the relative intensity of the peaks, as occurs for the sample of X^+ in HZSM-5. For the film sample, the absorption in the 500 nm region is very weak compared to that observed in the solid sample. For the sample of TMT^+ in HY, the film also displays a weaker absorption in the long wavelength region compared to the solid sample.

All of the film samples show a negative absorbance peak, corresponding to a bleaching effect. For the samples of X^+ in HZSM-5 and TMT^+ in HY, the bleaching was observed whether the monitoring of the transient absorption spectra was in transmission or diffuse reflectance mode, for films or solid samples, respectively. This is seen in Figures 6.8 and 6.9. In contrast, for the film samples of MG^+ in HY and DPP^+ in HZSM-5, a bleaching effect was not observed in the diffuse reflectance of the solid samples, but was in fact detected for the film samples. The bleaching in the case of MG^+ in HY is not as pronounced as it is for the sample of DPP^+ in HZSM-5.

The kinetics of transient decay for the film samples were very different than for the solid opaque samples. An observation made in all of the film samples containing organic cations is that the kinetic traces do not decay back down to the

preexcitation level. The kinetic traces for the film samples and the solid samples are shown in Figure 6.10 for the samples of MG^+ in HY and DPP^+ in HZSM-5.

Table 6-2: Comparison of transient absorption λ_{max} and rate constants for solid zeolite[a] and zeolite film samples.

	solid		film	
	λ_{max}, nm	k_{obs} (s^{-1})	λ_{max}, nm	k_{obs} (s^{-1})
DPP^+/HZSM-5	610, triplet	10^4	610, triplet 550, bleaching	~10^3
TMT^+/HY	380, 440 640 (triplet) 500 bleaching	$2x10^4$	370, 410, 520-640 490, bleaching	$1x10^4$
MG^+/HY	480, 530 triplet	$1.2x10^4$	470, 530 (sh) 610, bleaching	$4x10^3$
X^+/HZSM-5	300, 520-570 triplet 340 (radical) 370 bleaching	$2x10^4$	300, triplet 330, radical 375, bleaching	$3x10^3$

[a] Data taken from previous work[1,4,5]

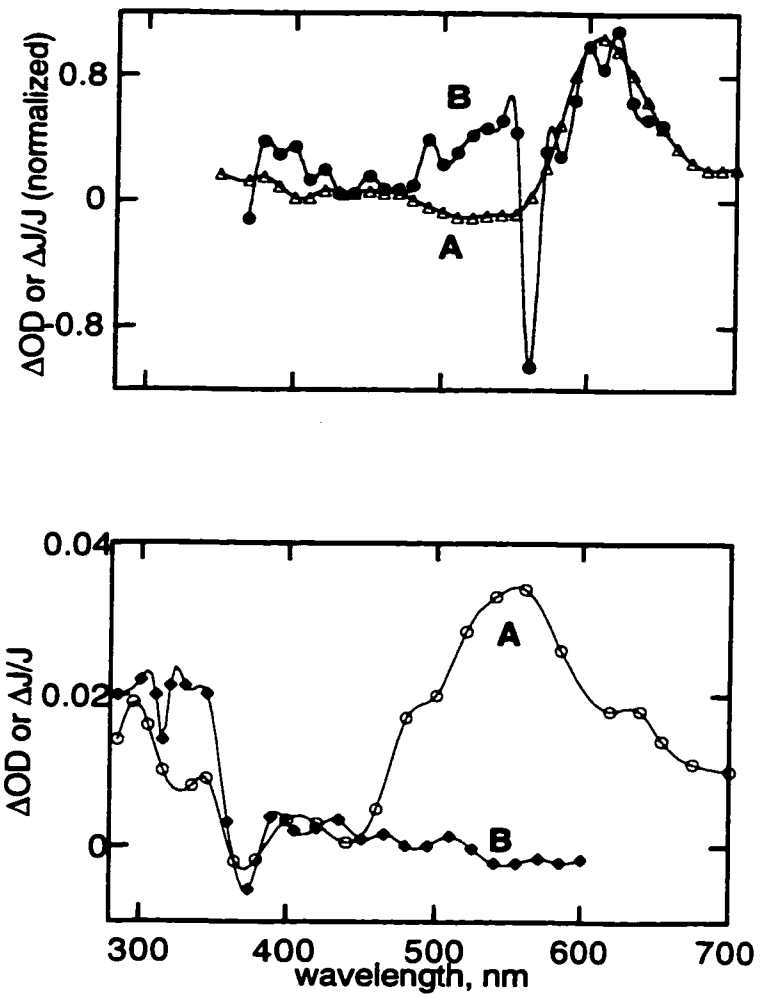

Figure 6-8: (*top*) Transient absorption spectra for DPP^{+} in HZSM-5 in (**A**) solid state, 6.4 μs after the laser pulse and (**B**) transparent film, 12 μs after the laser pulse.

(*Bottom*) Transient absorption spectra for X^{+} in HZSM-5 in (**A**) solid state,1 μs after the laser pulse and (**B**) transparent film, 24 μs after the laser pulse. The excitation wavelength for the solid is 355 nm and for the film is 308 nm. For both films, the loading of the organic cation in the zeolite is 5%.

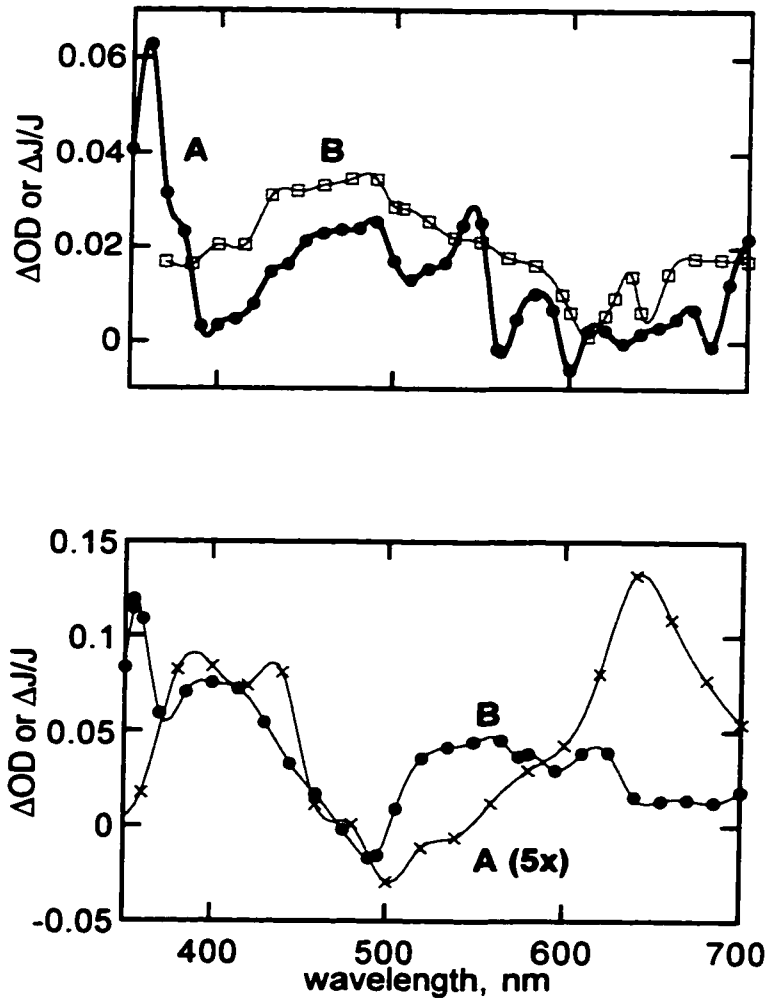

Figure 6-9: (*top*) Transient absorption spectra for MG^+ in HY in (**A**) solid state, 1 μs after the laser pulse and (**B**) transparent film, 24 μs after the laser pulse. Excitation wavelength in both cases is 355 nm.

(*Bottom*) Transient absorption spectra for TMT^+ in HY in (**A**) solid state, 1 μs after the laser pulse, upon 266 nm excitation, absorbance has been magnified 5x. (**B**) transparent film, 18 μs after the laser pulse upon 308 nm excitation. For both films, the loading of the organic cation in the zeolite is 5%.

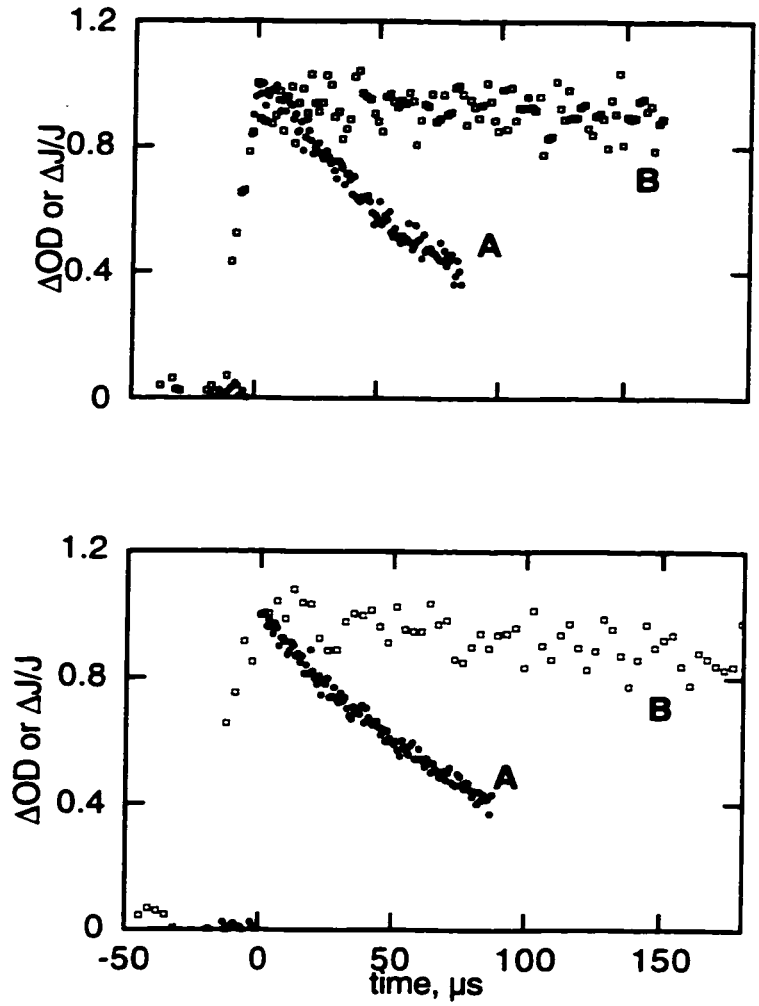

Figure 6-10: Normalized transient decay trace in (**A**) solid zeolite sample and (**B**) transparent zeolite film for (*top*) MG^+/HY monitored at 500 nm and (*bottom*) DPP^+/HZSM-5 monitored at 600 nm. Note that the lifetime of the transient in the film sample is considerably longer compared to that for the solid state sample.

6.3 Discussion

6.3.1 Comparison of Extinction Coefficients Measured in Films and in Solution

The transparency of the zeolite film and the accordance found with the Beer-Lambert law made it possible to determine the extinction coefficients of the organic cations included within zeolite cavities for the first time. These values were compared to the extinction coefficients of the organic cations in solution. The good correlation that resulted between the log ε values of the two sets of data indicates that confinement of these molecules in zeolite cavities does not significantly alter their molecular properties; that is, the frontier molecular orbitals of the guest, along with its preferred conformation, does not significantly change upon inclusion. This is also illustrated by the similarities in the ground state absorption spectra. Thus, we are measuring a physical property that is intrinsic to the organic chromophore. This method allows for the further application of determining the extinction coefficient of species that are not persistent in solution, but are stabilized within the zeolite interior.

6.3.2 *Determination of the Quantum Yield of Triplet Formation*

Two film samples of xanthone in NaY were prepared. The first sample contained xanthone included in the supercages of NaY, whereas the second sample had xanthone located on the outer surface. The certainty that xanthone is located on the outer surface of the zeolite is due to the fact that the zeolite in this

case was not calcined prior to use. It has been reported[13] that when zeolite cavities are filled with water, the incorporation of a guest molecule into the cavities cannot occur, resulting in the guest molecule residing on the zeolite exterior. The two samples contain the same amount of zeolite and xanthone, to ensure that the refractive index was similar in both samples. Therefore, any change in triplet formation between the two samples would reflect the photophysical properties of the organic guest and not simply a result of differences in sample content. An assumption that is made, which is a reasonable assumption based on the results presented above, is that the extinction coefficient of the triplet-triplet absorption of xanthone is the same on the zeolite surface as it is inside the zeolite cavities. The validity of this assumption and the superimposable triplet decay traces obtained for these two sets of samples (see Figure 6.4) indicates that the quantum yield of intersystem crossing is also the same within experimental error. This, once again illustrates that a photophysical property, the quantum yield of triplet formation of xanthone, is not greatly influenced by its confinement within the supercages of NaY.

6.3.3 Comparison of the Time-Resolved Absorption of Zeolite Films and Solid Zeolite Complexes

Some differences were noted between the transient absorption spectra of the zeolite films and solid zeolite complexes, in terms of relative peak intensities.

For the sample of X^+ included in HZSM-5, there is a weaker absorbance in the 500 nm region for the film sample compared to the solid sample. A similar difference was noted when comparing the transient spectra of the solid zeolite complex to solution. For example, there is a very weak absorption in the 540 nm region for the triplet state of substituted X^+ in homogeneous solution.[6] Thus, while an enhancement of the triplet signal at 540 nm occurs upon zeolite inclusion, this effect diminishes upon preparation of a PDMS film, which is stored under air. The weaker absorption seen in the longer wavelength region for the film sample of TMT^+ in HY may be due to O_2 quenching in the air-saturated films. The long wavelength band, which is assigned to the triplet of TMT^+, is known to be quenched by O_2 for the solid zeolite sample.

The bleaching effect that is seen in the film samples corresponds to ground state depletion. What is surprising is that for the samples of MG^+ in HY and DPP^+ in HZSM-5, the bleaching effect is only seen in the film samples, and not in the solid zeolite complexes. The bleaching is not as pronounced in the sample of MG^+ in HY, due to the transient absorbing in this region. The disappearance of the ground state absorption bands must occur during the laser pulse and is considered instantaneous on our timescale. Therefore, the difference that is seen between the diffuse reflectance and transmission mode may reflect the fact that the response time in diffuse reflectance is longer than in transmission, and thus not fast enough, in some some cases, to adequately follow the bleaching of the ground states. For each film sample, the recovery of the bleaching matches the decay of the excited states.

The differences in the kinetics are truly remarkable. The long lifetimes of the transients in the film samples indicate that there is a residual population of transients that persists longer than the timescale monitored on the nanosecond laser flash photolysis system. The lifetimes of the transients measured in the film samples are longer compared to those measured in the solid zeolite complex. It is well known that encapsulation of a guest molecule within zeolite cavities often results in the transient generated having a much longer lifetime compared to the same species measured in solution.[2,3] Some of the factors responsible for this phenomenon are the restricted motion and mobility of the guest molecule, rendering it unable to readily achieve the conformation required for decay as well as the greater protection that encapsulation in a zeolite achieves from O_2 ,which is an excellent triplet quencher. By dispersing the zeolite complex in a polymer matrix, the transients formed upon excitation are longer lived, at least for these organic cationic guests, due to an enhancement of the effects mentioned above.

6.3.4 *Stability of Zeolite Films*

The effect of consecutive purging of a film sample of xanthone included in NaY by N_2 and O_2 were reproducible over a period of a few days. Within this time period, it was found that purging the film sample with N_2 led to a long lived triplet, and subsequent purging with O_2 resulted in only a partial quenching of the triplet. The λ_{max} for both cases was the same, and indicative of inclusion of xanthone in NaY. Similar experiments performed on the same film sample a few months later resulted in very different observations. Purging by O_2 led to almost complete

quenching of the triplet. Subsequent purging by N_2 caused the λ_{max} of the triplet of xanthone to shift to ~ 610 nm. Combining these two observations leads to the conclusion that while the film sample of xanthone in NaY is stable for a period of a few days, guest migration from the cages to the polymer matrix occurs after many months. It should be noted that the film samples were stored under air at room temperature.

The film samples containing the organic cationic guests, MG^+, TMT^+, X^+ and DPP^+, did not display any changes in transient spectra or decay kinetics, even after more than a year of storage of these films under the same conditions as for the film sample of xanthone in NaY. This implies that the occurrence of guest migration is strongly dependent upon the size of the guest, as well as its charge. The stability of the samples containing the cationic guests are highly stabilized by the electrostatic field within the zeolite, and some of the cations generated by ship in a bottle synthesis are larger than the pore diameter. Thus guest migration of these cations does not occur.

6.4 Conclusions

The dispersion of an organic-embedded zeolite complex into a PDMS membrane results in the formation of a transparent zeolite film, regardless of the size of the zeolite crystals. These films can be studied using transmission techniques, and allows for the first time the quantification of some photophysical properties that previously were unattainable using diffuse reflectance techniques.

In this study, it was determined that the extinction coefficient of an organic cation measured in solution does not change upon inclusion into a zeolite. The quantum yield for intersystem crossing was also measured for xanthone, and once again confinement in the zeolite cavities does not influence the photophysical properties that are intrinsic to the molecule. Further applications of these films, which are highly stable, can be anticipated, along with the use of other instrumental techniques for characterization.

6.5 Experimental

Membrane Preparation

The PDMS silicone (RTV 615) was obtained from GE Silicones. Hexane (Omnisolv grade) was purchased from VWR Scientific and dried over molecular sieves prior to use. In a typical preparation of zeolite films, 1 g of RTV 615A with 30-70 mg of the zeolite included complex and 1 g of dry hexane was sonicated for a period of 6 hours. Then 100 mg of RTV 615B was added and the mixture was sonicated for an additional 20 minutes. This mixture was cast onto a glass plate and heated at 60°C overnight. Typically, film thicknesses range from 20 to 30 μm from sample to sample and have zeolite loadings < 15% (w/w). The dye loading in the zeolite is appoximately 5% based on composite weight, leading to a dye loading in the membrane of less than 1%. All films are air saturated. A PDMS-zeolite film of about 30 μm thickness has an appearance similar to an overhead transparency, with a somewhat more rubbery texture. The zeolite inclusion

complexes were prepared as described previously[4,1,5] and is also mentioned in Chapter 1 for ship in a bottle synthesis (for MG^+ in HY and TMT^+ in HY).

Quantum Yield Determination

The quantum yield for intersystem crossing was measured by matching the absorbance from xanthone encapsulated within NaY dispersed in a PDMS films and of xanthone located on the outer surface of hydrated NaY also dispersed in a PDMS film. The NaY used for the latter sample was not calcined prior to use to ensure that all of the xanthone remains on the outer surface. The zeolite was used in both film samples so that the xanthone molecule receives an equal laser dose. For this measurement, the film samples were prepared on the interior walls of a 3x7 mm quartz cell.

Purging of Film Sample with N_2 and O_2

To determine the accessibility of N_2 and O_2 to the organic molecule encapsulated in a zeolite film, a film of xanthone included in NaY was prepared and placed in a quartz cell. This was subsequently purged with N_2 for one hour followed by O_2 purging for specified periods of time. This study was done with freshly prepared film samples, as well as with those that had been aged for several months. The decay traces of the N_2 and O_2 purged samples were monitored at 600 nm, where triplet xanthone absorbs. Triplet xanthone was used as the probe in this study, since it is known to be quenched by O_2.

Instrumentation

Emission spectra were recorded on Perkin-Elmer LS-50 spectrofluorimeter. Absorption spectra were measured with a HP 8451A photodiode array spectrometer.

Laser Flash Photolysis

A detailed description of this method is given in Chapter 2. The sample setup used for the films in the transmission mode is as follows: front face excitation was used, with the film sample holder consisting of a stepping motor which moves the film after each laser shot, to ensure a fresh part of the sample is being irradiated.

6.6 References

(1) Cano, M. L.; Cozens, F. L.; García, H.; Martí, V.; Scaiano, J. C. *J.Phys. Chem.* **1996**, *100*, 18152.

(2) Casal, H. L.; Scaiano, J. C. *Can. J. Chem.* **1984**, *62*, 628.

(3) Casal, H. L.; Scaiano, J. C. *Can. J. Chem.* **1985**, *63*, 1308.

(4) Cozens, F. L.; Garcia, H.; Scaiano, J. C. *Langmuir* **1994**, *10*, 2246.

(5) García, H.; García, S.; Pérez-Prieto, J.; Scaiano, J. C. *J. Phys. Chem.* **1996**, *100*, 18158.

(6) Johnston, L. J.; Wong, D. F. *J. Phys. Chem.* **1993**, *97*, 1589.

(7) Valtchev, V.; Mintova, S.; Konstantinov, L. *Zeolites* **1995**, *15*, 679.

(8) Vankelecom, I. F. J.; Dotremont, C.; Morobé, M.; Uytterhoeven, J.-B.; Vandecasteele, C. *J. Phys. Chem. B* **1997**, *101*, 2154.

(9) Vankelecom, I. F. J.; Merckx, E.; Luts, M.; Uytterhoeven, J. B. *J. Phys. Chem.* **1995**, *99*, 13187.

(10) Vankelecom, I. F. J.; Scheppers, E.; Heus, R.; Uytterhoeven, J. B. *J. Phys. Chem.* **1994**, *98*, 12390.

(11) Vasenkov, S.; Frei, H. *J. Phys. Chem. B* **1997**, *101*, 4539.

(12) Yan, Y.; Chaudhuri, S. R.; Sarkar, A. *Chem. Mater.* **1996**, *8*, 473.

(13) Zhang, Z.; Turro, N. J.; Johnston, L.; Ramamurthy, V. *Tet. Lett.* **1996**, *37*, 4861.

7. Characterization of Photocatalyst TiO_2 Incorporated in Zeolite Pores

7.1 Introduction

Studies of titanium dioxide have received much attention in recent years.[1-12] Titanium dioxide has been used as a photocatalyst in many applications, including degradation of pollutants, solar energy conversion and the transformation of organic compounds. The mechanism for the degradation by TiO_2 involves its oxidative/reductive capabilities. Excitation of TiO_2 with light of energy greater than the band gap results in electron ejection from the semiconductor valence band, generating a positive hole and a conduction band (CB) electron. This process occurs on the femtosecond time scale.[6,13]

$$TiO_2 + h\upsilon \rightarrow e^-_{CB} + h^+_{VB} \qquad (1)$$

The hole and the electron that are generated are trapped, as demonstrated in equations (2) and (3):

$$h^+ + Ti^{IV}\text{-}O^{2-}\text{-}Ti^{IV}\text{-}OH^- \rightarrow Ti^{IV}\text{-}O^{2-}\text{-}Ti^{IV}\text{-}OH^{\bullet} \qquad (2)$$

$$e^-_{CB} + Ti^{IV}\text{-}O^{2-} \rightarrow Ti^{III}\text{-}O^{2-} \qquad (3)$$

The hole is believed to be trapped by a surface bound hydroxyl radical, produced by oxidation of surface water or OH^- ion. The electron is trapped by Ti^{IV}, which

yields Ti^{III} cation. It is these trapped species that undergo reaction through interfacial charge transfer, regenerating TiO_2:

$$Ti^{IV}\text{-}O^{2-}\text{-}Ti^{IV}\text{-}OH^{\bullet} + Red \rightarrow Ti^{IV}\text{-}O^{2-}\text{-}Ti^{IV}\text{-}OH^{-} + Red^{\bullet +} \quad (4)$$

$$Ti^{III}\text{-}O^{2-} + Ox \rightarrow Ti^{IV}\text{-}O^{2-} + Ox^{\bullet -} \quad (5)$$

The oxidant in most cases is O_2, which initially forms $O_2^{\bullet -}$ and eventually forms a peroxide. The reductant is the substrate that ultimately degrades as a result of its interaction with the trapped hole. The trapped hole and electron can also recombine through a back electron transfer, an inefficient process since it regenerates the catalyst with no net reaction occurring.

Many studies on the photocatalytic properties of TiO_2 have been performed, frequently aimed at improving its catalytic efficiency. The structure of the photocatalyst plays a vital role. Thus, studies of TiO_2 anchored on Vycor glass[14] or doped with transition metals[6] have been done in an effort to gain control on the catalytic efficiency of bulk anatase, one of the crystalline forms of TiO_2.

The incorporation of TiO_2 in zeolite cavities offers a new design of a photocatalytic system. This is due to the nanoscaled pores that zeolites contain, along with their ion-exchange capabilities that allow the preparation of clusters of TiO_2 of tailored dimensions within a rigid environment of variable polarity, hydrophilicity and wherein other cooperating sites can be present. There have been earlier reports on the incorporation of TiO_2 inside zeolite cages[15-18] or anchored to the surface of the zeolite.[18-20] These reports have focused primarily on the photocatalytic properties of these systems, such as the reduction of CO_2

with H_2O.[21] Some time-resolved measurements have also been reported, but we could not find any reports on the time-resolved fluorescence of such systems.[17] Time-resolved measurements that determine the photophysical properties of a system can also be vital for determining the structure of the TiO_2 clusters and their homogeneity that can help to anticipate the photocatalytic efficiency of these materials, leading to the preparation of more active and selective photocatalysts. For example, the active sites in the alkene epoxidation catalyzed by Ti - zeolites are due to tetrahedrally coordinated framework Ti. The presence of octahedrally coordinated Ti is inactive towards such reactions, due to a lack of free coordination sites.[22]

This chapter examines the picosecond fluorescence measurements of samples of TiO_2 included in zeolites Y, beta and mordenite. The effect of heating the samples at 300°C (referred to as "baked samples") is examined, and were compared to samples that have been stored at ambient temperature (referred to as "air-equilibrated samples"). Significant changes in intensity, emission wavelength and decay kinetics were found, dependent upon the sample history. The fluorescence was studied over the period of one month, to monitor any changes due to sample aging. Assignments of the ground state absorption bands are given, based on theoretical calculations of the electronic band structure of TiO_2.[23]

To analyze the electronic band structure of crystals, the Brillouin zone of the crystal is employed. The unit cell of TiO_2 is tetragonal, and the Brillouin zone is also tetragonal, which is defined in space by vectors. The edge of the Brillouin

zone is represented by X and the center of the zone is represented by Γ, using the notation of Daude et al.[23] who have calculated the band structure of TiO_2. The nature of the lowest allowed transition in the Brillouin zone will aid in classifying semiconductor materials. The lowest allowed transition for semiconductors consists of a transition from the maximum of the valence band to the minimum of the conduction band. For TiO_2, the valence band is mainly composed of O^{2-} 2p states and the conduction band consists of the 3d states of Ti^{4+}.

All semiconductors are classed as either direct or indirect semiconductors. A direct semiconductor is one in which the nature of the lowest allowed transition[24] occurs from the same point in the Brillouin zone. The maximum of the valence band and minimum of the conduction band are either both at the center of the Brillouin zone, Γ, or both at the edge of the Brillouin zone, X. Thus, a direct transition would occur from $X_a \rightarrow X_b$ or from $\Gamma_a \rightarrow \Gamma_b$.

For an indirect semiconductor, the class to which TiO_2 belongs, the maximum of the valence band and the minimum of the conduction band occur at different points in the Brillouin zone, Γ and X. That is, the maximum of the valence band may be located at the edge of the Brillouin zone, while the minimum of the conduction band is located at the center of the Brillouin zone, or vice versa. Thus an indirect transition would be from $X \rightarrow \Gamma$ or $\Gamma \rightarrow X$. Direct transitions in an indirect semiconductor can still occur, but the energies associated with these transitions will always be greater than the band gap energy. Radiative recombination in an indirect semiconductor is possible, but this process is not as

efficient compared to a direct semiconductor. Figure 7.1 illustrates some of these transitions in TiO_2.

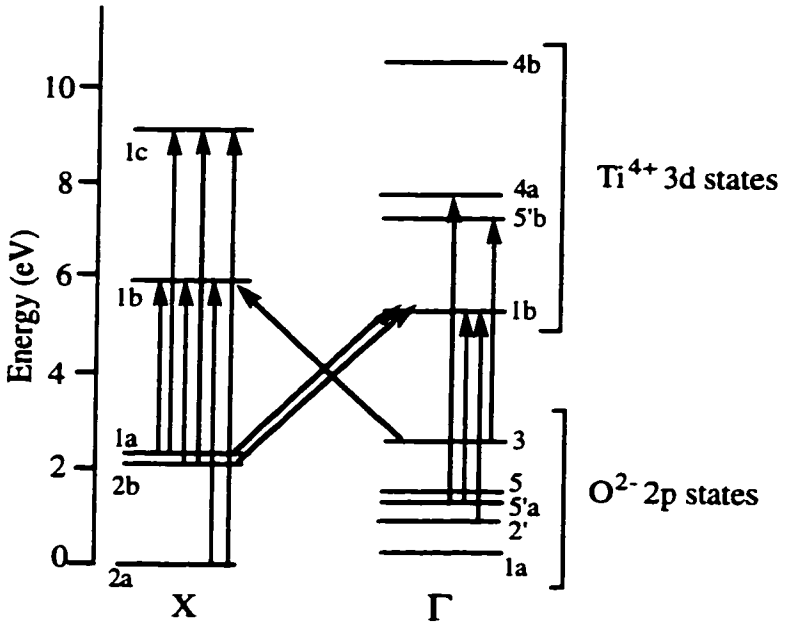

Figure 7-1: Energy level diagram showing the relative energy levels in TiO_2 as calculated by Daude et al. A few of the direct and indirect transitions are illustrated.

Controversial reports in the literature have debated whether the quantum size effect for nanoparticles of TiO_2 is applicable; quantum size effects have been used in characterizing other semiconductors such as CdS nanoparticles.[25] A quantum size effect was invoked to explain the shift in the absorption spectra of nanosized particles of TiO_2, compared to bulk anatase. This interpretation leads to the conclusion that there is a change in the band gap energy, associated with particle size. Using the effective mass model approach (EMM), a size determination of the nanoparticles can be made, based on the blue shift in the

absorption spectrum.[26,27] The other side to this debate argues that there is no size quantization for nanoparticles of TiO_2 > 4 nm; the band gap is the same as in bulk anatase.[28] The blue shift seen in the absorption spectra is attributed to a direct transition in the indirect semiconductor.

7.2 Results

7.2.1 *Absorption Spectroscopy*

The ground state absorption spectra of the air-equilibrated samples of TiO_2 included in zeolites Y, beta and mordenite are shown in Figure 7.2. The absorption onset for the three samples, which are the same as the baked ones, are at 3.45 eV for TiO_2 in Y, and at 3.65 eV for TiO_2 in zeolites beta and mordenite. These values are different from the absorption onset for bulk anatase, which occurs at 3.2 eV.[23]

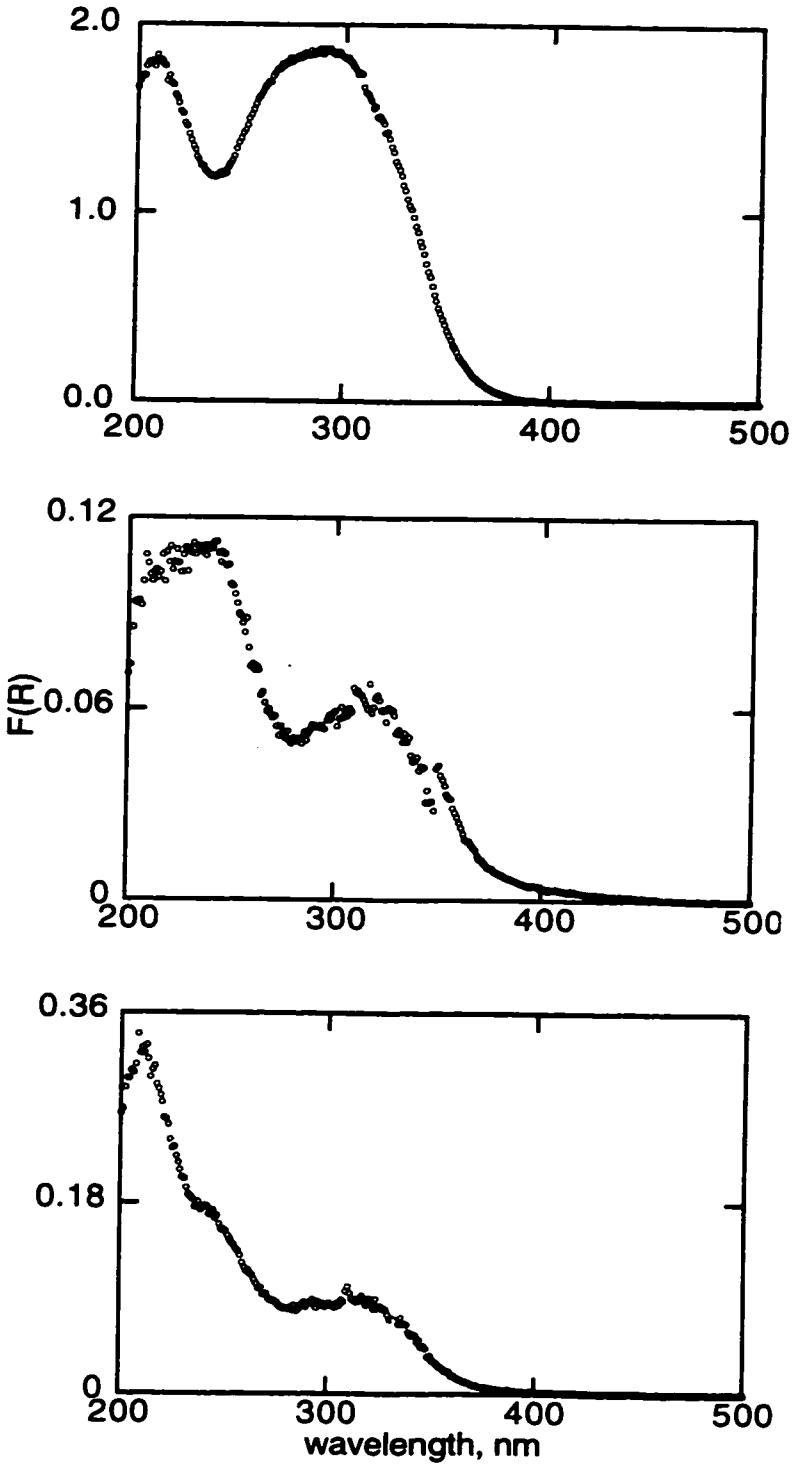

Figure 7-2: Ground state absorption spectra for TiO_2 included in zeolite Y (top), mordenite (middle) and beta zeolite (bottom)

7.2.2 *Transient Absorption Spectroscopy*

DR LFP studies of the samples of TiO_2 in zeolites, using an excitation wavelength of 355 nm were performed. The transient absorption spectrum for the sample of TiO_2 in zeolite Y had a broad absorption from 550 nm to 750 nm, with a λ_{max} centered at ~ 650 nm. The other TiO_2 - zeolite samples also displayed a broad transient absorption, but its center is blue-shifted by ~100 nm, with some absorption still occurring at 650 nm. This is assigned to the trapped electron that is produced shortly after irradiation. The transient decay traces recorded at 650 nm for TiO_2 in zeolite Y and in mordenite are shown in Figure 7.3. The decay trace obtained for TiO_2 in zeolite beta is superimposable with that of TiO_2 in mordenite and hence was not included in the figure. The decay traces indicate a long lived species, and in fact, a non-zero baseline is seen even at longer time scales.

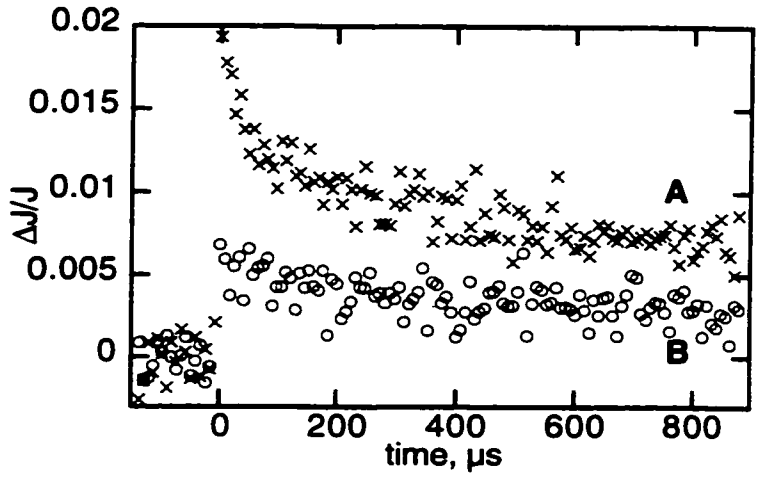

Figure 7-3: Transient decay trace of TiO_2 included in: **A**, zeolite Y and **B**, mordenite. The decays were monitored at 650 nm, using a 50 μs time scale.

7.2.3 *Luminescence Measurements*

Excitation of the samples at 290 nm produced a weak steady state luminescence with a λ_{max} at 490 nm. Time-resolved fluorescence measurements on the zeolite samples displayed an emission λ_{max} between 440 and 455 nm, with the emission extending past 550 nm. Spectral features were highly dependent upon sample conditioning (i.e. heated at 300°C or air-equilibrated) as well as on the time window for the emission (i.e. within the laser pulse or significantly after the pulse). These significant changes between the two sets of samples prompted us to examine the time-resolved emissions over an aging period of one month. The kinetics for all of the zeolite samples were adequately fitted by a biexponential decay. The fits obtained for all the samples under the different conditions started at 100 ps after the laser pulse and ended at 1.6 ns after the laser pulse.

The fluorescence intensity for all the zeolite samples was generally fairly weak. For TiO_2 incorporated in zeolite Y, heating the sample causes a significant change in the spectra as can be seen in Figure 7.4. The air-equilibrated sample, when looking at the full emission range, has a broad peak centered at ~460 nm. Examination of two time windows, one that includes the laser pulse, and the other which occurs well after the pulse has ended, (from 580 to 5700 ps) shows a shift in the emission λ_{max}, from 440 nm to 472 nm. Heating the sample at 300°C results in an emission spectrum that has a much sharper peak, with a λ_{max} centered at 450 nm, irrespective of the time window being monitored. There is also some emission at longer wavelengths (> 520 nm).

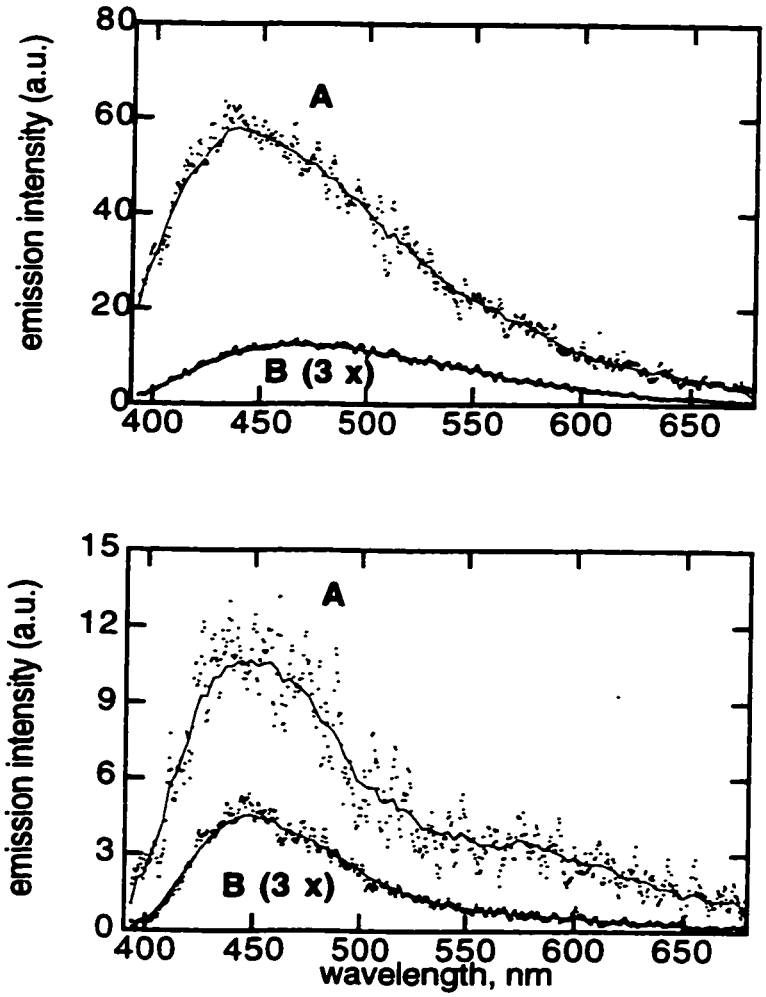

Figure 7-4: Time-resolved emission spectra of TiO_2 in zeolite Y. Air-equilibrated sample (*top spectra*) and baked sample (*bottom spectra*). **A** refers to a time window during the laser pulse and **B** refers to a time window taken between 580 and 5700 ps.

A comparison of the emission of the baked and air-equilibrated samples also reveals a difference in the relative intensities of the emission peaks. In addition, the lifetimes and preexponential factors for the emission decays vary between the baked and air-equilibrated samples of TiO_2 in zeolite Y. It should be noted that the

emission intensity of the air-equilibrated sample was much higher than for the baked sample.

The sample of TiO_2 in mordenite also shows major changes in the emission spectra when comparing baked and air-equilibrated samples, which contrasted the emission of TiO_2 in zeolite Y. This time, the emission for the air-equilibrated sample showed a single λ_{max}, at 450 nm, regardless of the time window being monitored, while TiO_2 -Y displayed two λ_{max} for the air-equilibrated sample (see above). The emission is still fairly broad, with some emission extending past 520 nm. Upon baking the sample, instead of obtaining a sharper emission peak, as was seen for TiO_2 in zeolite Y, a much broader emission occurs, with two resolvable peaks being detected for emission occurring within the laser pulse. Compared to the air-equilibrated sample, the emission intensity is much higher at longer wavelengths (λ > 500 nm). The spectra for these two sets of samples are shown in Figure 7.5. The lifetimes also varied, with a difference of > 200 ps for emission in the blue spectral region. This is best illustrated in Figure 7.6, which contains the decay traces for the baked and air-equilibrated samples. In contrast to what was seen for TiO_2 in zeolite Y, the intensity of the baked sample for TiO_2 in mordenite was greater than the air-equilibrated sample.

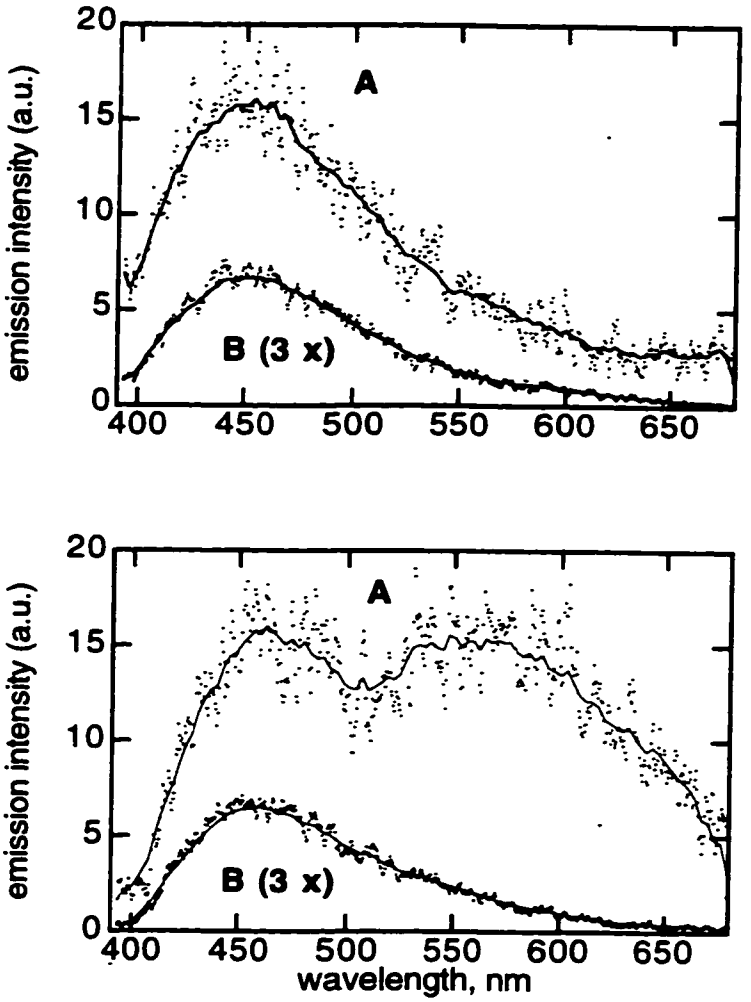

Figure 7-5: Time-resolved emission spectra of TiO_2 included in mordenite. Air-equilibrated sample (top spectra) and baked sample (bottom spectra). **A** refers to a time window during the laser pulse and **B** refers to a time window taken between 580 and 5700 ps.

The sample of TiO_2 in zeolite beta, on the other hand, did not show such major differences between air-equilibrated and baked samples, as occurred with the other zeolite samples. Both sets of samples displayed an emission λ_{max} at ~450 nm, with little emission intensity at longer wavelengths. The overall emission intensity of the baked sample was much less than the air-equilibrated

sample, which was also seen in the case of TiO_2 in zeolite Y. Some changes were noted in the lifetimes between the two sets of samples.

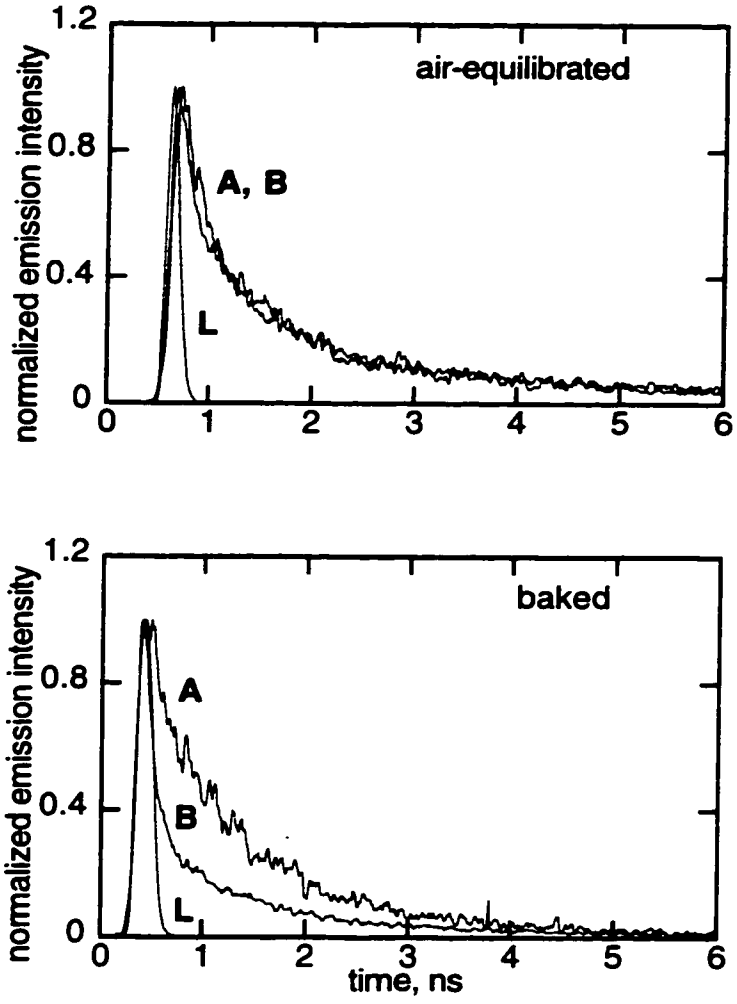

Figure 7-6: Fluorescence decay traces for TiO_2 in mordenite. Air-equilibrated sample (*top*) and baked sample (*bottom*). **L** refers to the laser pulse, **A** refers to the decay taken in the blue region of the spectrum and **B** refers to the decay taken in the red region of the spectrum.

For all of the zeolite samples studied, one trend was apparent: upon examination of the baked samples throughout a period of one month, the spectral features were similar to what was observed for the air-equilibrated samples. This

illustrates that the process being monitored in the baked sample is a reversible one. This holds true not only for the spectral features, but also for the decay kinetics. The spectra of the baked samples that have aged for one month are given in Figure 7.7 for samples of TiO_2 in mordenite and in zeolite Y. It is worth mentioning that the emission intensities cannot be directly compared when acquisitions are taken on different days; only the relative intensities of spectra taken on the same day can be compared. The lifetimes measured for these samples which varied according to sample conditioning, can be generalized in the following manner: two components were measured, one with a very short lifetime (within ~200 ps) and the second with a lifetime of around 1 ns, for both the blue and red spectral regions.

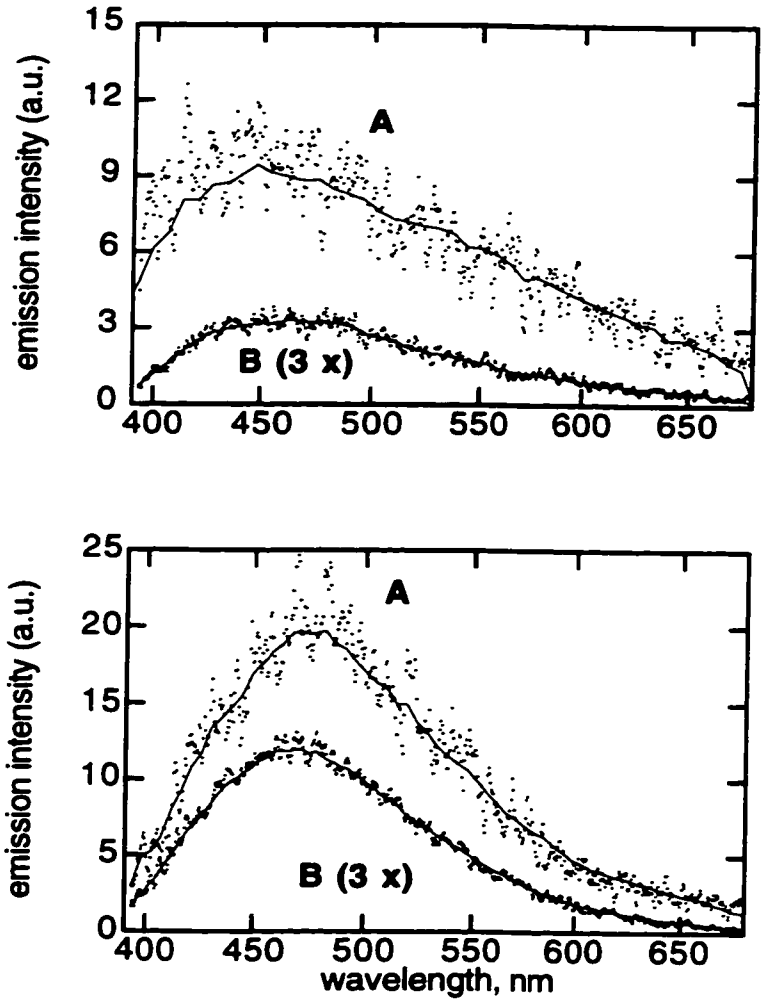

Figure 7-7: Time-resolved emission of baked TiO_2 samples in zeolite Y (*top spectra*) and mordenite (*bottom spectra*). These samples have aged for 1 month. Note the similarities in the spectra to those of the air-equilibrated samples shown in Figures 7.3 and 7.5. **A** refers to a time window within the laser pulse and **B** refers to a time window taken from 580 to 5500 ps.

Time-resolved emission experiments were also performed on suspensions of TiO_2 particles (32 nm size) in water and in perfluorocyclohexanes to aid in the understanding of the processes occurring in the zeolite samples. To parallel the zeolite experiments, two water suspensions were prepared, one

containing TiO_2 that had been heated at 300°C and the other containing TiO_2 that had not been heated. The resulting emission spectra for the two colloidal suspensions had a λ_{max} between 440 and 450 nm. No shift in the λ_{max} was observed as occurred in the zeolite samples. The only difference noted between the two emissions, which in general were much weaker than the zeolite samples, was that the emission of the suspension containing the TiO_2 that had been heated was less intense than the emission from the sample containing TiO_2 that had not been previously heated. A second set of colloidal suspensions was prepared, using perfluorocyclohexanes, since this solvent is inert to TiO_2 but its refractive index is similar to that of water. The resulting emission displayed a similar trend as occurred for the suspension of TiO_2 in water; the emission λ_{max} occurred at 450 nm, there were no shifts in the emission upon heating the TiO_2 particles, and the intensity of the sample containing the heated TiO_2 was much less than the sample containing TiO_2 that had not been heated.

7.3 Discussion

7.3.1 *Ground State Absorption Spectra*

The absorption onset for TiO_2 included in three different zeolites occurs at 3.45 eV for TiO_2 in zeolite Y and at 3.65 eV for TiO_2 in mordenite and in beta zeolites. However, the difference in the onset of the ground state absorption, which are blue-shifted compared to the value for bulk anatase, do not necessarily

imply that the band gap energy for the nanoparticles are different. Rather, the absorption onset values for TiO_2 in the three zeolite samples refer to direct transitions in TiO_2, from $X_{1a} \rightarrow X_{1b}$ and $X_{2b} \rightarrow X_{1b}$ that have calculated energies of 3.49 and 3.59 eV, respectively.[23] The absorption onset for bulk anatase occurs at 3.2 eV, corresponding to the indirect transition $\Gamma_3 \rightarrow X_{1b}$, which is the band gap energy. These results correlate well with those of Serpone et al.[28] for TiO_2 particles ranging in diameter of 2 - 27 nm.

The size and shape of the TiO_2 clusters in the zeolites are expected to differ between zeolite Y, containing spherical cages and mordenite, which has a channel structure. This is reflected in the significant change in the onset of absorption for TiO_2 in these two zeolites, suggesting that the zeolite structure does have an effect in controlling the shape of the TiO_2 particles. This has been seen in other work done on TiO_2 included in zeolites[17] where differences in absorption onsets were observed for zeolites containing different pore structures.

7.3.2 *Formation of Trapped Electrons*

The broad absorption in the region of 550 to 750 nm in the transient absorption spectra of TiO_2 in zeolite Y is characteristic of the trapped electron, seen in other systems.[2,8,29] The diffuse reflectance transient absorption spectra for TiO_2 in mordenite and beta zeolite are also broad, with its maximum shifted with respect to the zeolite Y sample. The broad absorption is also assigned to the trapped electron that is produced shortly following excitation. The decay traces for

all three zeolite samples at 650 nm indicate a long lived transient species. This is again consistent with the formation of a trapped electron, since these species have been reported to decay in the microsecond time scale. Studies of nanoparticles of TiO_2 have shown that the trapped electron decayed within 200 μs.[27] Pulse radiolysis[30] and time-resolved microwave conductivity experiments[31] have also demonstrated that charge carriers in small TiO_2 particles can have lifetimes in the microsecond to millisecond time scale. It is also common for a transient generated within a zeolite cavity to have a longer lifetime compared to that in solution. The species that may ultimately trap the electron is either Ti(IV) or the zeolite countercation. This results in the formation of Ti^{3+} or Na or K cationic clusters, respectively. (Note: K^+ is also introduced in zeolite Y during the procedure used to incorporate TiO_2 clusters into the zeolite). The exact nature of the trapped electron cannot be distinguished at the present time. For example, the absorption of Na_4^{3+} clusters has been reported in zeolite Y as a broad band at 500 - 550 nm, depending on the Si / Al ratio of the sample.[32,33] The absorption spectrum of K_4^{3+} is very similar but somewhat red-shifted.[34,35] The transient absorption spectra that we obtain for the TiO_2 - zeolite samples are fairly broad, and thus no accurate determinations of the formation of alkali metal cationic clusters can be made. The fluorescence studies, on the other hand, proved significantly more informative in understanding the behaviour of TiO_2 nanoclusters in zeolites.

7.3.3 *Interpretation of Luminescence Data*

The Ti species that are the focus of the present study involve clusters of TiO_2 inside zeolite pores. There have also been studies of Ti included in the framework of the zeolite structure. One such example is the characterization of Ti - silicalite, which has been accomplished by luminescence measurements combined with other techniques such as XANES (X-ray Absorption Near Edge Spectroscopy) and IR spectroscopies.[22,36] Through these studies, it was determined that there are two different framework Ti atoms in the zeolite, as could be seen by the two different emission wavelengths of 430 and 500 nm. It was also determined that framework Ti, in a tetrahedral coordination, upon interaction with a ligand such as water, expands the coordination sphere of Ti(IV), appearing as titanol groups (Ti-OH) that show a distinctive emission compared with Ti atoms lacking OH groups in their coordination sphere.[36] A return back to the initial tetrahedral coordination of Ti occurs upon prolonged outgassing at room temperature. These findings, particularly the different emission λ_{max} of titanol lumophores compared to the rest of Ti atoms not bonded to OH groups are valuable in the interpretation of the characteristics of TiO_2 nanoclusters in zeolites.

Applying these observations to our results, it is reasonable to assume that the changes in spectral features between baked and air-equilibrated samples are due to two different Ti species, where the difference lies in the coordination sphere of the Ti atoms; that is, the presence or absence of Ti(OH) sites. In order to explain the significant changes in intensity between baked and air-equilibrated

samples, an additional argument must be invoked, which is most likely due to a structural change in the TiO_2 nanocluster upon heating.

The thermal annealing of the (110) crystal surface of TiO_2 using a temperature > 200°C was found to produce defect sites on the crystal surface.[37] The nature of the defect site was suggested to be cleavage of the bridging oxygen atom, resulting in the exposure of two Ti^{3+} cations. This effect is reversed upon the addition of water, which acts reductively at the Ti^{3+} sites, ultimately restoring the bridging oxygen atom and producing H_2. For the samples of TiO_2 nanoclusters inside zeolites that have been heated at 300°C, the removal of an oxygen bridge, leaving two Ti^{3+} cations exposed, would result in a lower emission intensity. This is due to the nature of the emission band, which is generally assumed to be a charge transfer state from $(Ti^{3+} - O^-)^*$, in the case of tetrahedrally coordinated Ti. The fewer the oxygen bridges, the fewer charge transfer states that are possible and as a result, the decrease in the emission intensity.

To fully explain all the changes that occur upon baking the TiO_2 - zeolite samples, a combination of two arguments will be used. The first one is that through emission spectroscopy, it is possible to detect two different Ti species, one which is free of water and the other which has water as a ligand. We believe that this is responsible for the shifts in the emission wavelengths. The second argument, which explains the reduction in intensity of the baked samples, is the formation of defect sites that occurs upon sample heating. The two processes mentioned above are both reversible, which is essential in order to explain the

tendency of the baked samples to revert towards the characteristics of the air-equilibrated samples over time.

In order to apply the argument that Ti undergoes a change in coordination upon baking the sample, it must be assumed that the outgassing treatment at 300°C does not remove all of the water from the zeolite pores. This is necessary since the baked samples revert back to the air-equilibrated samples over time, which requires the presence of water. The assumption is a reasonable one, since temperatures of 400 - 550 °C are necessary to fully dehydrate hydrophilic zeolites.

The colloidal suspensions of 32 nm size TiO_2 in water or perfluorocyclohexanes showed that there was only a difference in emission intensities between suspensions containing baked TiO_2 and those containing TiO_2 that had not been heated, with the baked TiO_2 having the lower emission intensity. These experiments illustrate nicely the effect of producing defects on the TiO_2 surface upon heating the sample, resulting in a lower emission intensity.

Time-resolved fluorescence of the air-equilibrated sample of TiO_2 in zeolite Y shows two distinct emitting wavelengths, at 440 and 472 nm, which is evidence for the population of two different Ti sites in the sample. Baking the sample causes a sharpening of the fluorescence band and only one emitting wavelength at 450 nm. This indicates that under these conditions, the solid contains a uniform population of Ti sites. Based on the argument presented above, the emission at 450 nm must be due to Ti in a "closed" environment, and emission at longer wavelengths must be due to Ti atoms bonded to hydroxyl groups, probably from water acting as a ligand.

The sample of TiO_2 in beta zeolite did not show much change in the emission spectrum, even upon heating the sample. The emission wavelength occurred at 450 nm. This suggests that in this case the TiO_2 clusters are relatively free of hydration water. Based on these results, it is postulated that thermal treatment does not greatly affect the beta-TiO_2 sample, due to the small amount of hydration water present in the sample. Thus, the emission detected under both sample conditions arises from Ti in a "closed' environment.

The time-resolved fluorescence spectra of TiO_2 included in mordenite contrasted with observations for the sample of TiO_2 in zeolite Y, both in terms of emission intensities and band positions. For the air-equilibrated sample, there was only one fairly broad emission peak, centered at 450 nm. Upon heating the sample at 300°C, the emission becomes even broader with two resolvable emission maxima, with more fluorescence intensity at longer wavelengths (> 500 nm). It may be possible that sample heating results in changing the location of the water molecules, causing their relocation and coordination to the Ti, rather than its complete removal. The overall emission intensity for the air-equilibrated sample was less than that for the baked sample, the reverse of what is seen for the other two zeolite samples. This effect reflects the reduced dimensions of the mordenite pores that imposes steric restrictions to modifications in the size of the TiO_2 nanoclusters, making them more stable and less prone to the generation of defects.

The lifetimes measured for the zeolite samples, whether baked or air-equilibrated, are comprised of two components. The first component is short

lived, with a lifetime ≤ 200 ps. The second component represents a longer lived species, with a lifetime in the ns range (~ 1-1.3 ns). These fast and slow decay lifetimes, which vary somewhat upon sample treatment, probably originate from charge transfer recombination of shallow and deep sites on the nanocluster, respectively. This has also been observed in femtosecond studies in TiO_2 photocatalytic powders.[13]

Other possible explanations to account for the changes in the spectra observed between the air-equilibrated and baked samples of TiO_2 in zeolites were considered, such as a phase transition of TiO_2 from anatase to rutile. This possibility was rejected, since it has been reported that for TiO_2 particles with a diameter of 3-10 nm, the transition temperature is between 600 - 650°C, although rutile stabilization was found to occur below 350°C.[38] These phase transitions seem to occur at much higher temperatures than those used in the present work. A second possibility to be considered is the aggregation of TiO_2 clusters, resulting in an increase in the cluster size. This process, however, seems unlikely to reverse with the elapsed time after baking. Thus, these two possibilities do not appear as likely explanations for the present results.

7.4 Conclusions

The photophysical properties of TiO_2 included in zeolites Y, beta and mordenite have been studied using time-resolved techniques. A blue shift in the ground state absorption spectra of the zeolite samples compared to bulk anatase was observed and attributed to a direct transition in the indirect semiconductor,

rather than a change in the band gap energy due to a size quantization effect. Through time-resolved fluorescence measurements, it was determined that two different Ti sites are present in the nanocluster, depending on sample conditioning; one site consists of Ti in a "closed" environment and the other site has hydroxyl groups bonded to Ti atoms, due to the presence of hydration water, which acts as a ligand. The reduction in intensity that is seen upon heating the samples at 300°C is due to the formation of defect sites in the nanocluster, resulting in fewer charge transfer states, and thus a lower emission intensity. These studies are useful to expand upon catalytic studies of TiO_2 nanclusters in zeolites, since the coordination of Ti will play a crucial role in terms of catalytic activities and efficiencies.

7.5 Experimental Section

Preparation of samples for time-resolved measurements

The TiO_2-zeolite samples used in the present study were prepared by the group at the Instituto Tecnología Química in Spain. The formation of TiO_2 clusters inside the zeolite micropores was accomplished by ion exchange using aqueous solutions of commercial $(TiO)K_2(C_2O_4)$ (Aldrich) and subsequent mild calcination/polymerization at 150°C for 8 hours as previously reported. Characterization data based on FT-Raman spectroscopy showed the disappearance of $Ti{=}O^{2+}$ and the formation of TiO_2 clusters. Surface area measurements by isothermal nitrogen adsorption (Micrometrics) indicates a significant decrease after formation of the TiO_2 clusters.

The TiO_2 - zeolite samples were divided in half. One half of the samples were heated at 300°C for 18 hours, then placed on a vacuum line (P = 30 mTorr) and sealed. No special handling precautions were used with the other half of the samples (referred to as air-equilibrated samples throughout the paper). Slurry suspensions of TiO_2 in water or perfluorocyclohexanes were prepared as follows: 100 mg of 32 nm sized TiO_2 (mainly anatase form) was baked at 300°C for 18 hours and added to 1 ml of solvent, and was sonicated for 15 minutes. For laser flash photolysis experiments, the TiO_2-zeolite samples used were the air-equilibrated ones.

Instrumentation

Ground state diffuse-reflectance spectra were recorded on a Cary 1E spectrophotometer. Picosecond fluorescence measurements were carried out using a Hamamatsu C-4334 streakscope coupled with a spectrograph capable of simultaneous spectral and time-resolved data acquisition. The excitation source was the third harmonic of a Continuum PY-61 Nd:YAG laser (355 nm, < 4 mJ/pulse, 150 ps pulse width). The kinetic data were fitted with biexponential functions using the Hamamatsu software package.

Laser Flash Photolysis

A detailed description is given in Chapter 2.

7.6 References

(1) Trentler, T. J.; Denler, T. E.; Bertone, J. F.; Agrawal, A.; Colvin, V. A. *J. Am. Chem. Soc.* **1999**, *121*, 1613.

(2) Colombo, D. P., Jr.; Bowman, R. M. *J. Phys. Chem.* **1995**, *99*, 11752.

(3) Draper, R. B.; Fox, M. A. *Langmuir* **1990**, *6*, 1396.

(4) Morris Hotsenpiller, P. A.; Bolt, J. D.; Farneth, W. E.; Lowekamp, J. B.; Rohrer, G. S. *J. Phys. Chem. B.* **1998**, *102*, 3216.

(5) Zhang, Z.; Wang, C.-C.; Zakaria, R.; Ying, J. Y. *J. Phys. Chem.* **1998**, *102*, 10871.

(6) Martin, S. T.; Morrison, C. L.; Hoffmann, M. R. *J. Phys. Chem.* **1994**, *98*, 13695.

(7) Emeline, A. V.; Ryabchuk, V. K.; Serpone, N. *J. Phys. Chem. B* **1999**, *103*, 1316.

(8) Serpone, N.; Lawless, D.; Khairutdinov, R.; Pelizzetti, E. *J. Phys. Chem.* **1995**, *99*, 16655.

(9) Hoffman, M. R.; Martin, S. T.; Choi, W.; Bahnemann, D. W. *Chem. Rev.* **1995**, *95*, 69.

(10) Inoue, T.; Fujishima, A.; Konishi, S.; Honda, K. *Nature* **1979**, *277*, 637.

(11) Heller, A. *Acc. Chem. Res.* **1995**, *28*, 503.

(12) Ishitani, O.; Inoue, C.; Suzuki, Y.; Ibusuki, T. *J. Photochem. Photobiol. A: Chem.* **1993**, *72*, 269.

(13) Furube, A.; Asahi, T.; Masuhara, H.; Yamashita, H.; Anpo, M. *J. Phys. Chem. B* **1999**, *103*, 3120.

(14) Anpo, M.; Aikawa, N.; Kubokawa, Y.; Che, M.; Louis, C.; Giamello, E. *J. Phys. Chem.* **1985**, *89*, 5017.

(15) Yamashita, H.; Ichihashi, Y.; Anpo, M.; Hashimoto, M.; Louis, C.; Che, M. *J. Phys. Chem.* **1996**, *100*, 16041.

(16) Yamashita, H.; Fujii, Y.; Ichihashi, Y.; Zhang, S. G.; Ikeue, K.; Park, D. R.; Koyano, K.; Tatsumi, T.; Anpo, M. *Catalysis Today* **1998**, *45*, 221.

(17) Liu, X.; Iu, K.-K.; Thomas, J. K. *J. Chem. Soc. Faraday Trans.* **1993**, *89*, 1861.

(18) Fox, M. A.; Doan, K. E.; Dulay, M. T. *Res. Chem. Intermed.* **1994**, *20*, 711.

(19) Xu, Y.; Langford, C. H. *J. Phys. Chem.* **1995**, *99*, 11501.

(20) Xu, Y.; Langford, C. H. *J. Phys. Chem. B* **1997**, *101*, 3115.

(21) Anpo, M.; Yamashita, H.; Ichihashi, Y.; Fujii, Y.; Honda, M. *J. Phys. Chem. B* **1997**, *101*, 2632.

(22) Marchese, L.; Maschmeyer, T.; Gianotti, E.; Coluccia, S.; Thomas, J. M. *J. Phys. Chem. B* **1997**, *101*, 8836.

(23) Daude, N.; Gout, C.; Jouanin, C. *Phys. Rev. B* **1977**, *15*, 3229.

(24) Davies, J. H. *The Physics of Low-Dimensional Semiconductors: an Introduction*; Press Syndicate of the University of Cambridge: Cambridge, 1998.

(25) Logunov, S.; Green, T.; Marguet, S.; El-Sayed, M. A. *J. Phys. Chem. A* **1998**, *102*, 5652.

(26) Kormann, C.; Bahnemann, D. W.; Hoffmann, M. R. *J. Phys. Chem.* **1988**, *92*, 5196.

(27) Choi, W.; Termin, A.; Hoffmann, M. R. *J. Phys. Chem.* **1994**, *98*, 13669.

(28) Serpone, N.; Lawless, D.; Khairutdinov, R. *J. Phys. Chem.* **1995**, *99*, 16646.

(29) Rabani, J.; Yamashita, K.; Ushida, K.; Stark, J.; Kira, A. *J. Phys. Chem. B* **1998**, *102*, 1689.

(30) Lawless, D.; Serpone, N.; Meisel, D. *J. Phys. Chem.* **1991**, *95*, 5166.

(31) Warman, J. M.; de Haas, M. P.; Pichat, P.; Serpone, N. *J. Phys. Chem.* **1991**, *95*, 8858.

(32) Liu, X.; Iu, K.; Thomas, J. K. *J. Phys. Chem.* **1994**, *98*, 13720.

(33) Iu, K.; Liu, X.; Thomas, J. K. *J. Phys. Chem.* **1993**, *97*, 8165.

(34) Liu, X.; Zhang, G.; Thomas, J. K. *J. Phys. Chem.* **1995**, *99*, 10024.

(35) Liu, X.; Thomas, J. K. *J. Chem. Soc. Faraday Trans.* **1995**, *91*, 759.

(36) Bordiga, S.; Coluccia, S.; Lamberti, C.; Marchese, L.; Zecchina, A.; Boscherini, F.; Buffa, F.; Genoni, F.; Leofanti, G.; Petrini, G.; Vlaic, G. *J. Phys. Chem.* **1994**, *98*, 4125.

(37) Lu, G.; Linsebigler, A.; Yates Jr., J. T. *J. Phys. Chem.* **1994**, *98*, 11733.

(38) Ma, W.; Lu, Z.; Zhang, M. *Appl. Phys. A.* **1998**, *66*, 621.

8. Preliminary Results Towards Photochemical Chiral Induction in Zeolite Cavities

8.1 Introduction

Asymmetric synthesis for ground state reactions has received a great deal of attention over the past years.[1,2] In comparison, there has not been as much focus on asymmetric synthesis using a photochemical route. An excellent review summarizes the work that has been done in this area up to 1992.[3]

More recently, zeolites have been used as microreactors in which to host a substrate for the purpose of inducing chirality upon substrate irradiation.[4-8] The concept behind this procedure, known as the chiral auxilliary approach, is to coinclude in the zeolite cavities, along with the substrate undergoing the reaction, a chiral molecule or 'inductor' molecule. The purpose of the inductor molecule is to interact with the substrate during the course of the reaction in such a way that it causes the preferential formation of one enantiomeric photoproduct over another. This interaction will most likely be in the form of hydrogen bonds. The absorption of a chiral inductor molecule in the zeolite cavities renders a chiral zeolite medium, which is essential for inducing any asymmetry in a photoproduct included in a supramolecular host. The zeolite itself aids in this selective formation of an enantiomer by providing a rigid environment, thus hindering certain motions of the substrate molecule undergoing the photochemical reaction. In addition, the zeolite may enhance the inductor - substrate interaction. The combination of a chiral inductor molecule and the rigid zeolite host may serve to induce chirality in a

photoproduct where normally the product obtained upon solution irradiation is racemic.

Certain criteria that the inductor molecule must possess include:

(i) it cannot itself react during the photochemical reaction

(ii) it must be transparent at the irradiation wavelength

The simplest reaction type to use in order to test the concept of chiral induction in zeolites is a unimolecular photochemical reaction such as a Norrish Type II reaction.

There have been only a handful of literature reports on using this method, with very low to moderate % ee. The first report on asymmetric induction in zeolite cavities looked at the Norrish Type II reaction of cis-4-tert-butylcyclohexyl ketones into the corresponding cyclobutanols.[6] The chiral inductor molecule used which rendered the highest ee % was (-)-ephedrine, giving an ee of 10-30%, depending on the loading of the inductor in the supercages of NaY. Turro's group have also reported on chiral induction in zeolites by examining the α-photocleavage of aryl ketones such as benzoin methyl ether and the subsequent recombination of the radical pairs.[7] The % ee reported when using a chiral inductor such as ephedrine and diethyl tartrate ranged from 3-9%. Such low ee values are, nevertheless, promising. They demonstrate that using a 'chirally modified' zeolite is a viable approach to inducing chirality in the product of a photochemical reaction. All of the factors that optimize this ee yield are yet to be determined. However, it is apparent from these studies that a loading of one chiral inductor molecule per cage is

necessary in order to achieve satisfactory results, and that there must be a tight fit between the substrate and the chiral inductor.

There have been no previous reports on the examination of the transient features of substrates loaded into a zeolite containing a chiral inductor molecule. This type of study may shed some light into the mechanism of chiral induction in zeolites and what criteria are required to optimize these conditions. For this purpose, the transient lifetimes of a particular enantiomer included in zeolite NaY along with both R and S forms of a chiral inductor will be examined and compared to the other enantiomeric form of the substrate under the same conditions. Thus, differences in the lifetimes that result from specific interaction of a chiral substrate with the R and S form of an inductor molecule may lead to additional evidence that a 'chiral zeolite' host is an alternate and unique medium for inducing chirality in substrate molecules undergoing a photochemical reaction.

This chapter will look at the preliminary results obtained in the transient lifetimes of a substrate molecule, methyl-p-methoxy-β-phenylpropiophenone (MePMPP) when included in NaY with a chiral inductor molecule, (R)-(+)-α-methyl-4-pyridinemethanol and (S)-(-)-α-methyl-4-pyridinemethanol.

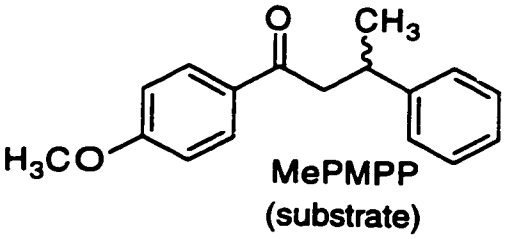

MePMPP
(substrate)

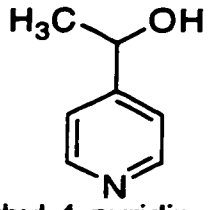

methyl-4-pyridinemethanol
(inductor)

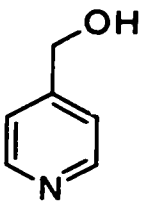

4-pyridylcarbinol
(control)

The triplet lifetimes of the enantiomeric and racemic forms of MePMPP in the crystalline state have previously been reported.[9] Differences between the racemic and pure enantiomers of MePMPP were found, with the racemic form having a triplet lifetime of 733 ns, whereas the enantiomeric forms have similar triplet lifetimes of 420 ns. The mechanism of triplet deactivation for this substrate is through β-phenyl quenching, as described in Chapter 3. The differences in lifetimes exhibit an interesting example of chiral discrimination in the solid state. Powder x-ray diffraction of both the racemic and S-enantiomer forms reveal that the shape of the unit cell and the respective volumes are significantly different. The unit cell of the S-enantiomer is long and rectangular, compared to the nearly cubical unit cell of the racemic compound. Although no conclusive evidence about the orientation of the molecules in the racemic form could be made, the triplet lifetime data indicates a significant difference in crystal packing between the racemic and enantiomeric forms. This results in chiral discrimination in the decay

kinetics of this ketone in the crystalline state. Inclusion of this molecule into a zeolite cavity results in an increase in triplet lifetime compared to both solution and solid state values, due to the inefficiency in the zeolite medium to readily achieve a conformation required for quenching of the excited carbonyl by the β-phenyl ring.

The choice of an inductor molecule was based on work reported on in other chapters, mainly that pyridine has an enormous effect on the triplet lifetimes of carbonyl molecules included in zeolite NaY[10] (see Chapter 3). Thus, the use of a chiral pyridine derivative seemed an attractive candidate for a chiral inductor molecule in these systems. As a control, 4-pyridylcarbinol was also incorporated into NaY containing the MePMPP substrate. This molecule was chosen because it is of similar size as the inductor molecules, but it does not contain any chiral centers.

8.2 Results

8.2.1 *Transient Spectroscopy*

The transient absorption spectrum of MePMPP included in NaY has a broad peak centered at ~ 400 nm. This is seen in Figure 8.1 for a sample of S-MePMPP included in NaY. This peak is assigned to the triplet of MePMPP, as was seen in the solid state.[9] The triplet-triplet absorption spectra does not change upon the addition of any of the inductor molecules.

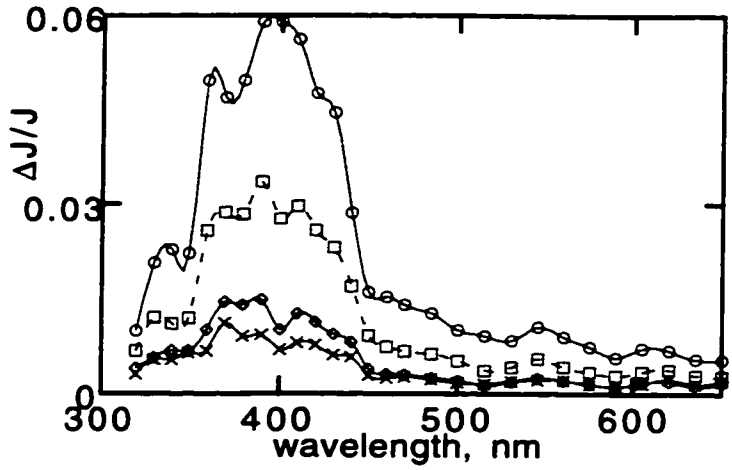

Figure 8-1: Transient absorption spectra of S-MePMPP in NaY sample that has been sealed under vacuum. The excitation wavelength was 308 nm using a 5 μs instrumental time scale. The maximum at 400 nm is assigned to the triplet state of S-MePMPP.

The triplet decay traces for all of the samples prepared were monitored at 420 nm. A comparison of the decay traces obtained when the inductor molecules are added to the zeolite cavities is shown in Figure 8.2 for the substrate (R)-MePMPP. These decay traces reflect samples that were sealed under vacuum prior to LFP measurements. As can be seen in the figure, the decay traces of the samples containing the 4-pyridylcarbinol and the (S)-methyl-4-pyridinemethanol are superimposable; the decay trace of the sample containing (R)-methyl-4-pyridinemethanol is much longer lived. Thus, a significant difference in triplet lifetime of (R)-MePMPP is observed when different enantiomers of methyl-4-pyridinemethanol are coincluded into the zeolite cavities.

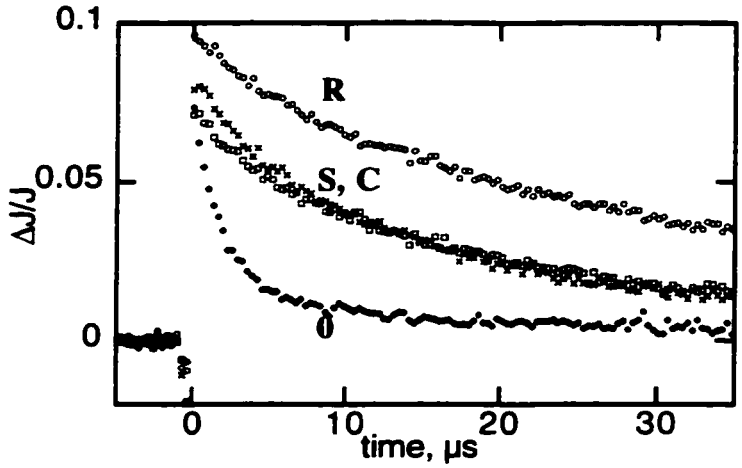

Figure 8-2: Kinetic decay traces monitored at 420 nm for vacuum sealed samples of R-MePMPP in NaY containing various inductor molecules. The instrumental time scale used is 2 μs. **0** refers to a sample containing no inductor molecule, **C** refers to a sample containing 4-pyridylcarbinol, and **R** and **S** refer to the enantiomeric forms of methyl-4-pyridinemethanol

Samples containing (S)-MePMPP as the substrate were also prepared. These samples, however, were not sealed under vacuum prior to LFP measurements. A comparison of the triplet decay traces for this set of samples is given in Figure 8.3. This time, the triplet decay traces of the samples containing (R)-methyl-4-pyridinemethanol and 4-pyridylcarbinol are superimposable, while the sample containing (S)-methyl-4-pyridinemethanol has the longest triplet lifetime. Thus, the sample giving the longest triplet lifetime of MePMPP contains an inductor molecule that is of the same enantiomeric configuration as the substrate.

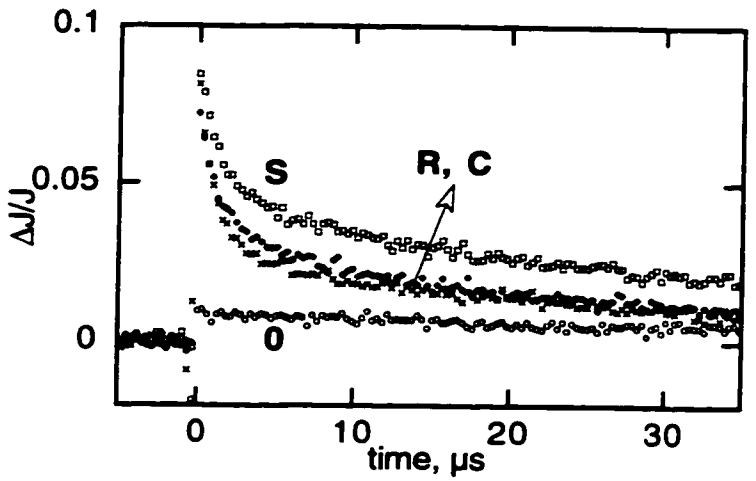

Figure 8-3: Kinetic decay traces monitored at 420 nm for vacuum dried (but not sealed) samples of R-MePMPP in NaY containing various inductor molecules. An instrumental time scale of 2 μs was used. **0** refers to a sample containing no inductor molecule, **C** refers to a sample containing 4-pyridylcarbinol, and **R** and **S** refer to the enantiomeric forms of methyl-4-pyridinemethanol

The samples containing the R-substrate were examined some weeks later to determine if sample aging has any effect on the triplet decay traces. The only change that occurs when comparing normalized triplet decay traces of the fresh and aged samples is that there is a decrease in lifetimes for the sample containing 4-pyridylcarbinol. This sample has also changed colour upon laser irradiation, from white before LFP experiments to purple after LFP experiments. The ground state absorption spectrum for this sample contains a weak absorption at 500 nm compared to the absorption spectrum for the fresh sample. Figure 8.4 displays the ground state spectrum for the aged carbinol sample.

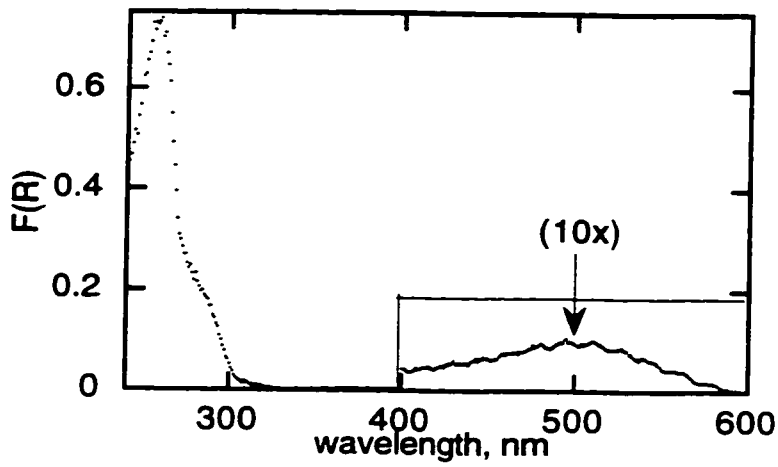

Figure 8-4: Ground state absorption spectrum of aged sample of R-MePMPP in NaY containing carbinol (sample sealed under vacuum).

8.3 Discussion

8.3.1 *Effect of Sample Preparation*

The manner in which the samples are prepared for these experiments is very important. First, the chiral inductor molecules must be included in the zeolite cavities before the substrate molecule; otherwise, the substrate molecule MePMPP will be forced out of the cavities, rendering an unknown occupancy number for the ketone. The handling of the samples prior to LFP measurements, that is, sealing the samples under vacuum or not sealing the samples at all has a great effect on the triplet lifetimes. Thus, while the trend that is seen when comparing the samples containing (R)-MePMPP and (S)-MePMPP is apparent and real, the triplet lifetimes cannot be directly compared because of the different sample conditions. The samples containing the (S)-MePMPP substrate which

have not been sealed have shorter lifetimes compared to the sealed samples, since there will also be an effect of oxygen quenching the triplet state of (S)-MePMPP. Thus, the effect that is observed can only be explained in a qualitative rather than a quantitative manner.

8.3.2 *Interpretation of Triplet Decay Traces*

The decay traces of the two sets of samples show that the substrate, either (R)-MePMPP or (S)-MePMPP have different rates of triplet decay when an additional molecule, a chiral inductor molecule, is also included in the NaY cages. This effect was already shown in Chapter 3, where the triplet decay of certain aryl ketones was altered by the presence of pyridine in the cavities, which quenched the acid sites of the zeolite. Thus, the use of 4-pyridylcarbinol as a standard becomes apparent: it does not contain any chiral centers, it is of similar size to the chiral pyridine derivatives used, and it contains a pyridine moiety. Thus, any changes in triplet lifetime of MePMPP that occur when 4-pyridylcarbinol is also included in the cages compared to a sample of NaY that contains only MePMPP reflects interactions of the pyridine moiety with the acid sites in the zeolite, or with MePMPP. They do not indicate that there is any sort of 'chiral induction' taking place. The fact that the inclusion of 4-pyridylcarbinol to the cavities of NaY does cause an increase in the triplet lifetime of MePMPP is indicated in Figures 8.2 and 8.3.

Following the above argument, it can be concluded that any of the samples that give a triplet decay trace that is superimposable with that of the sample

containing the non-chiral pyridine derivative also does not reflect any chiral interaction occurring.

The most interesting and exciting observation is that the use of (S)-MePMPP afforded the optical antipode of transient decay traces produced by the use of (R)-MePMPP, indicating that the system is well-behaved. The longest triplet lifetime of MePMPP occurs when the configuration of the inductor molecule matches that of the substrate. Based on these preliminary results, this observation most likely reflects an optimal and tight fit between the substrate and inductor that cannot be achieved in any other conformation. The sample containing the inductor that is of the opposite enantiomeric form compared to the substrate has no effect on the triplet lifetime of MePMPP compared to the standard sample, indicating no chiral interaction taking place. The location and fit between the substrate and inductor molecule in this case probably does not allow for the chiral centers in the two molecules to interact.

8.4 Conclusions

The preliminary results presented do indicate that further experiments must be performed in order to obtain a more complete picture of the events that are occurring. In any event, these results do show that using a chiral zeolite medium may be a versatile host for performing asymmetric photochemical reactions. The details of the conditions and criteria needed to optimize this process have not completely been elucidated, but it is expected that the field of chiral induction using

zeolite cavities will see an increasing effort by many research groups in the near future.

8.5 Experimental Section

Preparation of Samples for LFP Studies

Zeolite NaY (250 mg) was activated at 500°C overnight. The zeolite was then added to 20.2 mg of the specific pyridine derivative dissolved in a 1:1 solution of dichloromethane and hexane (10 ml in total). The resulting mixture was stirred for 3 hours, at which point it was filtered and washed with dichloromethane to ensure that none of the molecules were absorbed to the surface of the zeolite. The zeolite complex was dried in air for 1 hour, then vacuum dried at 20-30 mTorr of pressure overnight. The dried zeolite complex was then added to 1 mg of MePMPP substrate dissolved in 10 ml of hexane. The inclusion of MePMPP substrate is followed in the same manner as inclusion of the inductor molecule in NaY. The zeolite complexes containing both inductor and substrate molecules were either sealed under vacuum (P = 8 mTorr) or stored under air. LFP measurements for fresh samples were taken immediately following the sealing of the samples, or immediately following vaccum drying the samples (for the samples that were not sealed prior to LFP measurements).

Preparation of Substrate Molecules MePMPP

Two methods were used to synthesize the substrate molecules. The first method has previously been reported in the Scaiano group.[9] The other method,

which was used to synthesize R-MePMPP used in this work, consisted of an alternative to a Friedel-Crafts acylation. Trifluoroacetic anhydride (0.52 ml, 3.66 mmol) was added to 300 mg (1.83 mmol) of R-3-phenylbutyric acid. The solution was cooled down to 10°C and 21 mg (0.183 mmol) of 85% phosphoric acid was added. The dissolution of the phosphoric acid takes place within 20 minutes (the solution is now bright yellow). Anisole (0.20 ml, 1.83 mmol) was added and the solution refluxed overnight, resulting in a bright red solution. The mixture was then quenched with 10% NaOH and extracted three times with 10 ml of CH_2Cl_2. After drying over $MgSO_4$, the solvent was removed in vacuo. Purification was achieved by preparative TLC, using hexane and ethyl acetate. The NMR and GC-MS data matched what was previously reported for this compound.[11]

8.6 References

(1) Noyori, R. *Asymmetric Catalysis in Organic Synthesis*; Wiley-Interscience: New York, 1994.

(2) Cervinka, O. *Enantioselective Reactions in Organic Chemistry*; Ellis Horwood: London, 1995.

(3) Inoue, Y. *Chem. Rev.* **1992**, *92*, 741.

(4) Joy, A.; Robbins, R. J.; Pitchumani, K.; Ramamurthy, V. *Tet. Lett.* **1997**, *38*, 8825.

(5) Joy, A.; Scheffer, J. R.; Corbin, D. R.; Ramamurthy, V. *Chem. Commun.* **1998**, 1379.

(6) Leibovitch, M.; Olovsson, G.; Sundarababu, G.; Ramamurthy, V.; Scheffer, J. R.; Trotter, J. *J. Am. Chem. Soc.* **1996**, *118*, 1219.

(7) Kaprinidis, N. A.; Landis, M. S.; Turro, N. J. *Tet. Lett.* **1997**, *38*, 2609.

(8) Sundarababu, G.; Leibovitch, M.; Corbin, D. R.; Scheffer, J. R.; Ramamurthy, V. *Chem. Commun.* **1996**, 2159.

(9) Boch, R.; Bohne, C.; Scaiano, J. C. *J. Org. Chem.* **1996**, *61*, 1423.

(10) Scaiano, J. C.; Kaila, M.; Corrent, S. *J. Phys. Chem. B.* **1997**, *101*, 8564.

(11) Boch, R. Ph.D. Thesis, University of Ottawa, 1995.

9. Final Comments and Future Directions

This thesis presents research on the photophysical and photochemical properties of guest molecules included within zeolite pores. While each individual chapter investigated distinct processes, they all relate to each other in that a deeper understanding of the influence of the constrained zeolite media on the photobehaviour of encapsulated guest molecules was achieved.

One of the more important results reported in this thesis includes the significant influence that the acid sites in the 'non-acidic' zeolite NaY has on the transient lifetime of included arcmatic carbonyl molecules. Many researchers in this field do not consider NaY to have any acidity. However, the one hundred fold increase in the triplet lifetime of xanthone whcihc occurs uon initial pyridine addition strongly suggests that the acidic nature of this zeolite, while small, does have a trememdous impact on the photobehaviour of included molecules. This was seen with other probe molecules as well, including coumarin 6 and 1-azaxanthone.

The interaction of pyridine with the acid sites in faujasite zeolites led to the idea that a chiral pyridine derivative may be ideal for use as a chiral inductor molecule for asymmetric reactions carried out in zeolite cavities. This possibility was probed in Chapter 8, where preliminary results on the chiral selectivity of a chiral ketone probe incorporated into a chirally modified zeolite, through monitoring the triplet decay kinetics of the probe, were presented. Inclusion of the chiral pyridine derivative leads to a chirally modified zeolite.

Optimizing the degree of chiral selectivity through modifying the substituents of the chiral probe, as well as altering the charge-balancing cations, may prove insightful into designing highly enantioselective photochemical reactions. Changing the substituent may influence the positioning of the probe in relation to the chiral inductor molecule, thereby affecting their interaction. Using zeolites with different charge-balancing cations may stabilize the interaction between the probe and inductor molecule, through an electrostatic effect, or through a reduction of the free volume of the cages, or both. Modifying the chiral inductor molecule, such that two asymmetric centers are present, rather than one as the inductor used in Chapter 8 had, should also improve upon the chiral selectivities. This area of zeolite research, which is still a fairly new and exciting field, has the potential of opening up a whole new set of possibilities towards enantioselective photochemical reactions in zeolites. Numerous examples have been provided in this thesis and in the literature that show how unique a medium zeolites are in altering and modifying photochemical reactions. Employing some of the characteristics and properties discovered from these areas to the conceptual design of asymmetric induction reactions could prove invaluable to the success of chiral selectivity in zeolite cavities.

Another significant contribution was described in Chapter 6, which examined the photophysical properties of transparent zeolite-PDMS films. This project provided a correlation, for the first time, between properties of organic molecules included in zeolite pores and in solution. These properties, such as ground state extinction coefficients and quantum yield of ISC, could not previously

be quantified due to the restrictions and limitations of DR techniques. The transparent film overcomes these difficulties.

Other applications of these materials are surely forthcoming. For example, it may be possible to use transparent zeolite films for circular dichroism (CD) studies. This would accompany the techniques used in the study of asymmetric induction in zeolites, since the presence of specific interactions between the probe and the inductor may result in an absorption peak in the CD spectrum. This would help to identify the combination of probe and inductor molecules best suited for asymmetric induction, rather than performing time-consuming product studies reactions on a random basis.

Claims to Original Research

(1) The determination that NaY, which has been considered a 'non-acidic' zeolite, does contain enough acid sites to significantly affect the photobehaviour of included guest molecules. This was demonstrated by the fluorescence of the monocation species of coumarin 6 in NaY, as well as by the one hundred fold increase in the lifetime of xanthone with inclusion of pyridine.

(2) First quantization of photophysical properties such as absorption coefficients and quantum yields of ISC of included guest molecules were accomplished through use of transparent PDMS zeolite films.

(3) Determination of two Ti sites in TiO_2 nanoclusters included in zeolites, depending on sample water content. Measured using time-resolved fluorescence techniques.

(4) First investigation of chiral discrimination in zeolites using time-resolved DR techniques. This was achieved through monitoring changes in the triplet decay of a chiral probe molecule as different enantiomers of chiral inductor molecules were introduced into the cavities.

Publications Resulting from the Research Described in this Thesis

S. Corrent, L.J. Martínez and J.C. Scaiano. "Intrazeolite Photochemistry. 25. Photochemistry of 1-Azaxanthone in Zeolites in the Presence of Hydrogen Donors, Electron Donors and Energy Acceptors" *J. Phys. Chem. B.*, 103, p8097 (1999)

M. Alvaro, H. García, S. Corrent and J.C. Scaiano. "Intrazeolite Photochemistry. 23. Transparent PDMS Films of Zeolites Incorporating Organic Guests: Quantitative Determination of Photophysical Parameters by Transmission Techniques" *J. Phys. Chem B.*, 102, 39, p7530 (1998)

S. Corrent, P. Hahn, G. Pohlers, T.J. Connolly, J.C. Scaiano, V. Fornés and H. García. "Intrazeolite Photochemistry. 22. Acid-Base Properties of Coumarin 6. Characterization in Solution, the Solid State and Incorporated into Supramolecular Systems" *J. Phys. Chem. B.*, 102, 30, p5852 (1998)

J.C. Scaiano, M. Kaila and S. Corrent. "Intrazeolite Photochemistry. 19. Effect of the 'Spectator' Pyridine on the Behavior of Carbonyl Triplet States in the Zeolite NaY" *J. Phys. Chem. B.*, 101, 42, p8564 (1997)

S. Corrent, G. Cosa, J.C. Scaiano and H. García. "Intrazeolite Photochemistry 26. Photophysical Properties of Nanosized TiO_2 Clusters Included in Zeolites Y, Beta and Mordenite" submitted *Chemistry of Materials.*, October 1999

A.M.C. Kwok, S. Corrent and J.C. Scaiano. "Intrazeolite Photochemistry. 27. Stereoselective Photocyclization of 2,6-Diphenylcyclohexanone in Faujasite Zeolites. Effect of Spectators Pyridine and Ammonia" manuscript in preparation